Elettra Sincrotrone Trieste

X-ray imaging and tomography

Giuliana Tromba

Elettra - Sincrotrone Trieste

SYnchrotron **R**adiation for **ME**dical **P**hysics (SYRMEP) beamline

School on Synchrotron and Free-Electron-Laser Methods for Multidisciplinary Applications,
ICTP – Miramare, 7-18 May 2018

The Abdus Salam International Centre for Theoretical Physics

Elettra Sincrotrone Trieste

Outline

Characteristics and potentials of synchrotron X-rays

SR X-rays imaging techniques

- Absorption, K-edge imaging
- Phase contrast techniques:
  - *Propagation Based Imaging (PBI)*
  - *Analizer Based Imaging (ABI)*
  - *X-ray interferometry with crystals*
  - *Grating interferometric imaging (GI)*
  - *Grating non-interferometric imaging*

Applications

- Biomedical imaging and biology
- Cultural Heritage and Paleoantropology
- Volcanology

Advantages of SR for hard X-ray imaging

Monochromaticity allows for:

- *optimization* of X-ray energy according to the specific case under study (dose reduction)
- quantitative CT evaluations
- no beam hardening
- convenient use of contrast agent (K-edge and L-edge imaging)

Spatial coherence enables the applications of ***phase sensitive imaging techniques***

- Phase contrast overcomes the limitation of conventional radiology
- It brings to a dose reduction
- Improved contrast resolution, edges enhancement
- Use of phase retrieval algorithms

High fluxes

- Short exposure time
- Dynamic studies (4DCT)

Collimation

- parallel beams, scatter reduction
- beam shaping (micro-beams)

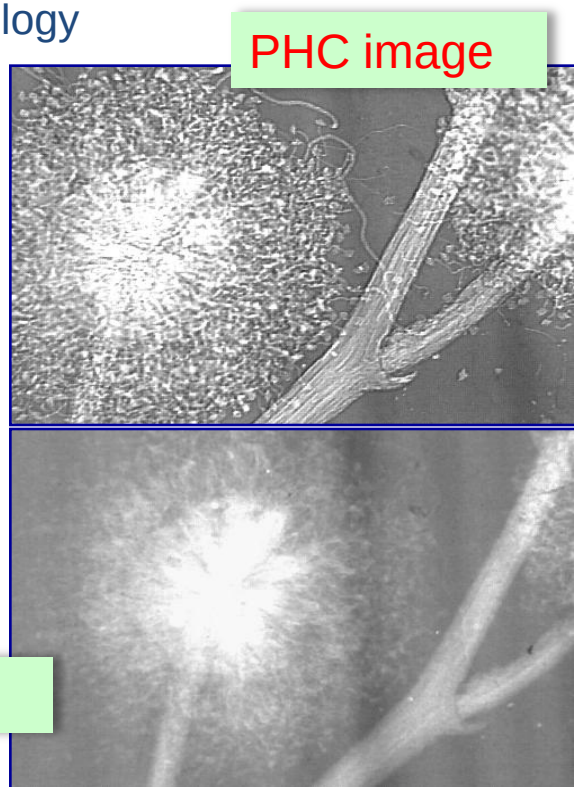

Elettra
Sincrotrone
Trieste

SR X-rays imaging techniques

K-edge subtraction imaging

Exploiting the monochromaticity of SR…

K-edge Subtraction Imaging

1. Contrast agent: Iodine, or Gadolinium, etc.
2. Two Images are acquired : Above (A) and Below (B) the K-edge of Contrast agent
3. From image processing : Iodine and Tissue images can be obtained

Energy E_{K-} (B)

Energy E_{K+} (A)

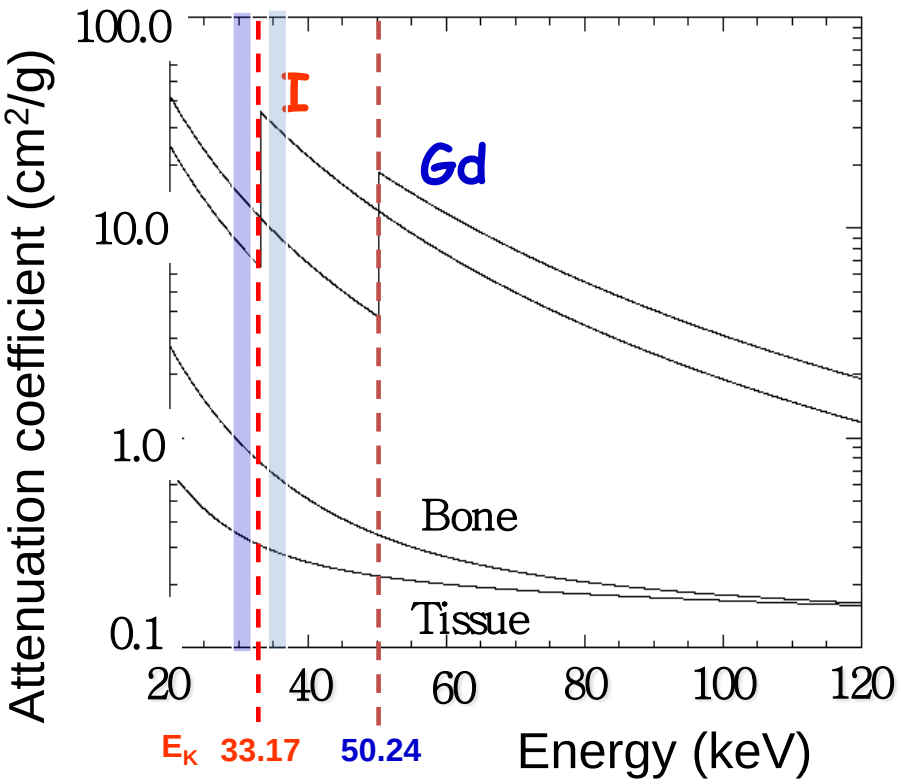

μ_{xy} : Attenuation coefficients : x = energies (A or B), y = material (tissue (t) or iodine (i)).

$$x_i = \frac{\mu_{Bi}\ln(A) - \mu_{Ai}\ln(B)}{\mu_{Bi}\mu_{At} - \mu_{Ai}\mu_{Bt}}$$

$$x_t = \frac{\mu_{Bi}\ln(A) - \mu_{Ai}\ln(B)}{\mu_{Bi}\mu_{At} + \mu_{Ai}\mu_{Bt}}$$

Below Above K-edge

Iodine Image

Phase – contrast imaging techniques: main cathegories

Propagation-based Imaging (PBI)

Analizer-Based Imaging (ABI)

X-ray interferometry with crystals

Grating interferometric imaging (GI)

Grating non-interferometric imaging

Exploiting the spatial coherence of SR…

Phase Contrast vs. Absorption imaging

Radiation – matter interaction is determined by **refraction index :** $n = 1 - \delta + i\beta$, β = absorption term, δ = phase shift term

Absorption properties are expressed through β in the attenuation coefficient μ. $\mu = \frac{2\pi\beta}{\lambda}$

The **effect on phase** of incident radiation produced by the sample *(φ or phase shift)* is related to δ

for soft tissue@17 keV: $\beta \sim 10^{-10}$; $\delta \sim 10^{-6}$, $\delta \propto \lambda^2$, $\beta \propto \lambda^3$

Absorption radiology -> **contrast** is generated by differences in the x-ray absorption ($C_{abs} \sim x\,\Delta\beta$),

Phase Radiology -> **contrast** is generated by phase shifts ($C_{\phi} \sim x\ \Delta\delta$) with x = object size // to beam direction

$\delta >> \beta$ ➔ phase shifts effects >> absorption

In conventional radiology image formation is based on differences in X-ray absorption properties of the samples (β term). The image contrast is generated by density, composition or thickness variation of the sample. Main limitation: poor contrast in soft tissue differentiation.

***Phase contrast* techniques** are based on the observation of the *phase shifts* produced by the object on the incoming wave (δ term). Contrast arises from interference among parts of the wave front differently deviated (or phase shifted) by the sample. Edge enhancement effects.

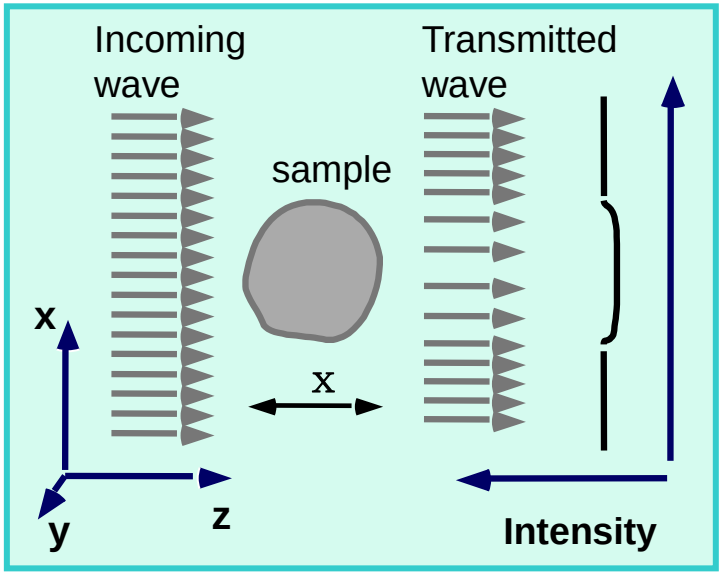

Absorption

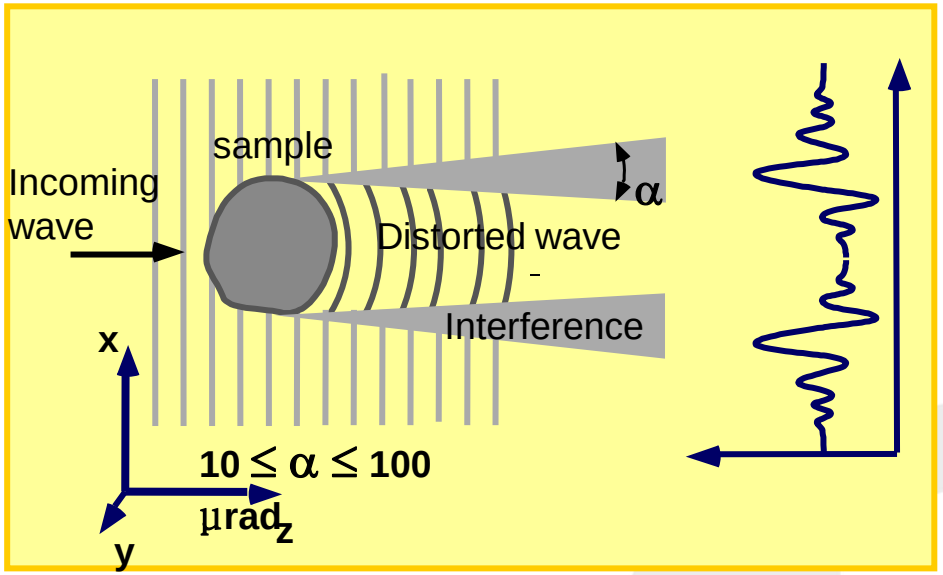

Phase Contrast

Propagation based imaging (PBI)

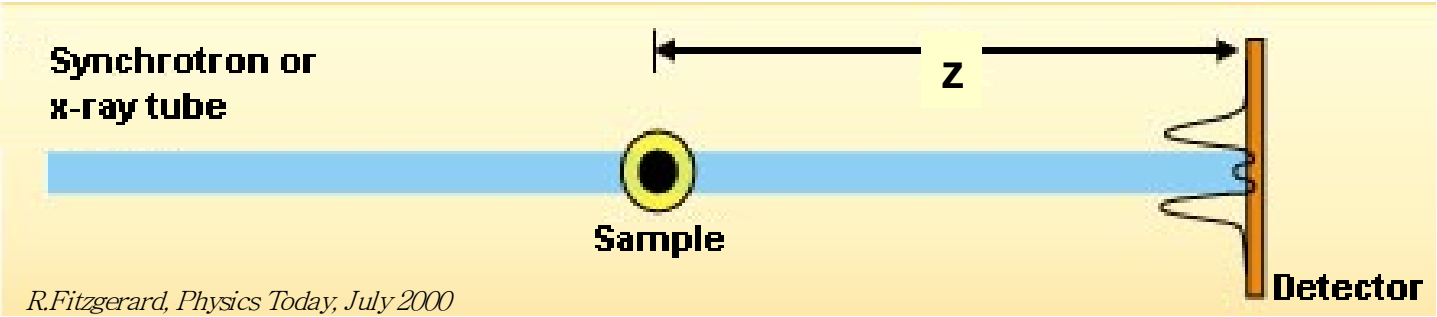

- The technique exploits the high spatial coherence of the X-ray source.
- z =0 -> absorption image
- For z > 0 -> interference between diffracted and un-diffracted wave produces edge and contrast enhancement. A variation of δ is detected
- Measure of $\nabla^2\Phi(x,y)$
- The technique requires a high spatial coherence source, monochromaticity is not needed

Regimes

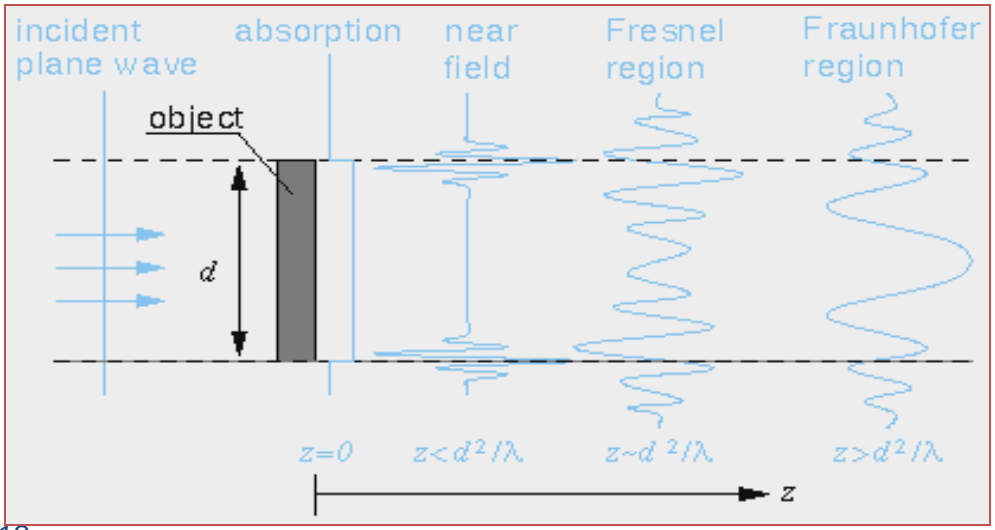

Snigirev A. et al., Rev. Sci. Instrum. 66, 1995
Wilkins S. W. et al., Nature 384, 1996
Cloetens P. et al., J. Phys D: Appl. Phys. 29, 1996
Arfelli F et al., Phys. Med. Biol. 43,1998

Analyzer Based Imaging (ABI)

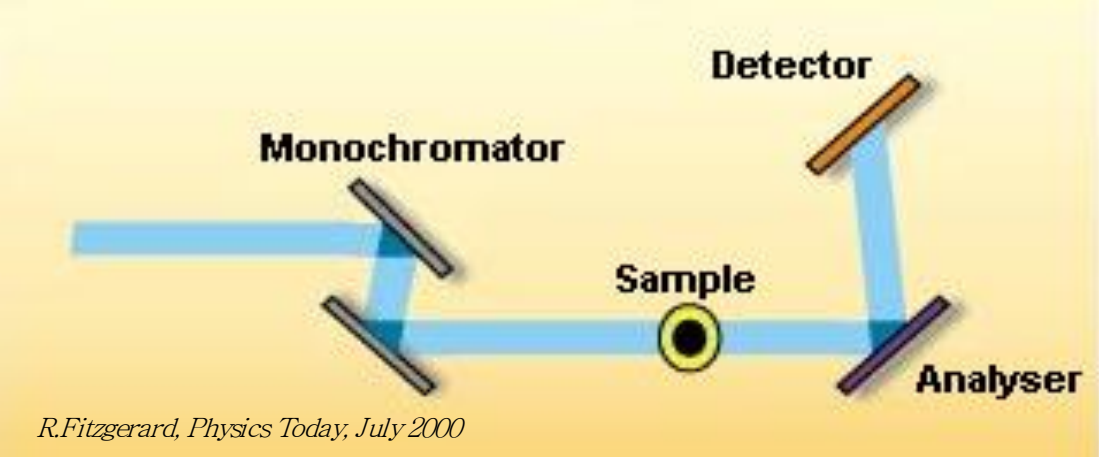

- A perfect crystal is used as an angular filter to select angular emission of X-rays. The filtering function is the rocking curve (FWHM: 1-20 μrad)
- Image formation with ABI is sensitive to a variation of δ in the sample. Indeed, **refraction angle is roughly proportional to the gradient of δ**
- Analyzer and monochromator aligned -> X-ray scattered by more than some tens μrad are rejected
- Small misalignments -> investigation of phase shift effects
- With greater misalignments the primary beam is almost totally rejected and pure refraction images are obtained
- Sensitive to $\nabla\Phi(x,y)$
- The technique requires the beam monochromaticity.

Podurets K. M. et al., Sov. Phys. Tech. Phys. 34(6), 1989
V. N. Ingal and E. A. Beliaevskaya, J. Phys. D: Appl. Phys. 28, 1995
Chapman D et al., Phys. Med. Biol. 42, 1997

ABI image manipulation (original algorithm)

I_L

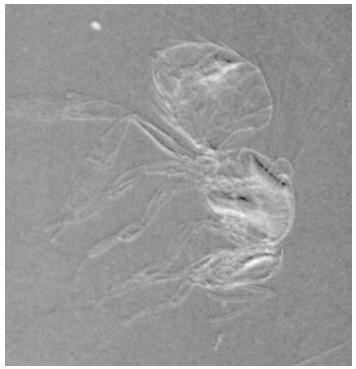

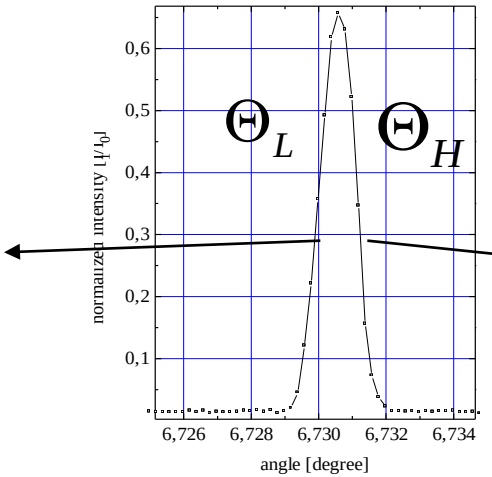

I_H

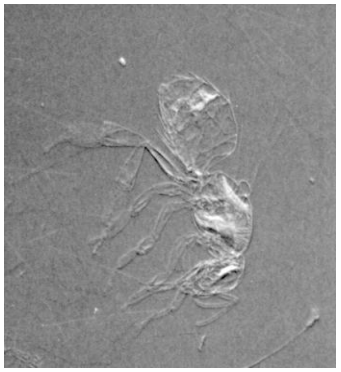

Linear approximation of rocking curve at half values (I_R and I_L)

$$I_L = I_R\left(R(\Theta_L) + \frac{\partial R}{\partial \Theta}(\Theta_L)\Delta\Theta_z\right)$$

$$I_H = I_R\left(R(\Theta_H) + \frac{\partial R}{\partial \Theta}(\Theta_H)\Delta\Theta_z\right)$$

Θ_Z = refraction Image

I_R = apparent absorption image (absorption+extinction)

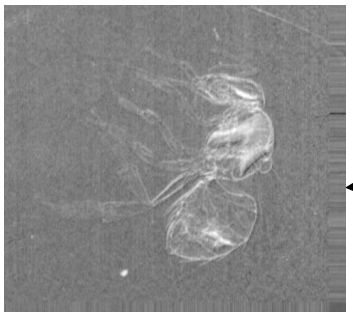

Apparent Absorption Image

$$I_R = \frac{I_L \cdot \left.\frac{dR}{d\Theta}\right|_{\Theta_H} - I_H \cdot \left.\frac{dR}{d\Theta}\right|_{\Theta_L}}{R(\Theta_L)\cdot \left.\frac{dR}{d\Theta}\right|_{\Theta_H} - R(\Theta_H)\cdot \left.\frac{dR}{d\Theta}\right|_{\Theta_L}}$$

$$\Theta_Z = \frac{I_H \cdot R(\Theta_L) - I_L \cdot R(\Theta_H)}{I_L \cdot \left.\frac{dR}{d\Theta}\right|_{\Theta_H} - I_H \cdot \left.\frac{dR}{d\Theta}\right|_{\Theta_L}}$$

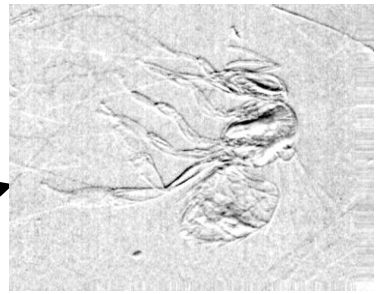

Refraction Image

Ref: Chapman et al, Phys.Med.Biol, 42,1997

Limitations and Requirements

PBI

- It is the simplest method as it requires the detector to be set at a certain distance from the sample. It does not require monochromaticity.
- Requirements:
  - a high spatial coherence of the beam
  - adequate spatial resolution of the detector to detect interference fringes (edge-enhancement)
- Exposure time related to beam intensity
- The recorded signal is proportional to the second derivative of the phase term ($\nabla^2\Phi(x,y)$)
- Adequate to study samples with important variations of refractive index

ABI

- It requires the implementation and control of at least one crystal
- Requirements:
  - high monochromaticity
  - parallel beam
- Sensitive to beam instabilities
- The recorded signal is proportional to the first derivative of the phase term ($\nabla\Phi(x,y)$)
- Adequate to study cartilages, joints, samples with wide variation of refractive intex

Elettra Sincrotrone Trieste

Interferometry: from phase shift to image contrast

- Interferometry is a family of techniques in which waves are superimposed in order to extract information.
  - Widely used in optics (visible light)
  - It can be used in X-ray phase contrast imaging to transform the phase shift introduced by the object into image contrast
- Two different interferometric approaches:
  - **Crystal interferometry** (Bonse and Hart, 1965)
  - **Grating interferometry** (David et al, 2002; Momose et al., 2003)

Bonse, U. and Hart, M. (1965). Appl. Phys. Lett. ***6****, 155–156.*
David, C., Nöhammer, B. et al. (2002). Appl. Phys. Lett. 81, 3287–3289
Momose, A. et al. (2003). Japan J. Appl. Phys.: 2 Lett. 42, L866– L868

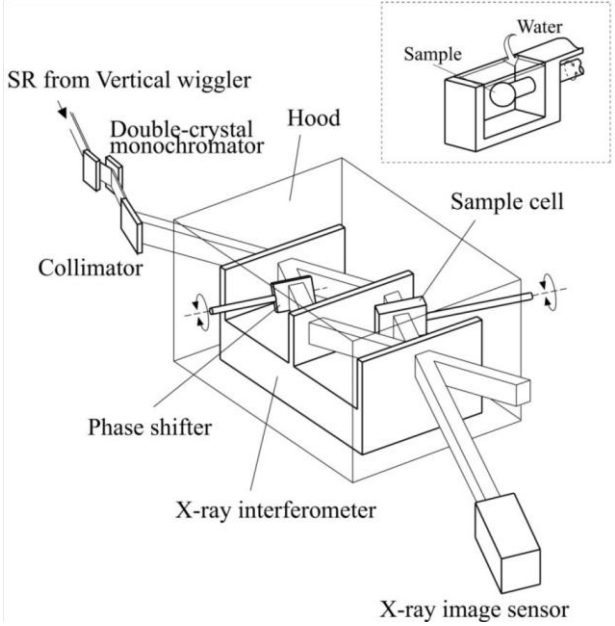

X-ray interferometry with crystals

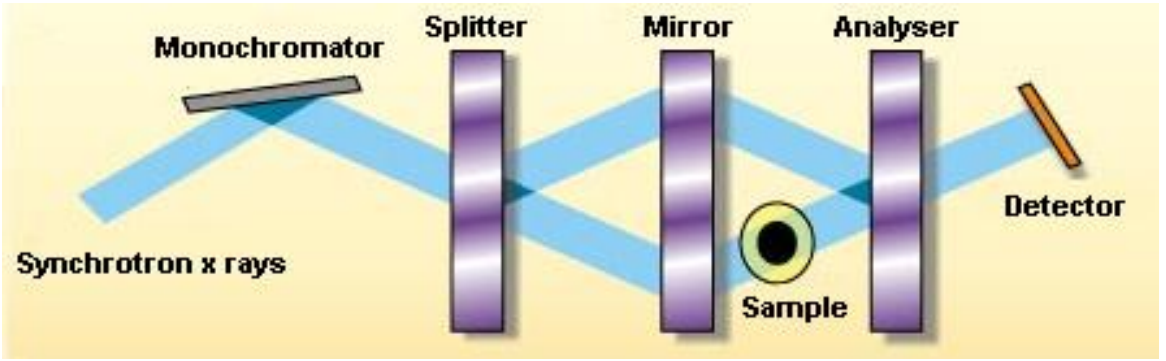

- The method has been pioneered by U.Bonse and M.Hart. A.Momose, T.Takeda et al. have refined the technique for medical applications.
- the I crystal splits the monochromatic beam into two beams with the same phase, the II crystal acts as a mirror, the III crystal recombines the two beams
- A phase shift on the probe beam is produced by the presence of the sample
- The beams re-combinated at the analyzer position generate an interference pattern registered by the detector
- Direct access to $\Phi(x,y)$
- Using monolithic Si crystal the limitation of the technique concerns the maximum size of samples to be studied. Interferometers based on double crystal systems are very sensitive to vibrations and require very accurate alignment systems: this limit their applications for imaging purposes.

Refs.: U.Bonse, M.Hart, Appl.Phys.Lett. 6,1965; A.Momose et al:, NIMA 352, 1995, A.Momose et al.: Opt. Express 11 2003, A. Momose et al., Japan J. Appl. Phys. 44, 2005

Grating interferometric imaging (GI)

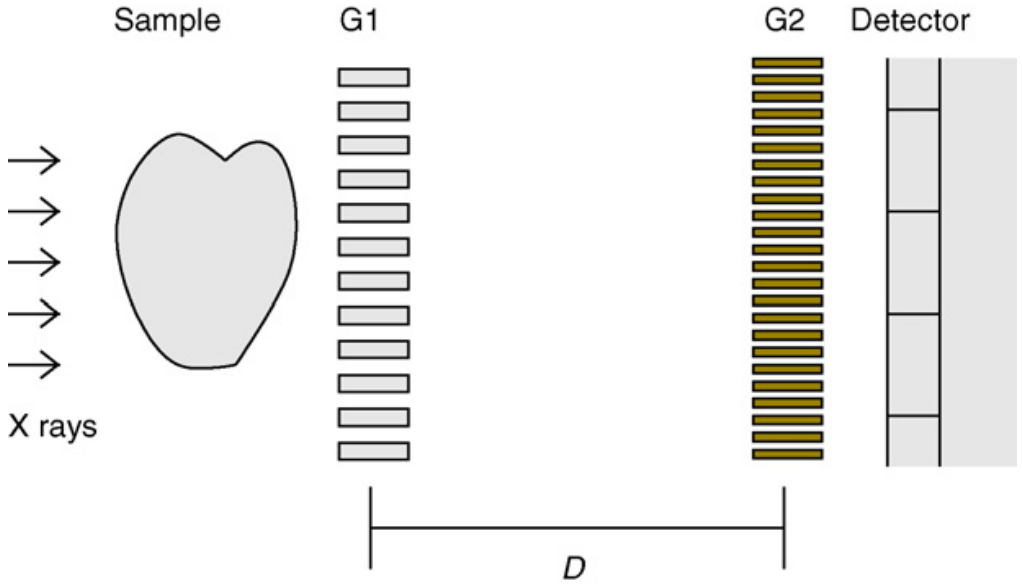

Based on an optical phenomenon discovered by Talbot (1936) and explained by Rayleigh (1881).

With a coherent radiation, the image of the grating is repeated at regular distances behind the grating, $D = 2d^2/\lambda$ (d=grating period, λ=wavelength).

The beam is split and analyzed by means of two gratings, introduced between the object and the detector:

The X-ray wavefront transmitted by the sample go through a **linear diffraction grating G1** (*beam splitter*). Downstream G1, a pattern of interference fringes is formed. The local distortions of the fringe pattern from its ideal regular shape contain information on the sample structure.

Since the fringes are too closely spaced to be resolved by the pixel detector, **an additional absorption grid** (**G2**, called *analyzer*) in front of the detector is needed to transform fringe-position information into intensity values on the detector.

A modified set-up can be applied to polychromatic spectrum from an X-ray tube.

T. J. Davis et al., Phys. Rev. Lett. 74, (1995), A.Momose et al.: Opt. Express 11, 2003, Weitkamp, T., et al., Opt. Express, 13(16), 2005, Weitkamp T et al, Eur. J. Radiol. 68, 2008

Note: Talbot effect

Talbot interferometry is based on the Talbot effect (1836), which is known as a self-imaging effect observed downstream a grating (object with a periodic structure), under coherent illumination.

The distances z_T between the object and self-imaging planes are determined by the light wavelength λ and the period d of the structure

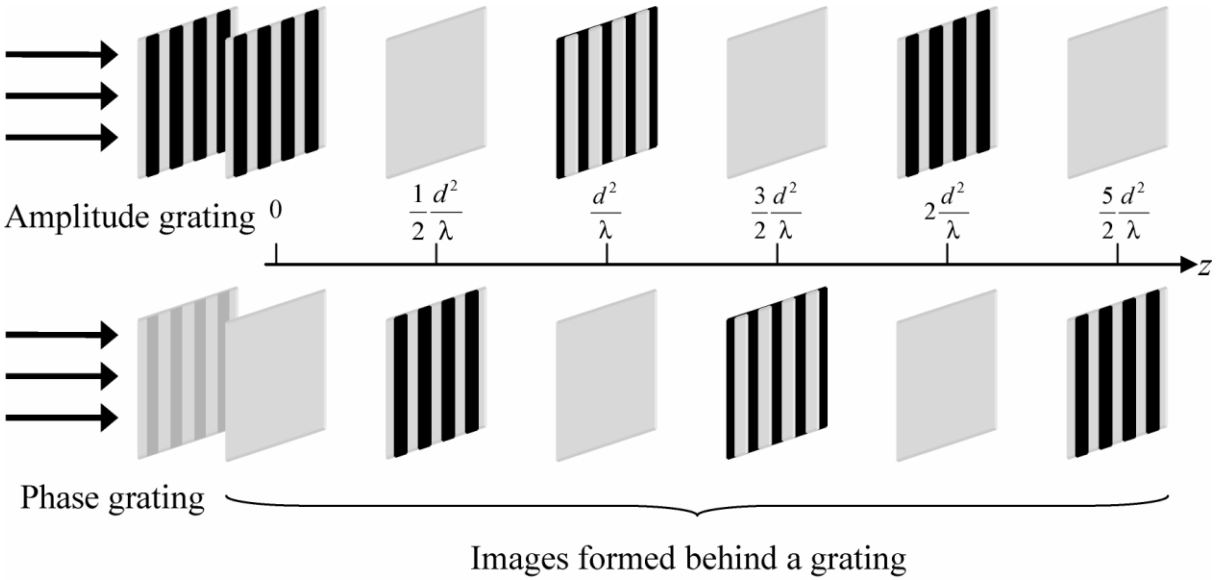

Talbot effect in the case of plane-wave illumination. For **an amplitude grating**, self-images are generated at $z_T = 0$, d^2/λ, $2d^2/\lambda$, and so on. (d is the period of the grating, λ is the wavelength). For a **phase grating**, similar patterns are observed at intermediate positions.

Grating Interferometry- Limitations

Demanding mechanical requirements (precision ~ 20-30 nm)

- Field of view must be increased to clinical size
- At the moment 5 cm x 5 cm

Limited exploitation of X-ray output

- 20% - 30% due to source grating
- grating silicon substrates (~ 300 μm)

Long exposure time and high delivered dose

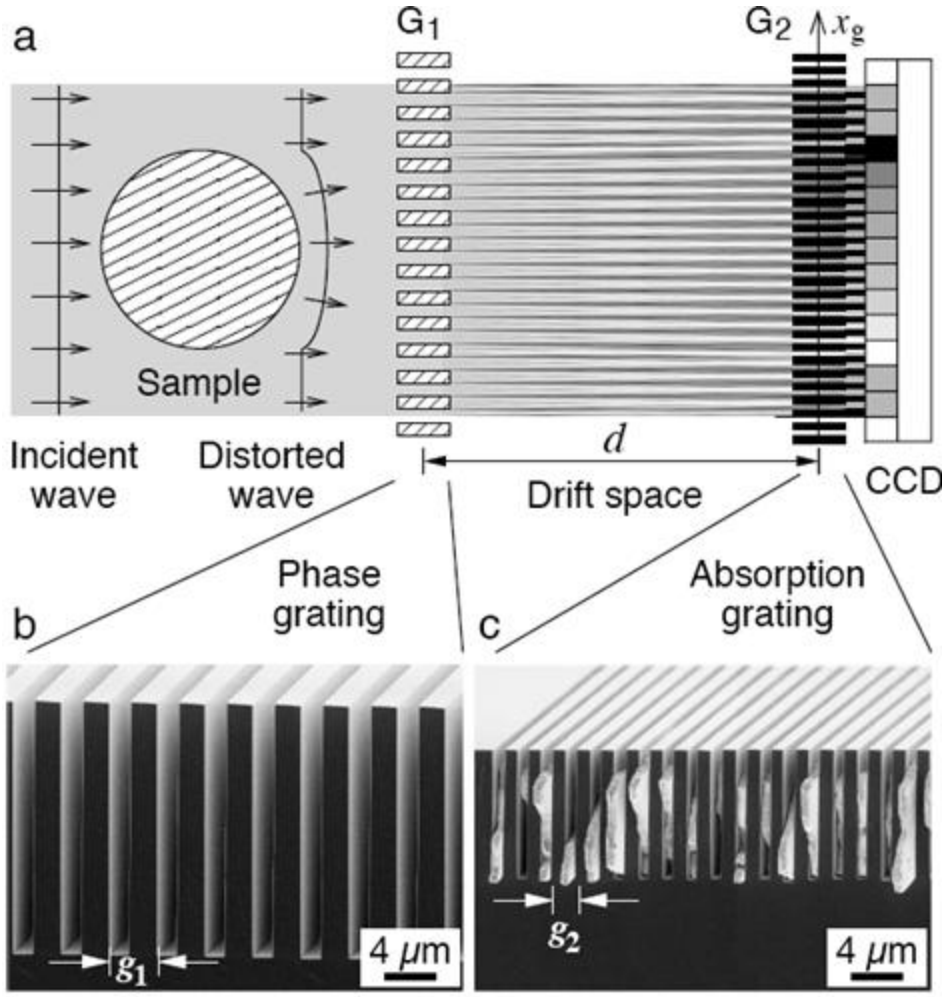

Grating non-interferometric imaging - Edge Illumination method: principles

Like ABI, Edge Illumination (EI) is based on the detection of the refraction angles suffered by photons when crossing the object. Simplified setup is used in synchrotron.

A **first slit** placed before the sample (***pre-sample slit***) collimates the beam (aperture some micrometers, depending on the image resolution). In front of the detector, there is then a second slit, (***detector slit***), aligned with one pixel's row of the detector.

The two slits have a small misalignment, so the beam exiting from the first slit, reaches the edge of the detector slit, i.e. the beam is partially stopped by the second slit (partial illumination condition).

The sample produces beam refraction, thus the portion of the beam reaching the detector is shifted by:

$\Delta y = z \tan(\Delta\theta_y)$, (z = sample-det. distance, $\Delta\theta_y$ is the component of the refraction angle in the vert direction).

For small refraction angles, $\Delta y \approx z\, \Delta\theta_y$, the displacement is typically less than few micrometers for z ~ 1m.

When beam is shifted **towards the aperture** -> detector counts **increase**,
When beam is shifted **towards the slit** -> detector counts **decrease**

This allows to translate **the refraction angle** caused by the object, into a **modulation of the intensity** on the detector.

The whole image of the sample is obtained scanning the sample, step by step, in the direction orthogonal to the slits and then pasting together all the single lines.

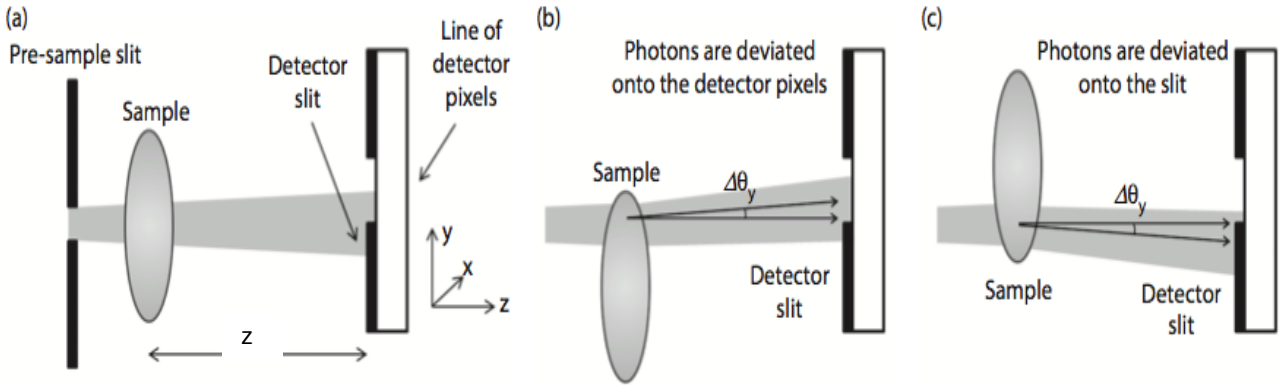

Edge Illumination method - Implementation

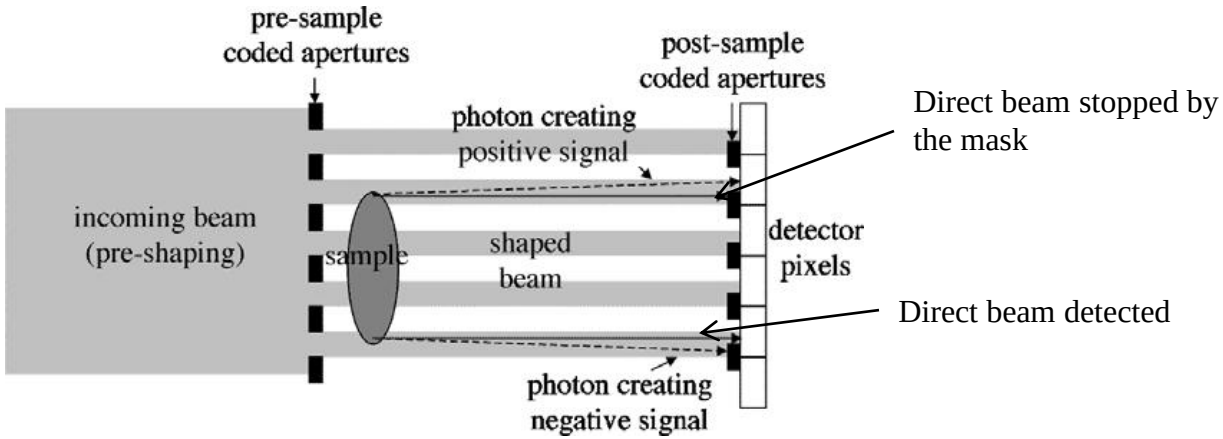

- ✓ the detector is divided by a mask (‘detector mask’) into a pattern of sensitive and insensitive regions between adjacent pixels, and a pre-sample mask creates the same pattern of beams that impinges on the boundaries of sensitive and insensitive regions.
- ✓ The beams are deviated by refraction in the sample, resulting in intensity variation at the detector.
- ✓ The pre-sample coded-aperture system (‘sample mask’) is placed immediately before the sample, and it creates an array of individual beams each one impinging on the edge of the detector pixels, as defined by the detector mask.
- ✓ the pre-sample mask prevents unnecessary radiation from transversing the sample, thus ensuring efficient dose delivery.
- ✓ It can be applied to polychromatic radiation from an x-ray tube

Olivo A et al., Med. Phys. ***28****, 2001, Olivo A and Speller R, Appl. Phys. Lett. 91, 2007*

SYRMEP layout for PHC imaging

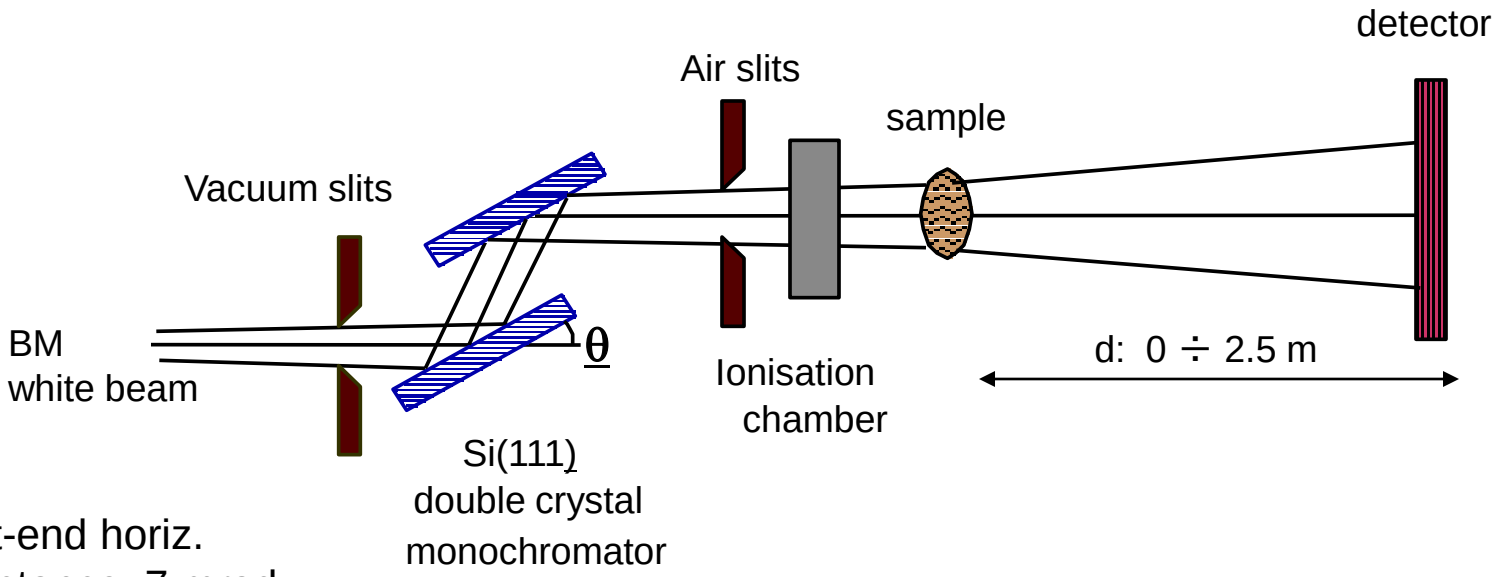

Front-end horiz.
acceptance: 7 mrad

ABI setup

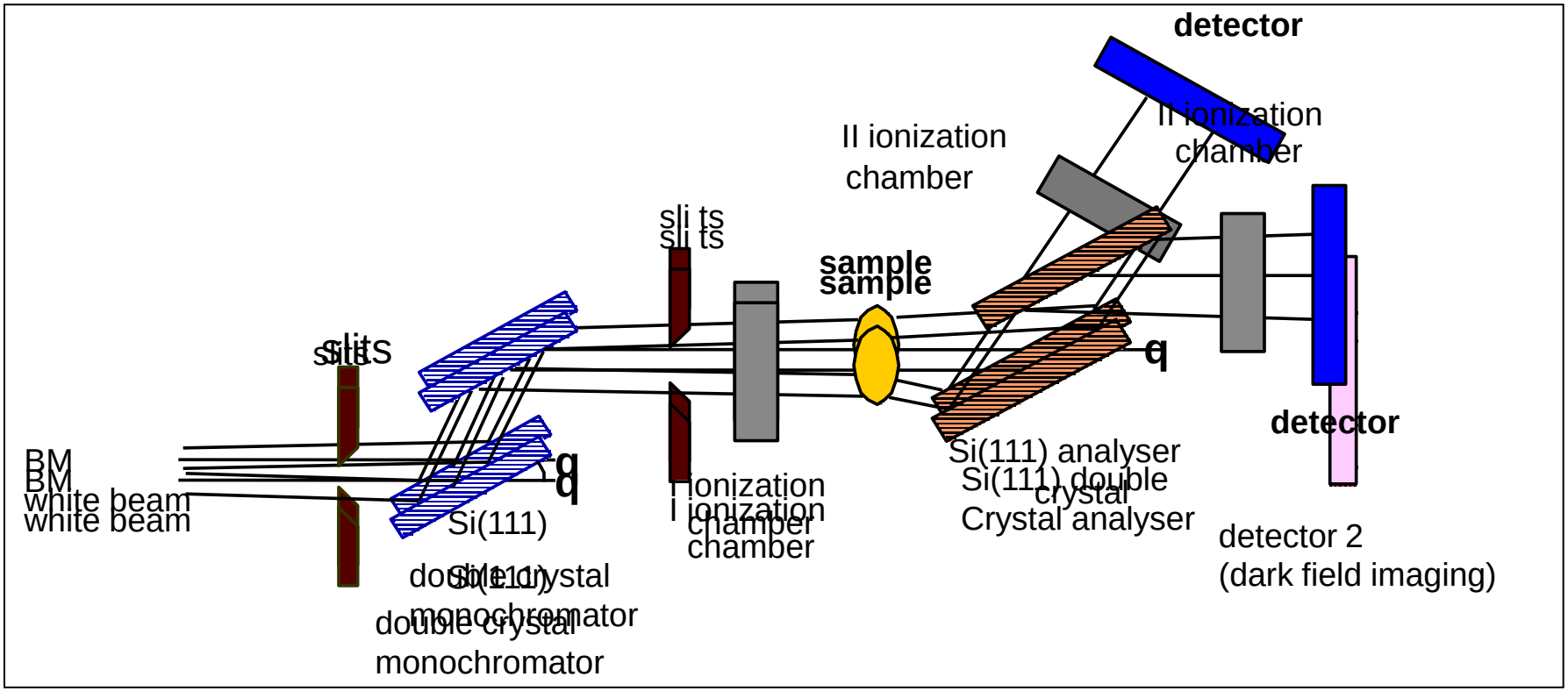
detector
II ionization chamber
II ionization chamber
sli ts
sli ts
sample
sample
slits
slits
q
q
BM
BM
white beam
white beam
Si(111)
double crystal
monochromator
Si(111)
double crystal
monochromator
I ionization chamber
I ionization chamber
Si(111) analyser
Si(111) double crystal
Crystal analyser
detector
detector 2
(dark field imaging)

ABI images for different analyzer positions

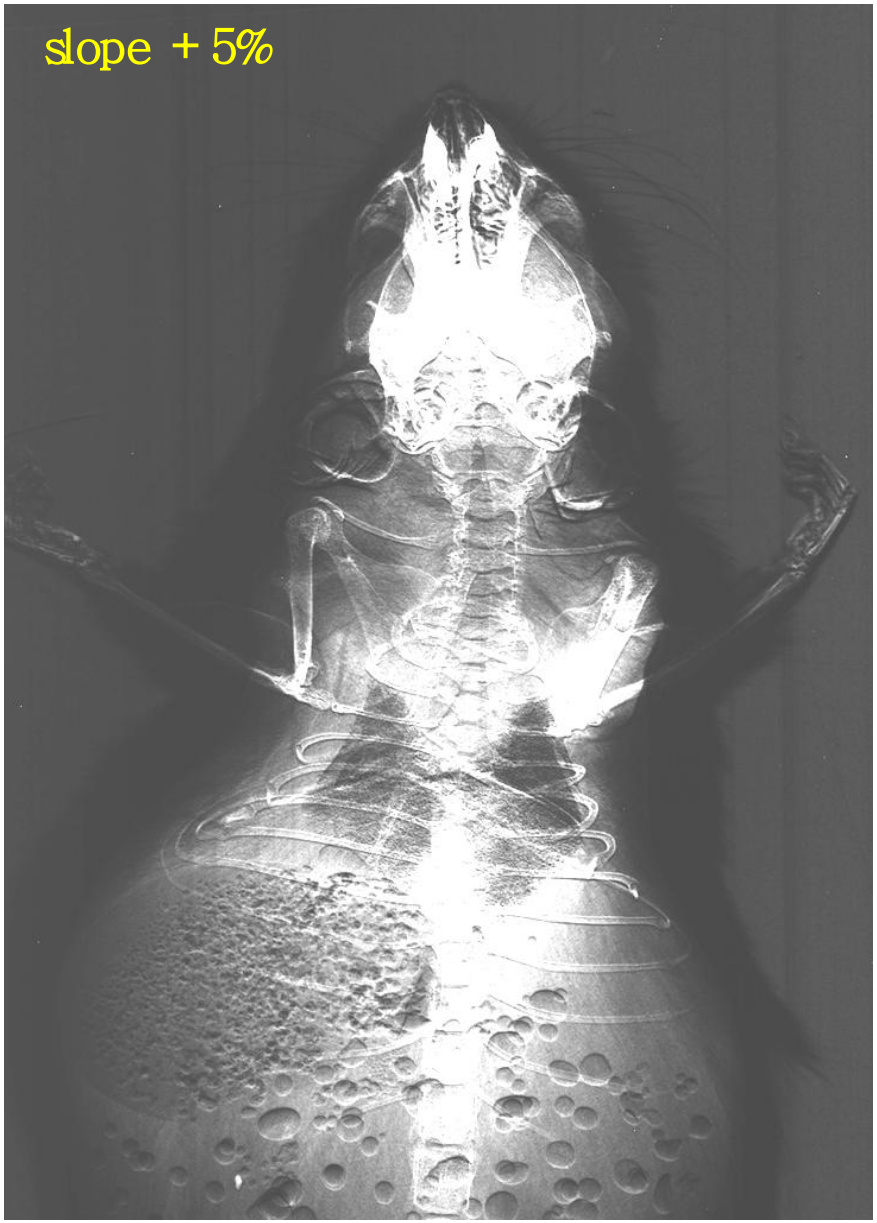

Images obtained from application of the algorithm

Apparent absorption

Refraction image

Elettra
Sincrotrone
Trieste

Application of
K-edge absorption imaging:

Bronchography (pre-clinical – animal model)

Bronchography - CT imaging at ESRF

Dual Line Ge Detector
w: 150 mm, 350 mm pitch, beam thickness 700 mm

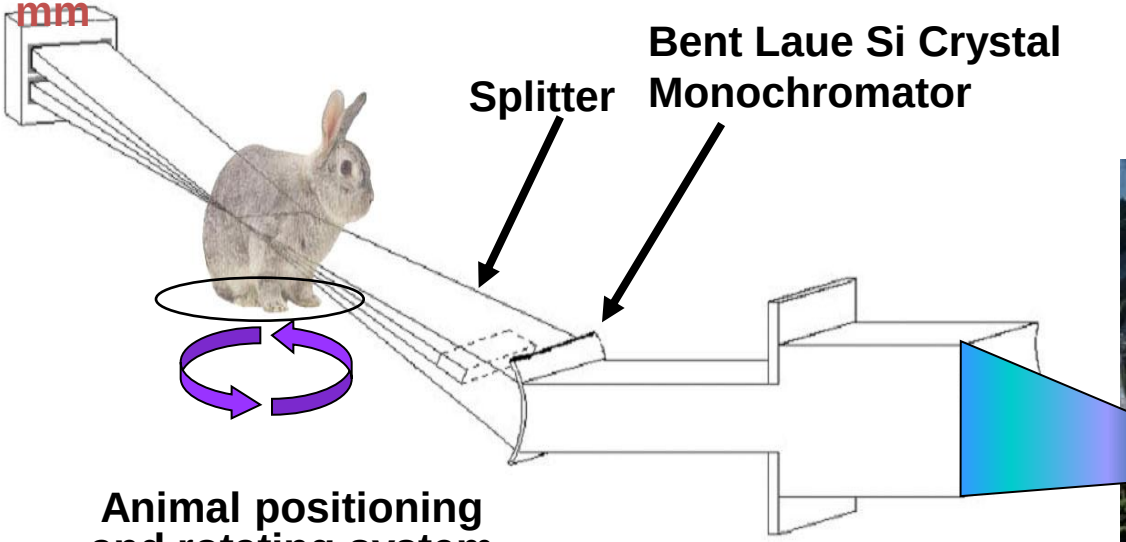

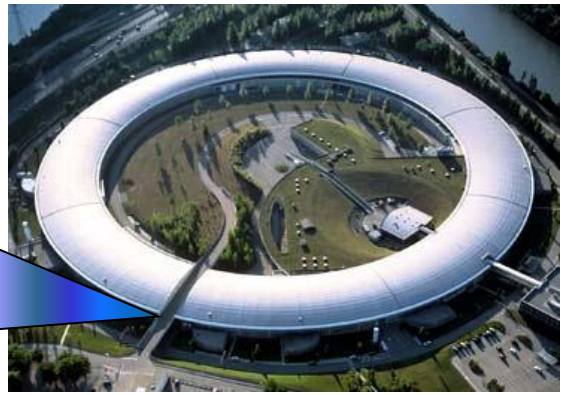

System Control

Image Processing

Courtesy of A.Bravin (ESRF)

K-edge Subtraction - Lung Tomography: use of Xenon

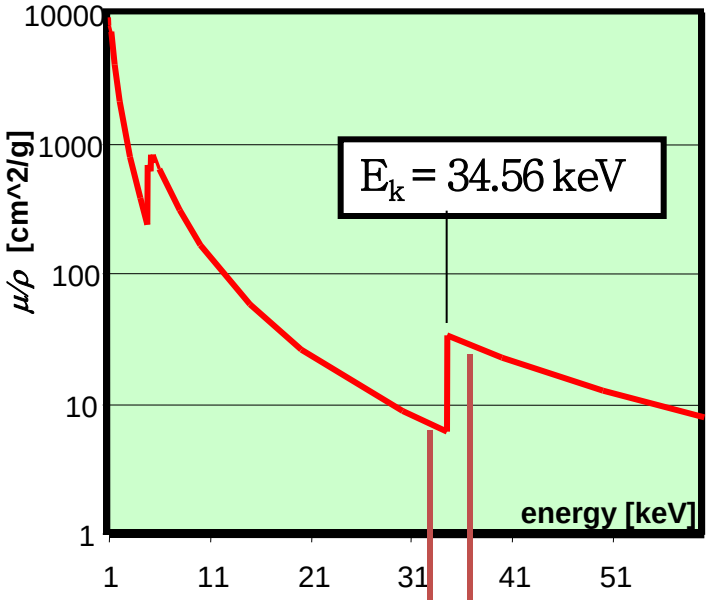

$E < E_k$

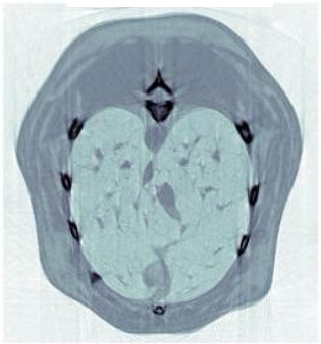

$E > E_k$

$$(\rho t)_I = \frac{\ln(\frac{I}{I_0})^+ - \ln(\frac{I}{I_0})^-}{(\frac{\mu}{\rho})_I^+ - (\frac{\mu}{\rho})_I^-}$$

Subtraction

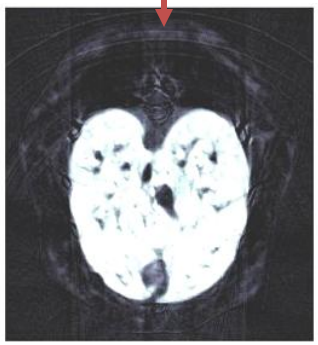

Courtesy of A.Bravin (ESRF)

Imaging Sequence

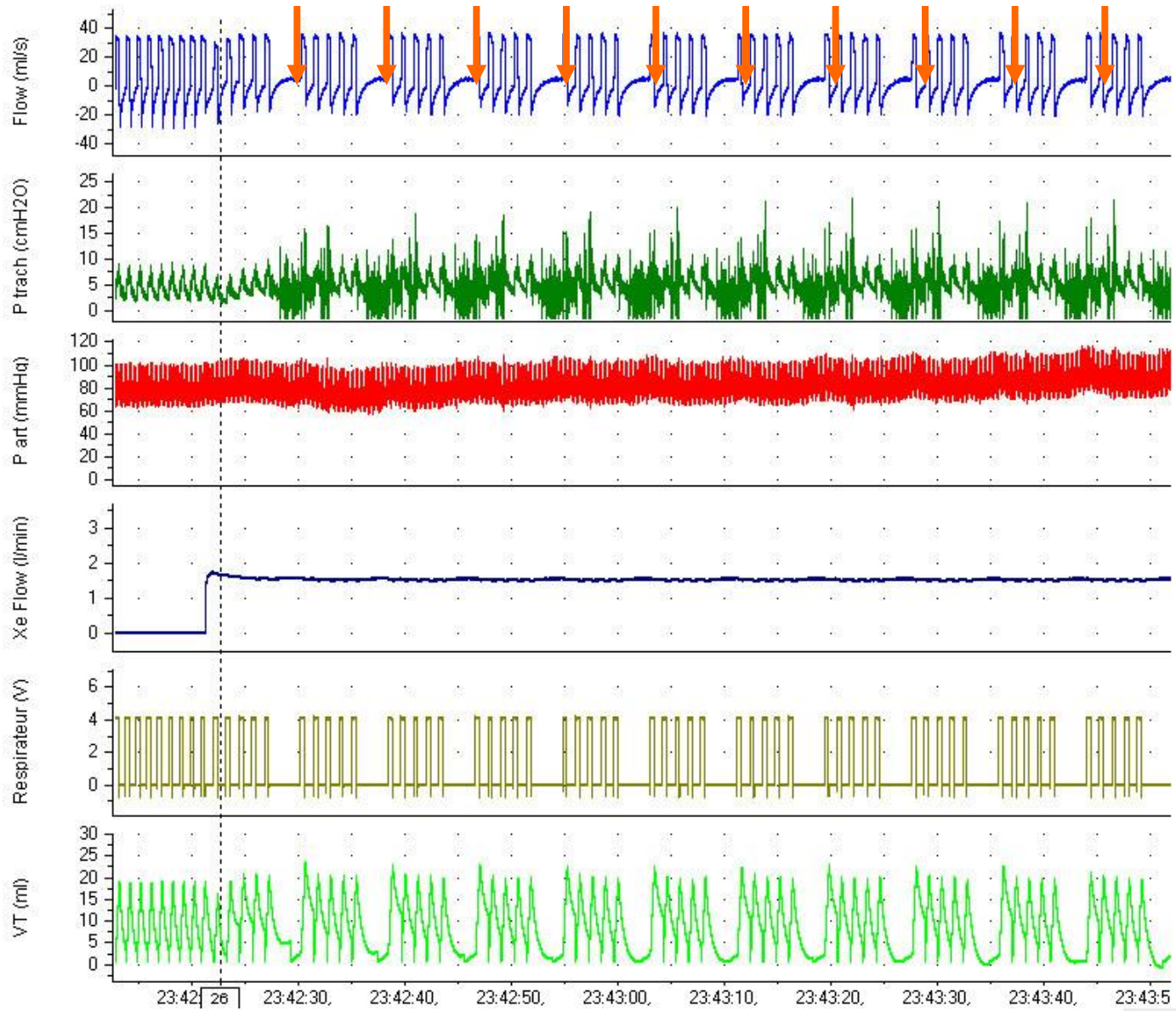

Elettra Sincrotrone Trieste

ESRF The European Synchrotron

Projection Images
In Vivo Rabbit Lung
Xenon K-edge Imaging

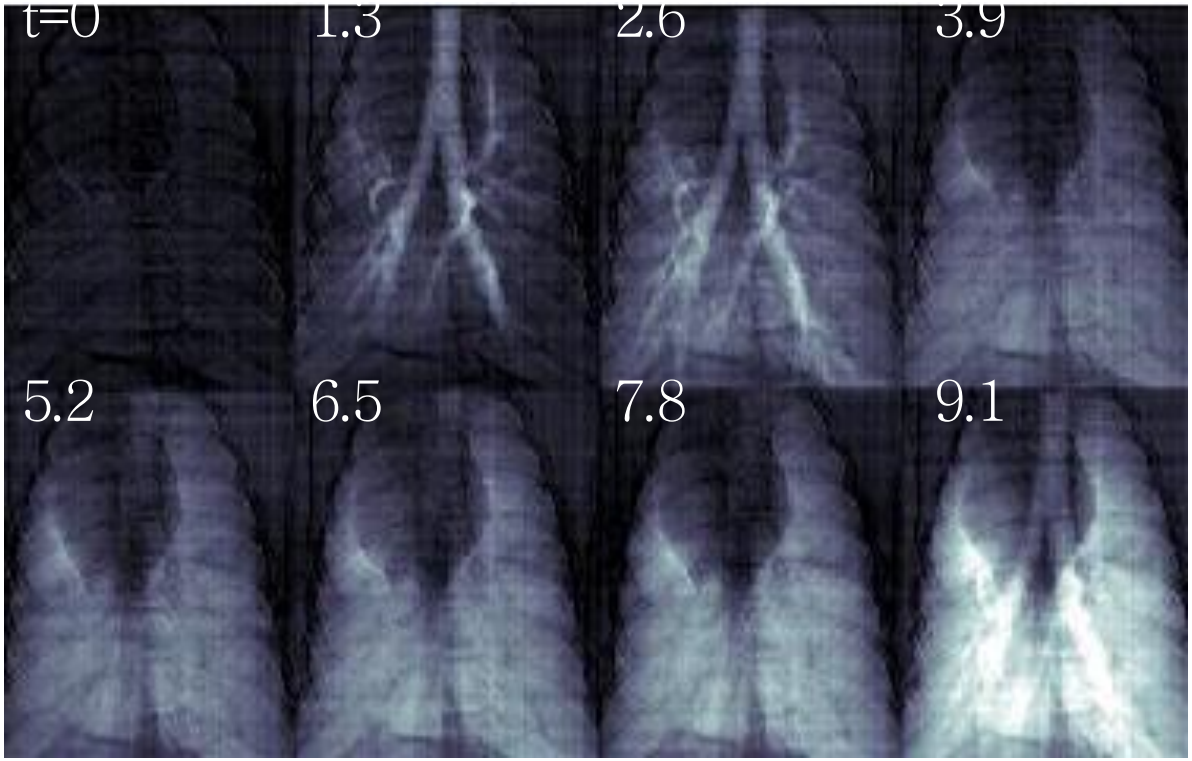

Time between images = 1.3 sec

Courtesy of A.Bravin (ESRF)

Effects on lungs ventilation induced by different treatments on healthy or asthmatic animals

Experimental asthma studies have been carried out to study allergic reactions by using **ovalbumine-sensitized rabbit model**. These allergic reactions were compared with asthma reactions caused by non-specific drug provocation (Methacholine, Mch). Mch caused **airway narrowing** mainly on the central large airways, while ovalbumine induces **a predominantly peripheral and heterogeneous lung response**.

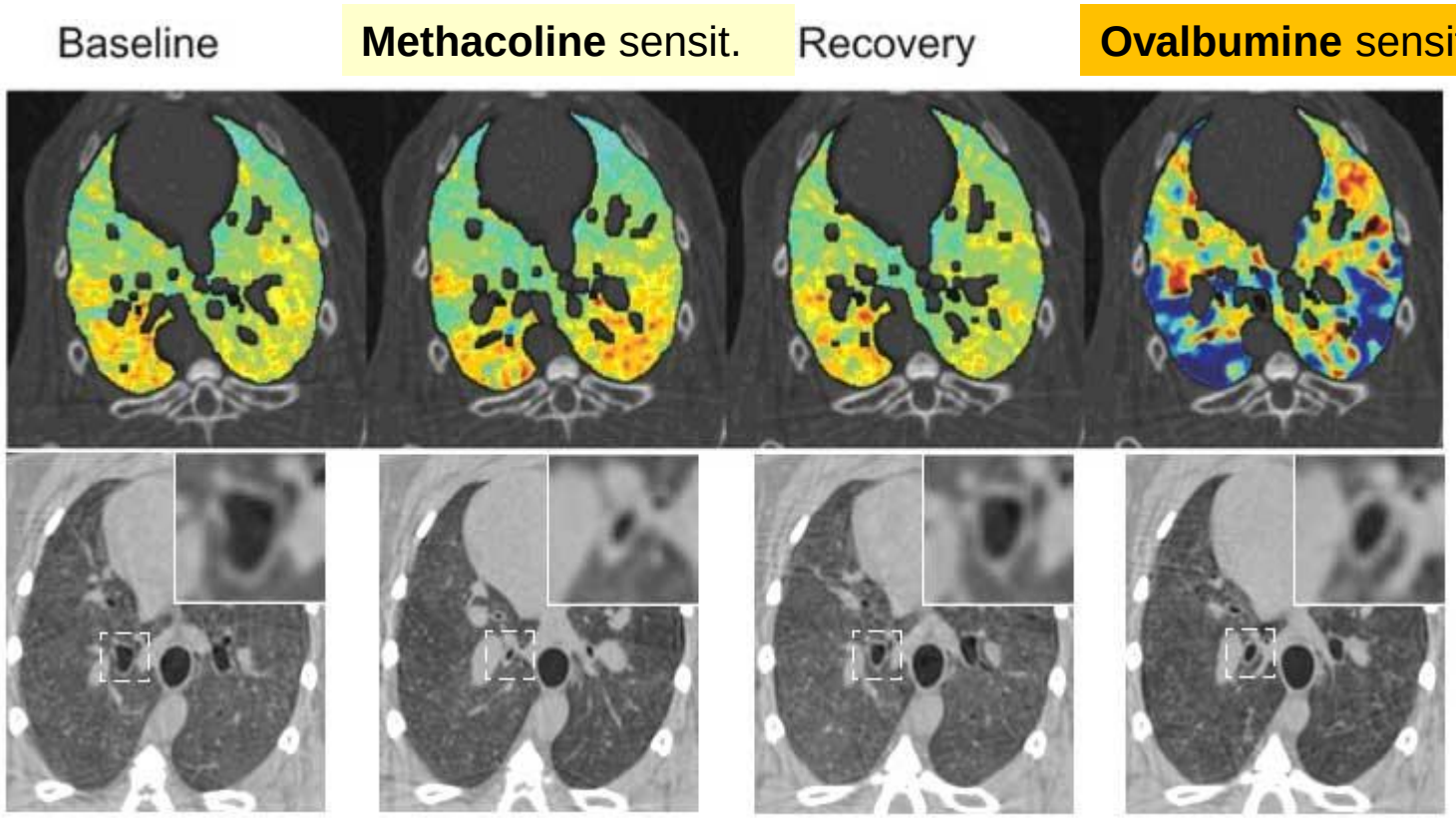

Upper part: **images of specific ventilation** in a sensitized rabbit at baseline, during Mch infusion, upon recovery and after Ovalbumine allergen provocation. Lower part: **absorption CT slices** showing changes in the central airway cross-sectional area at the different experimental stages in one representative animal. Magnifications of the indicated square areas are shown in the right-upper corners.

Bayat S. et al:, Am J Respir Crit Care Med. Aug 15;180(4):296-303 (2009).

Breast imaging – first protocol with patients at Elettra

Agreement among the Public Hospital of Trieste, the University of Trieste and Elettra

Aim: Explore the potential of phase contrast imaging on selected cases

Target: Patients whose conventional diagnosis gave uncertain results.

Modality:

I) PHC radiography with film systems

II) PHC imaging with digital detectors

Projection imaging
X-ray energy: 17– 22 keV

III) Tomo-mammography (X-ray energy > 30 keV)

Outcomes from the first protocol (I, II)

SR exams have:
- higher specificity,
- better agreement with the golden standard (biopsy),
- improved image quality,
- strong reduction of delivered doses.

Elettra Sincrotrone Trieste

Clinical Mammography

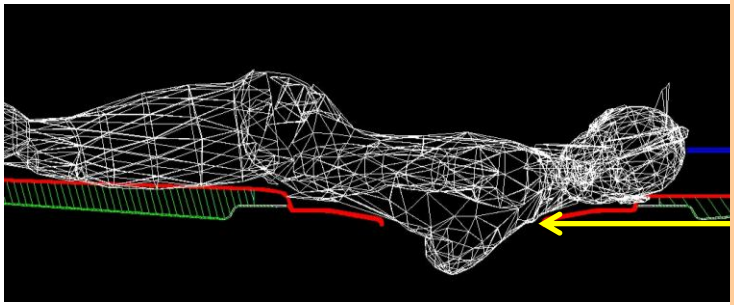

Outcomes of first protocol

Images with SR have:

- *higher specificity,*
- *better agreement with the golden standard (biopsy),*
- *improved image quality,*
- *strong reduction of X-ray doses.*

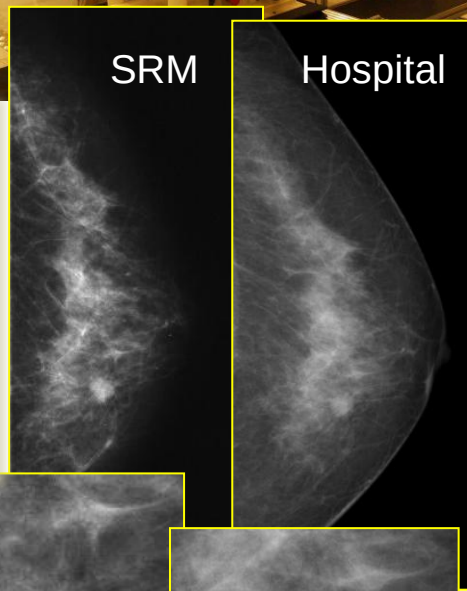

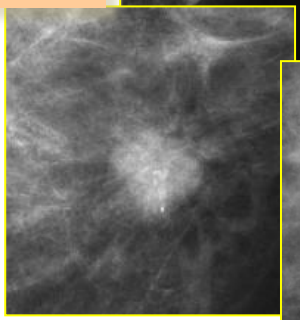

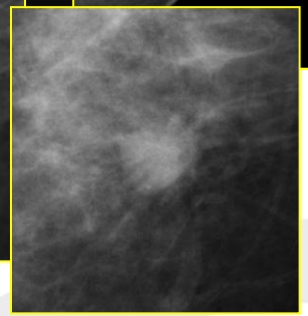

Next step: Low dose phase contrast breast CT

PiXirad Chromatic Photon Counting

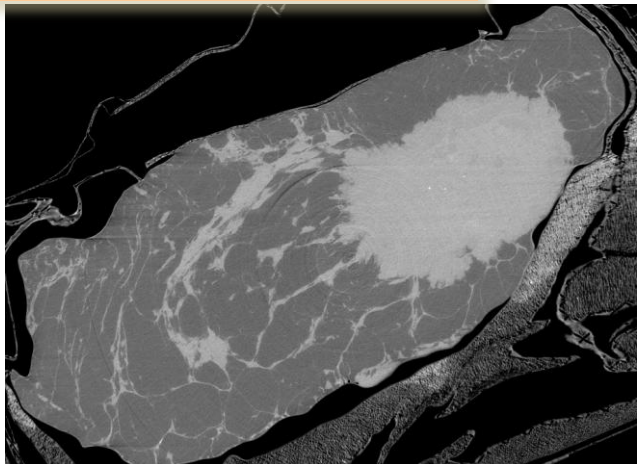

CSIRO THE UNIVERSITY OF MELBOURNE UNIVERSITÄTSMEDIZIN GÖTTINGEN UMG

Computed μ-Tomography (μCT)

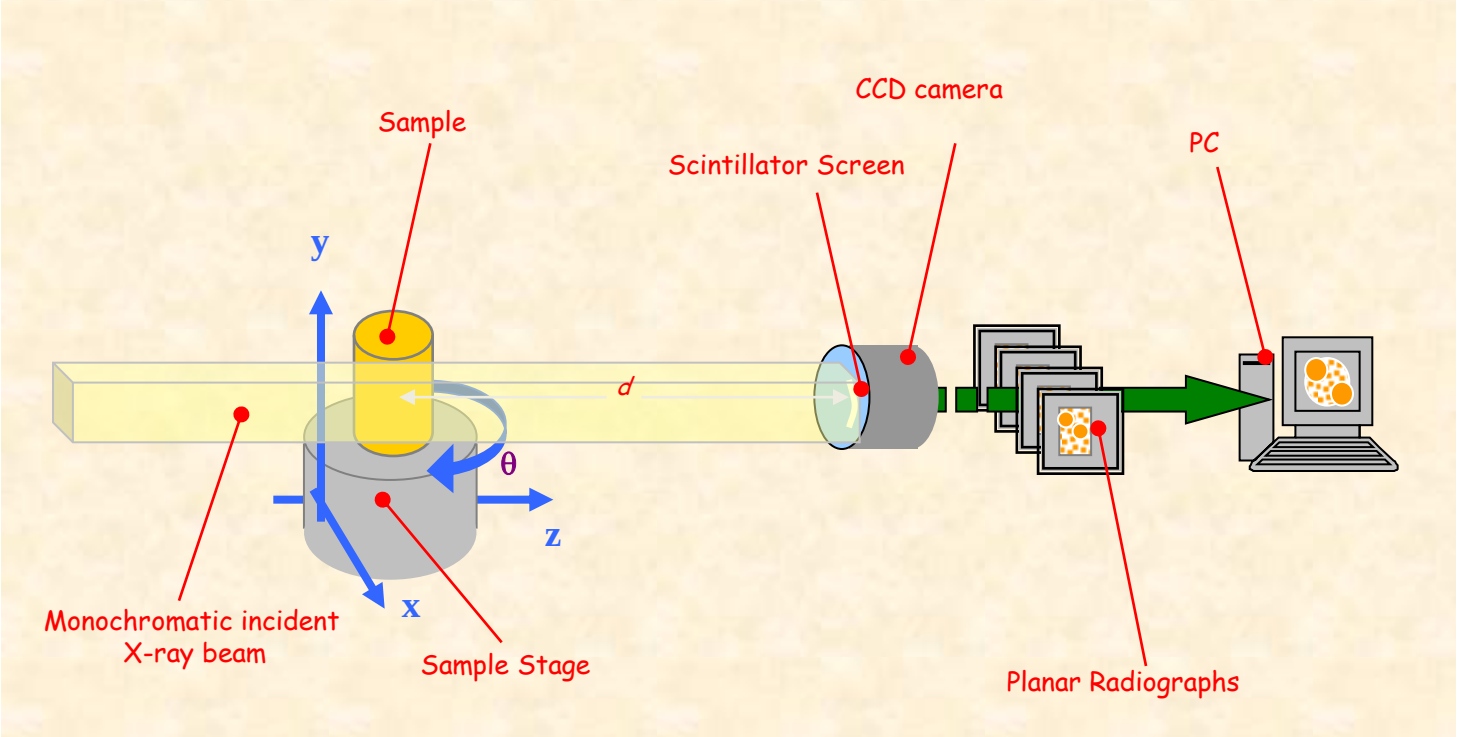

- *not destructive tool* to study the ***internal structure*** of any kind of sample
- no sample preparation
- it gives access to quantitative information on the *density maps* of the irradiated volumes
- suited for *in vivo* imaging of small animals

Potentials of ABI

Pre-clinical studies:

- Studies of cartilages and bones interfaces

ABI studies of Cartilage and bone interface

Osteoarthrosis (OA) is a disease characterized by the progressive degeneration of articular cartilage and the development of altered joint congruency. It has a high incidence in the adult population. Affecting mainly the elderly population, it is one of the main causes of disability worldwide. Conventional radiography detects only **important osseous changes**, at advanced OA or RA stages, when therapeutic strategies are less effective. **Early changes** in the **cartilage** and other **articular tissues** are **not** directly visible. MRI imaging works better but the maximum achievable spatial resolution is not always adequate.

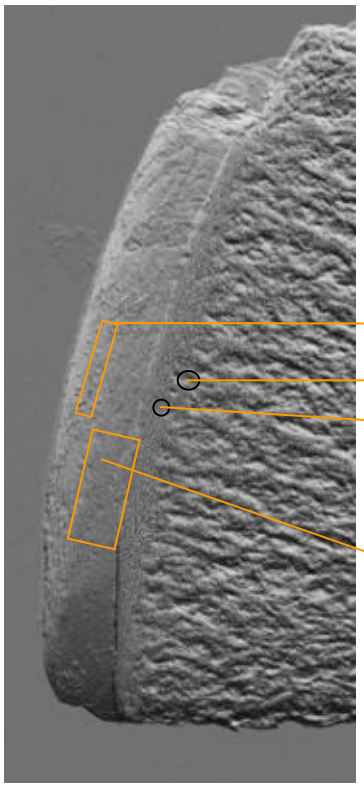

Need to study:
- cartilage
- cartilage-bone interfaces
- changes in the bone structure

Superficial Layer (Zone of horizontal collagen fibers with flat cells)

Subchondral Bone Plate (**Important for diagnostic purposes in OA**)

Tidemark (Border between normal and mineralized cartilage)

Transitional and Deep Layer (round cells, collagen fiber switches from horizontal to vertical orientation, increasing stiffness and material density)

Aim: detect the architectural arrangement of collagen within cartilage and evaluate how the cartilage degeneration affects the underlying subchondral and trabecular bone.

Femur head core cuts: collagen arcades structure

- The ABI technique allows to visualize the discontinuities in the sample and the inner structures invisibles by means of conventional X-Ray imaging.
- The transition bone-cartilage is emphasized.
- The articular cartilage striations are well visible due to X-ray diffraction at edges of fibers

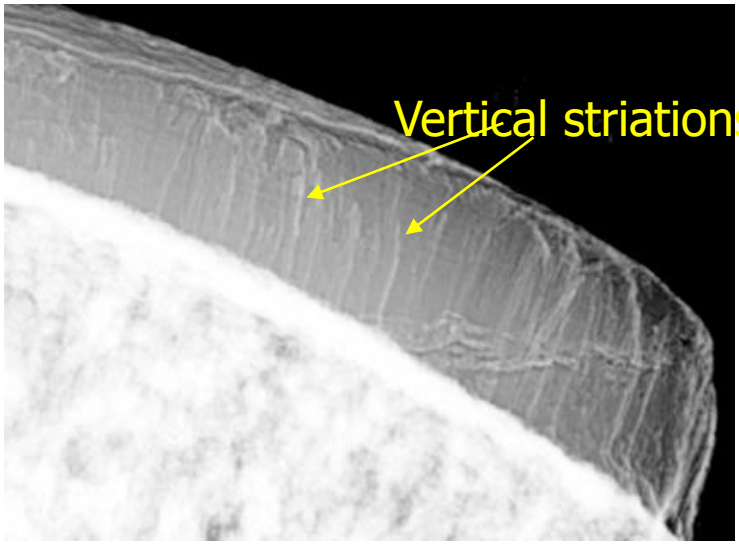

Apparent absorption image

Refraction image

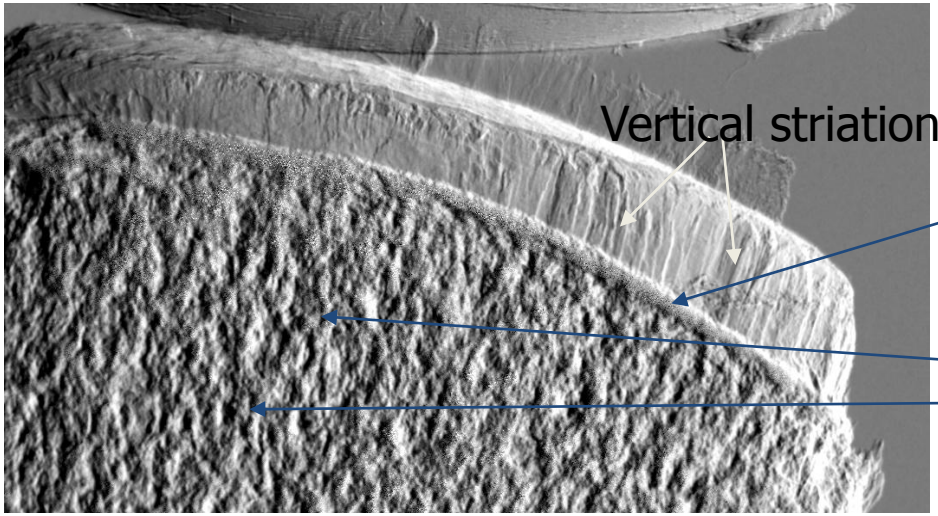

Elettra
25 keV

Muehleman C, Majumdar S, Issever AS, Arfelli F, Menk RH, Rigon L, Heitner G, Reime B, Metge J, Wagner A, Kuettner KE, Mollenhauer J, Osteoarthritis and Cartilage 12 (2): 97-105 FEB 2004

Femur head core cuts: comparison with MRI

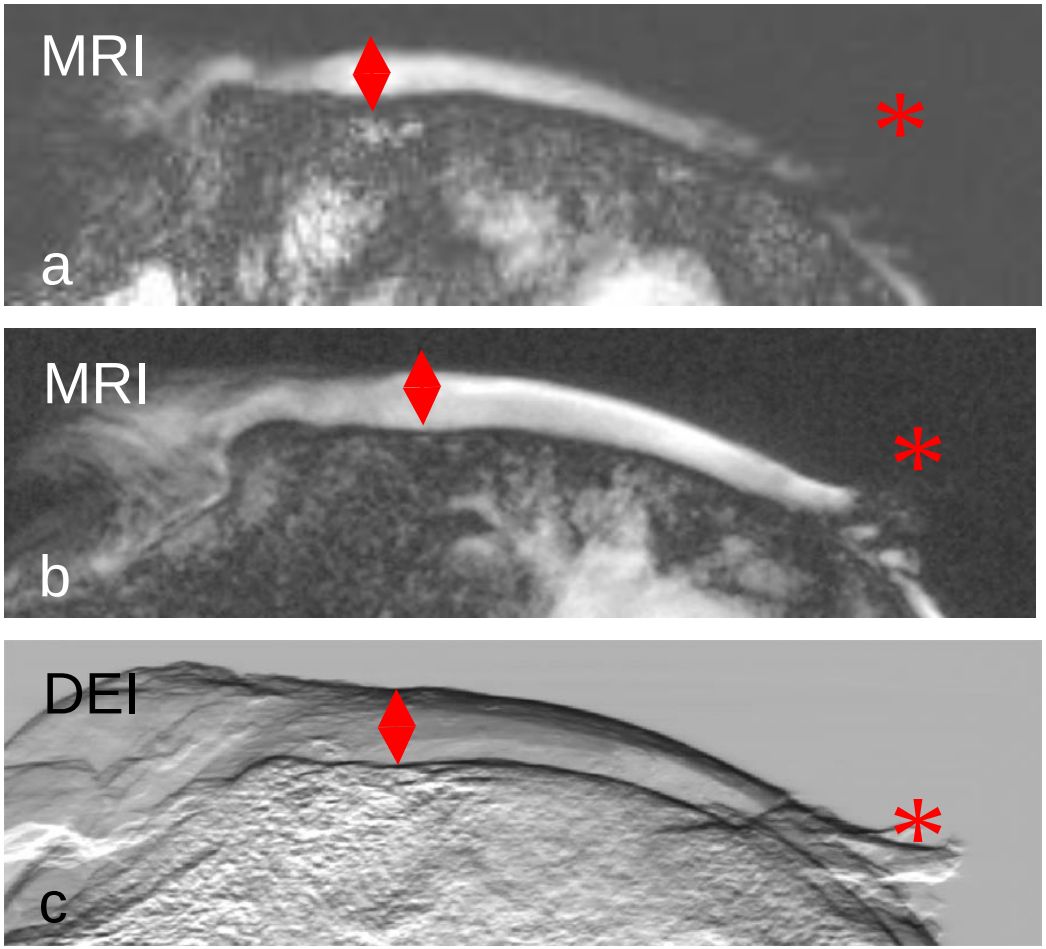

5 sec

150 sec

A Wagner, M Aurich, N Sieber, M Stoessel, WD Wetzel, K Schmuck , M Lohmann, B Reime,
J Metge, P Coan, A Bravin, F Arfelli, L Rigon, RH Menk, G Heitner, T Irving, Z Zhong, C Muehleman, J A Mollenhauer sumbitted to NIM A

Lungs imaging

Technique: Propagation Based

+ contrast agent (Barium)

Modalities: micro-CT *ex-vivo* images on mice

planar for *in-vivo* images on rabbits

Cell tracking technique

Multi resolution CT approach (ZOOM CT)

Use of phase retrieval to increase the tissue differentiation and allow quantitative analysis

Imaging of asthmatic mice – feasibility study

Animal model of allergic asthma induced by ovalbumin based on balb/c mice developed by CBM in collaboration with the University of Wien.

Aim: evaluate the potential of SR-based technique for **functional** and **morphologic** imaging of mice lungs

Available techniques: optical imaging and PHC micro-CT

Linköping University

Programme on Scientific and Technological Cooperation between Italy and Sweden financed by Ministero degli Esteri

Imaging protocol: use of macrophages with double staining

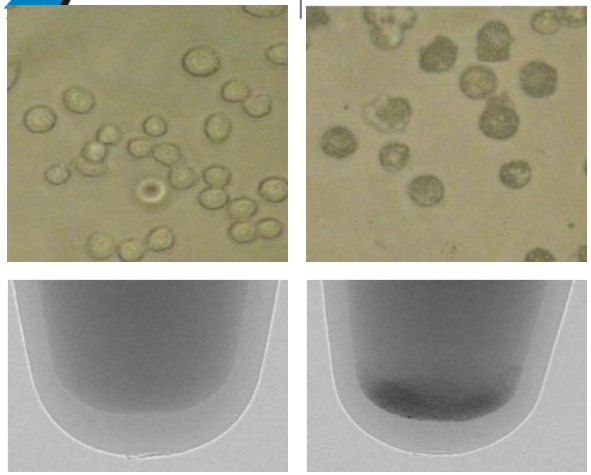

Unlabeled macrophages

Macrophages labeled with Ba

Use of immortalized Murine Alveolar Macrophage Cell line with double staining:

- Barium sulfate (clinical contrast agent Micropaque CT (Guerbet, F))

-DiD fluorescent dye to be used for cells localization inside the lungs using fluorescence microscopy.

Macrophages were adminstered intra tracheally 48 hours after asthma induction

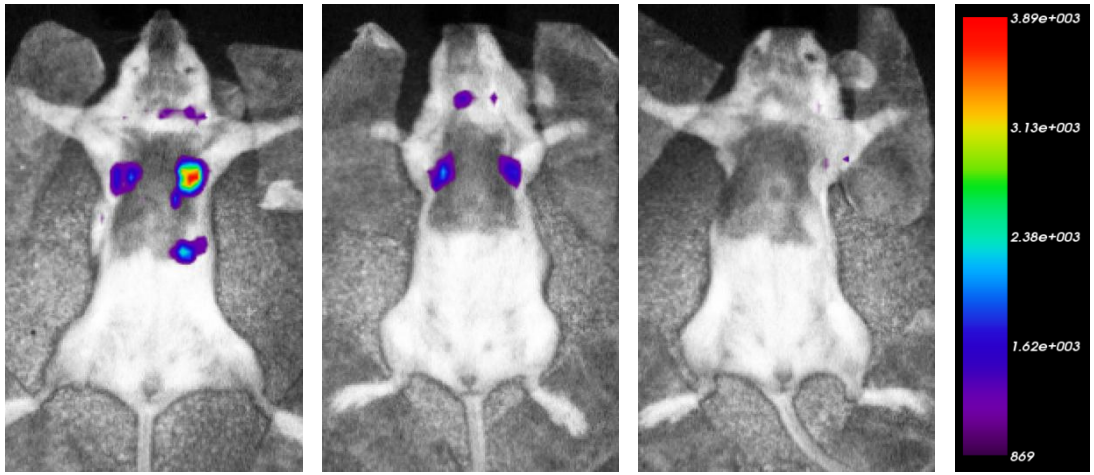

Asthmatic mouse treated with macrophages

Normal mouse treated with macrophages

Native mouse untreated

In vivo validation of homing of the macrophages to inflammation sites. Images performed 24 hours after macrophages administration.

Elettra Sincrotrone Trieste

Reconstructed slice –

Filtered back projection standard reconstruction procedure

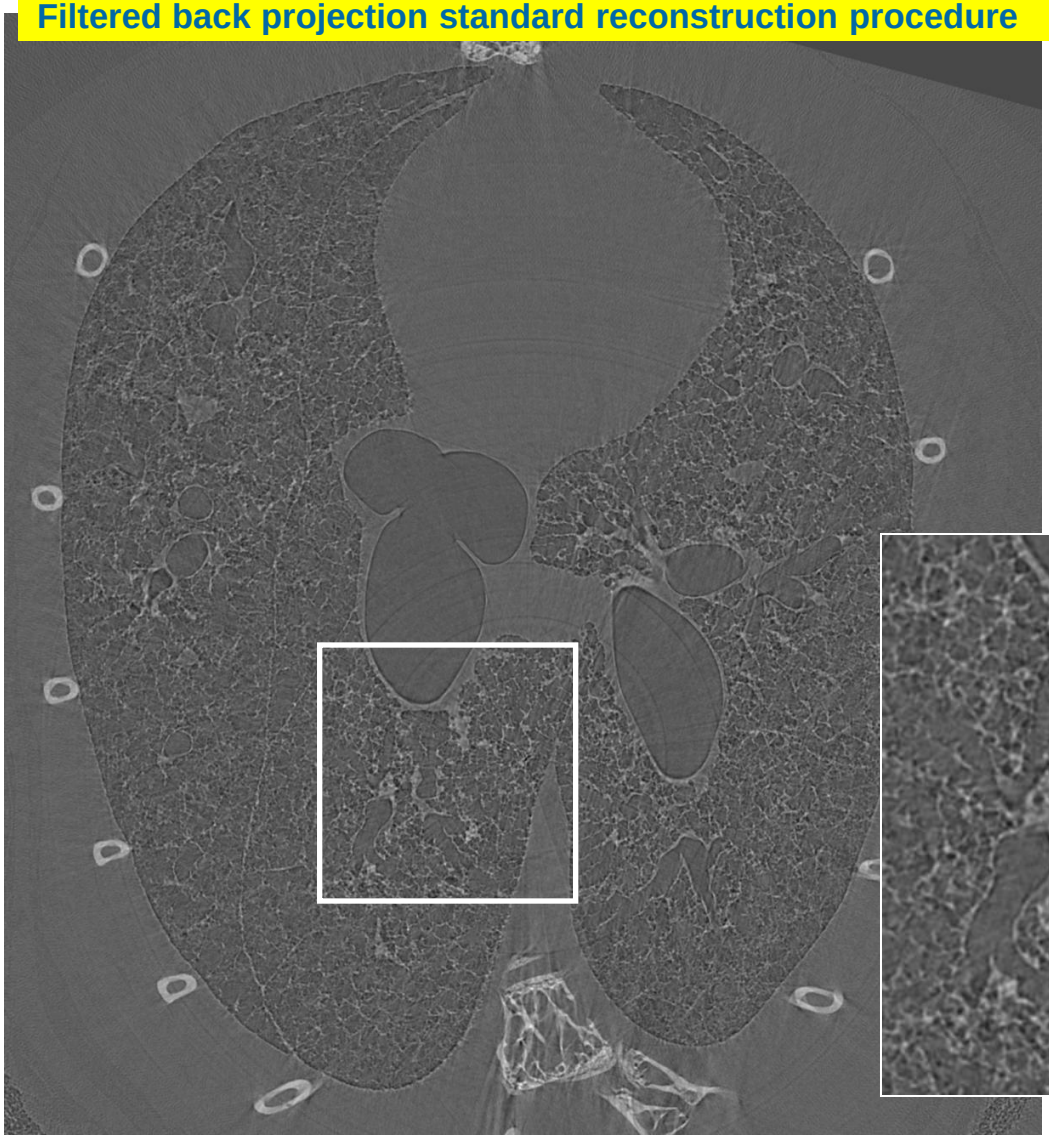

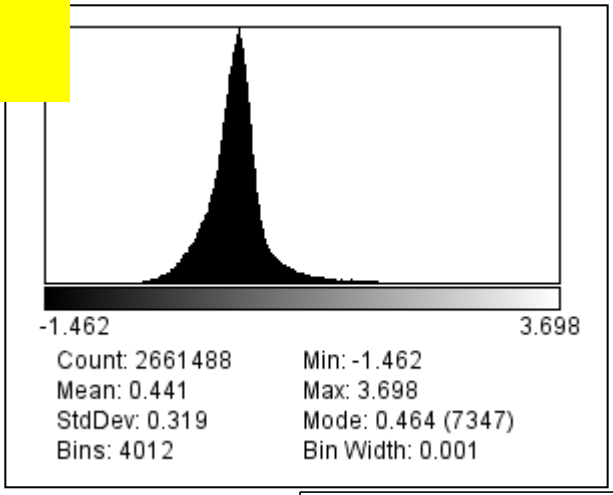

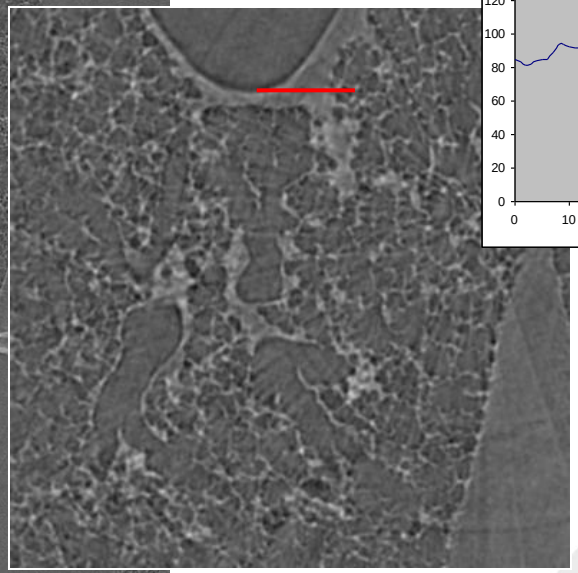

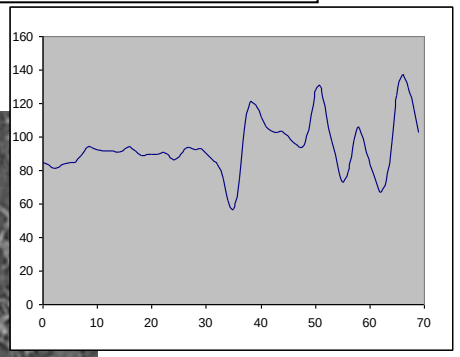

Typical edge enhancement effects due to phase contrast

Elettra Sincrotrone Trieste

Visualizing Barium brought by macrophages into the inflammation sites

Sample: acute asthma mouse treated with macrophages labeled with Barium

Phase Retrieval pre-processing *algorithm* is applied to CT projections, (prior to the reconstruction) to enable the decoupling of *phase* from *absorption*

Assumptions (Paganin et al., 2002):
-near field phase contrast regime
- materials with δ/β = const

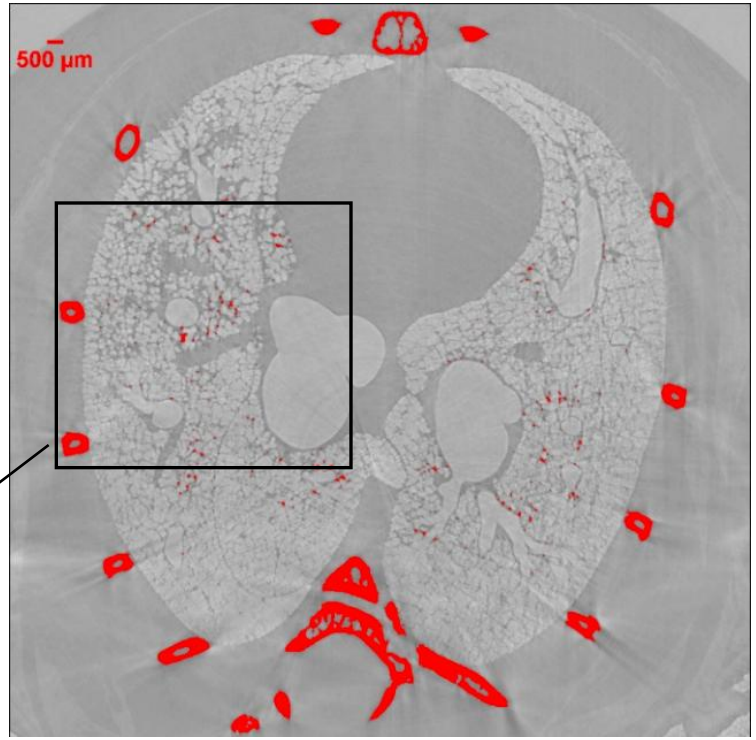

E=22 keV
PHC dist=30 cm

Bones
Barium

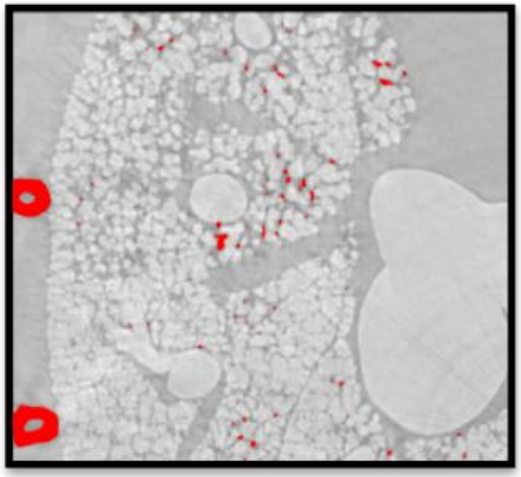

Application of Phase Retrieval for:

- Reducing the artefacts due to PHC effects around the tissue edges
- Reducing the noise
- Enhancing the phases separation

Visualization of labeled macrophages

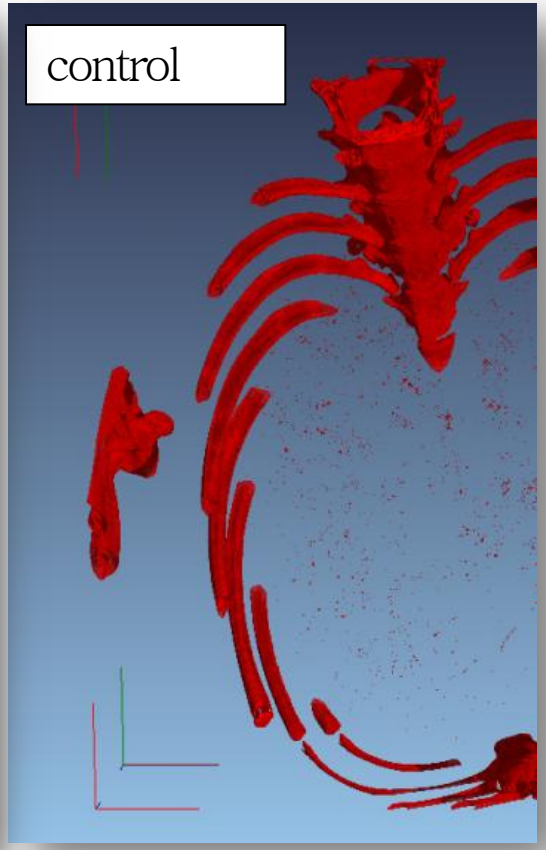

Quantification performed by Larsson E, using pore3D

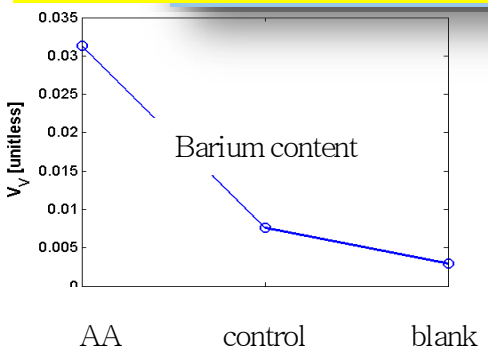

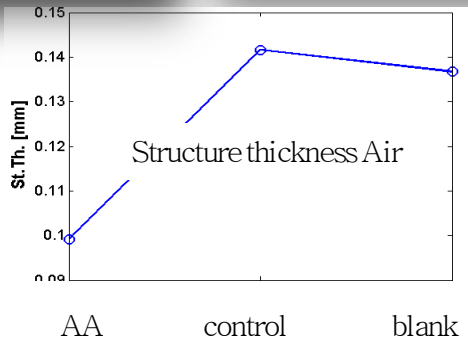

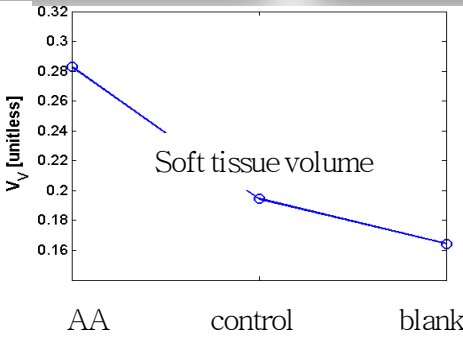

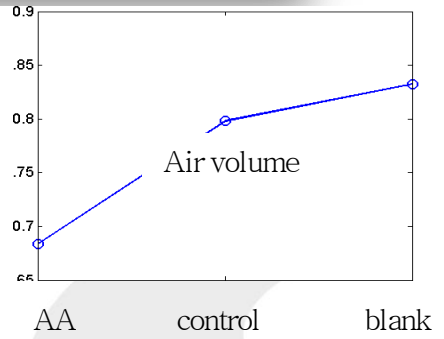

VOI of soft lung tissue

Soft Tissue (green), Macrophages with barium (red), Medial axis/skeleton (blue)

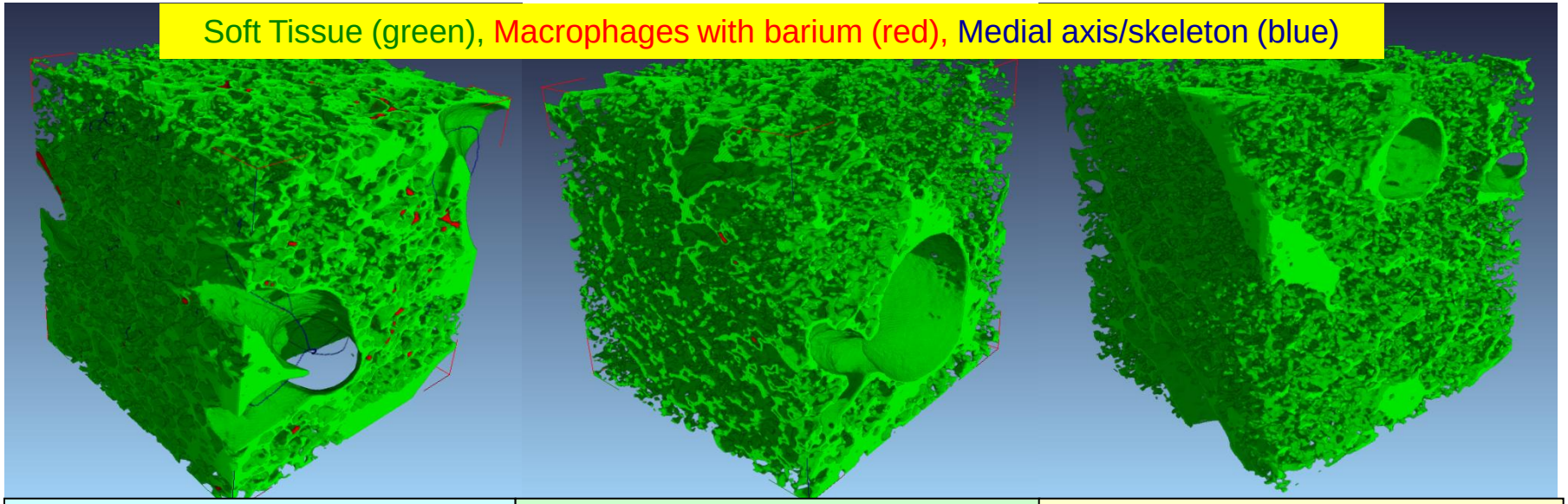

a) asthmatic mouse treated with macrophages labeled by Barium	b) healthy mouse treated with macrophages labeled by Barium	c) control: healthy mouse untreated (no Barium)

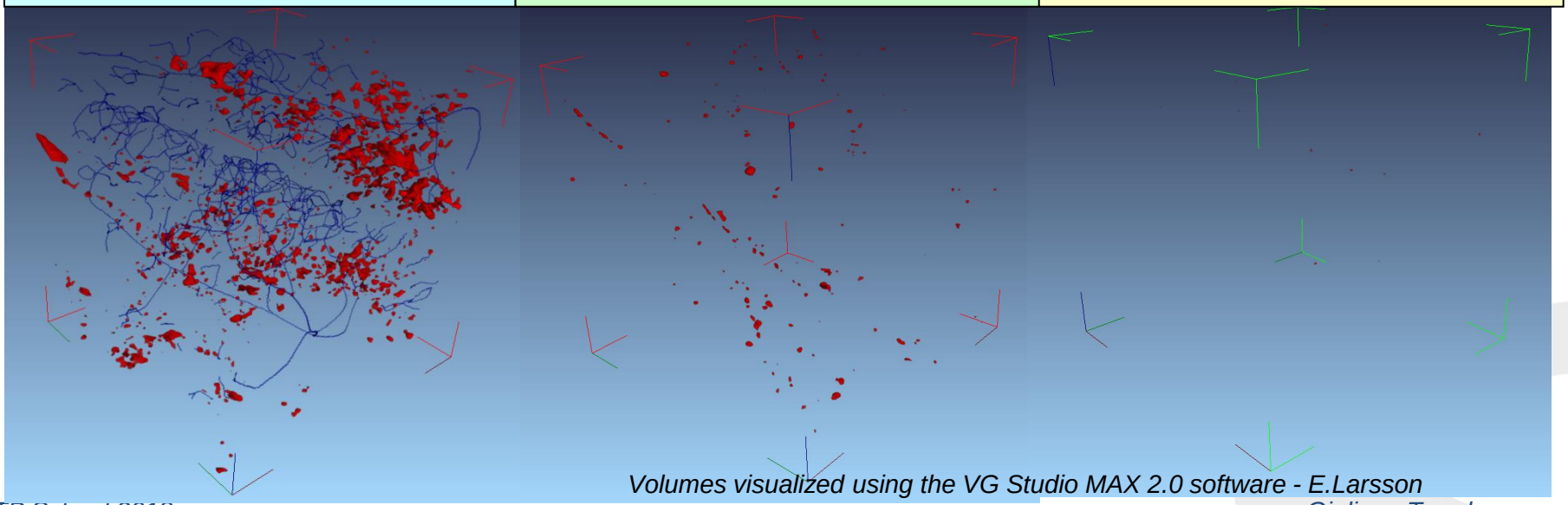

Volumes visualized using the VG Studio MAX 2.0 software - E.Larsson

In vivo studies at Spring 8 (Japan)
Effects of Ventilation on Lung Liquid Clearance at Birth

Aim: to observe lung aeration on a breath-by-breath basis.

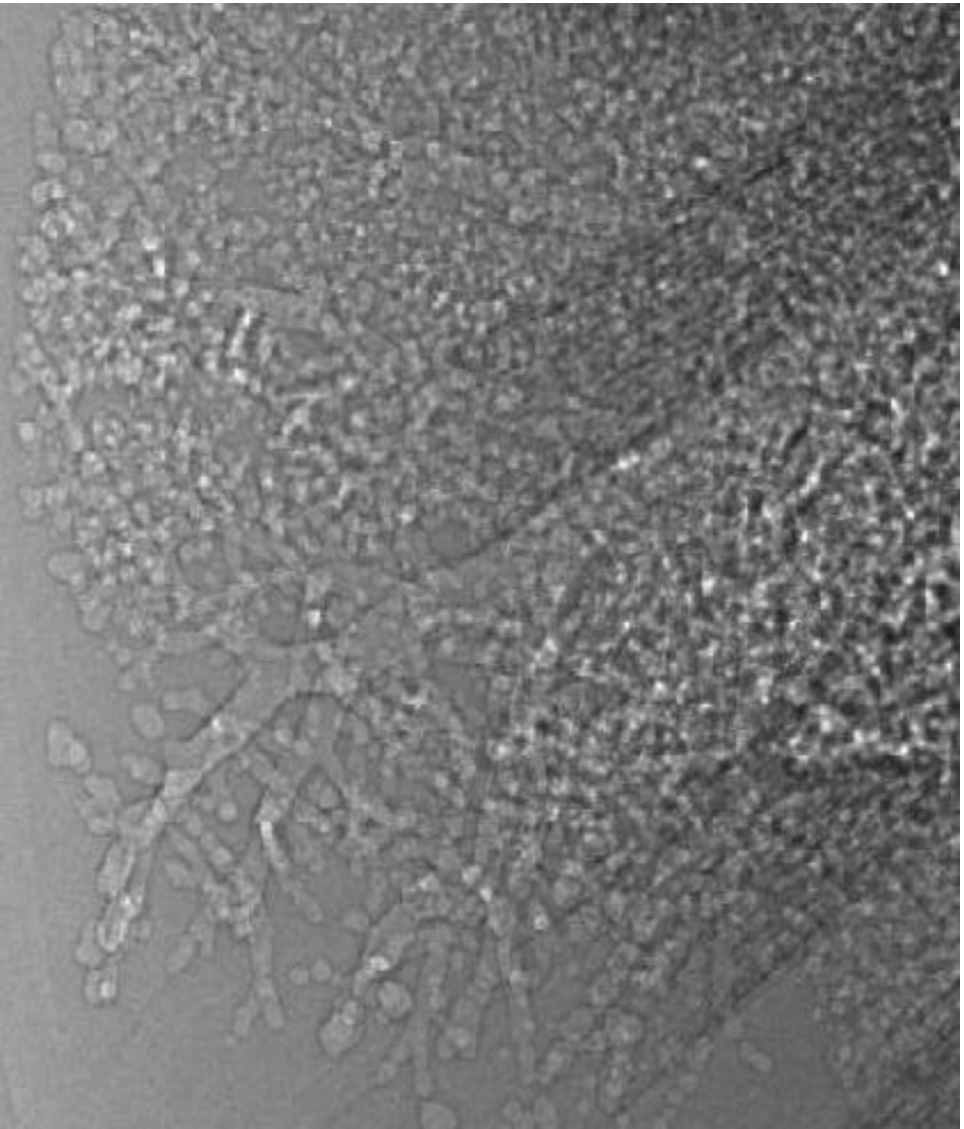

Birth: a major physiological challenge

- ✓ Clear the airways of liquid
- ✓ Entry of air generates surface tension
- ✓ Separation of the pulmonary and systemic circulations
- ✓ 10 fold increase in pulmonary blood flow
- ✓ Large increase in blood oxygenation

- ➢ Animal model: rabbit pups
- ➢ Imaged pups with phase contrast imaging (FPI), either before the first breath (fetus) and at fixed intervals after birth (up to 2h)

Courtesy of M. Kitchen, School of Physics

MONASH University
Science

X-ray imaging of the lung

Absorption Contrast

Phase Contrast, 25 keV, z=2 m

Courtesy of : M.Kitchen

Kitchen, M. J., et al., Phys. Med. Biol., 53(21), 6065-77 (2008).

Elettra Sincrotrone Trieste

MONASH University Science

Exp. time:
80 ms

Interval:
0.8 s

Skin Dose:
~ 0.15
mGy
per frame

Pixel Size:
22.5 μm

Kitchen, M. J., et al., Phys. Med. Biol., 53(21), 6065-77 (2008).

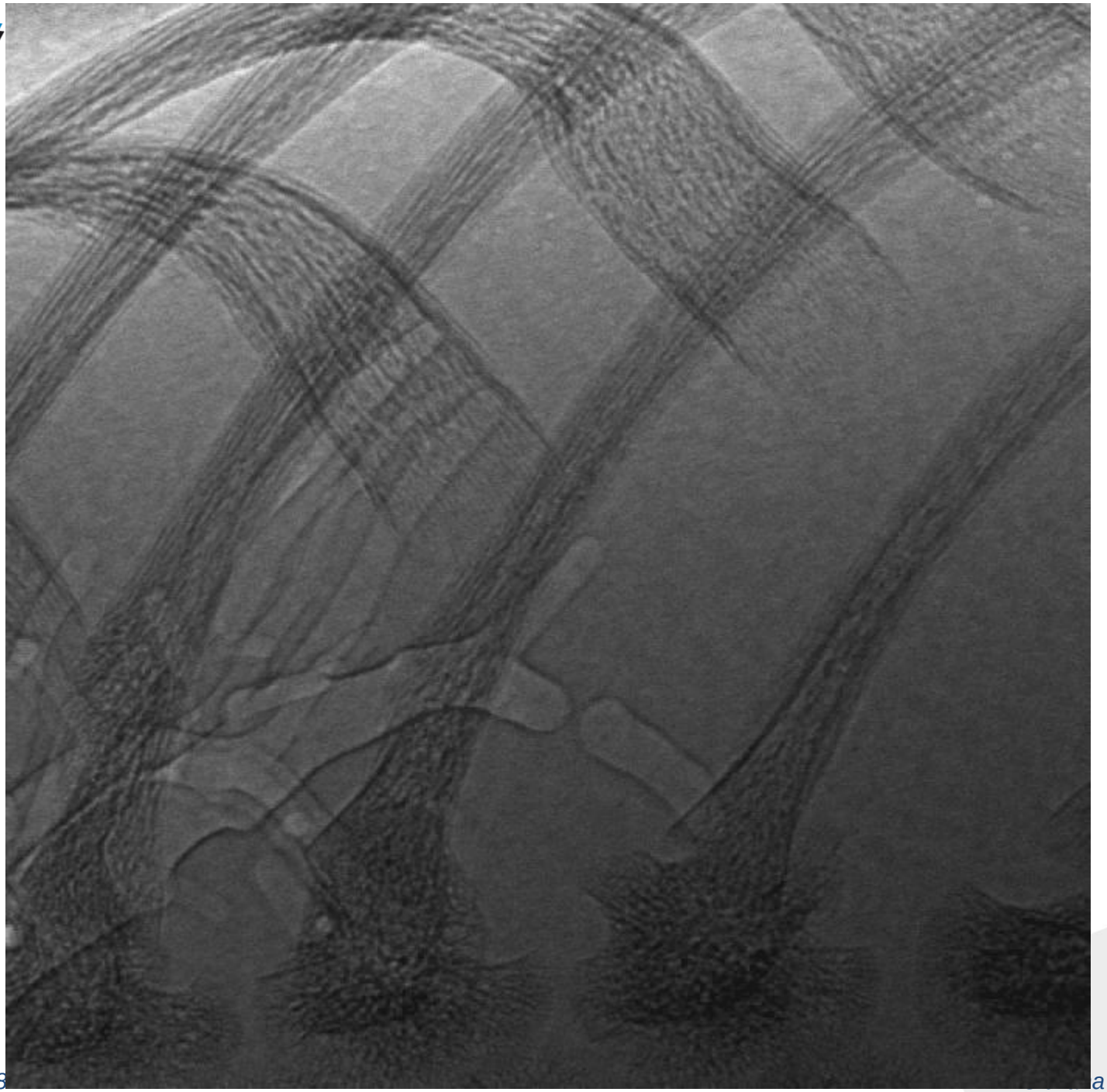

Multi-resolution CT: Zoom CT

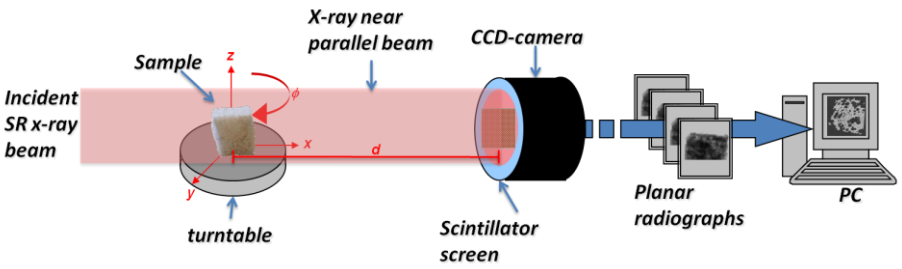

Agarose embedded mice

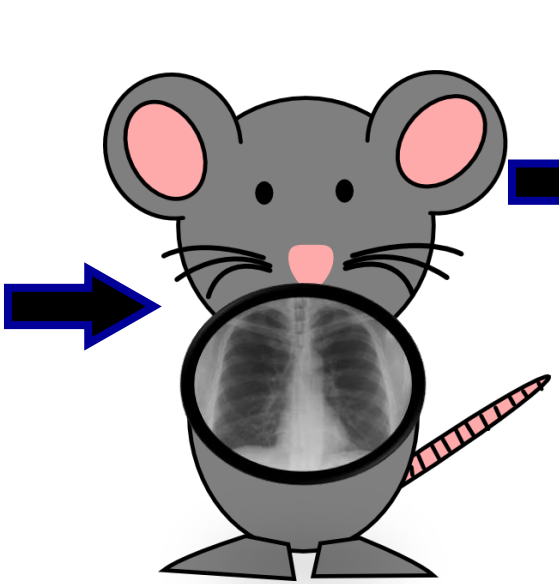

9 µm voxel size overview scan

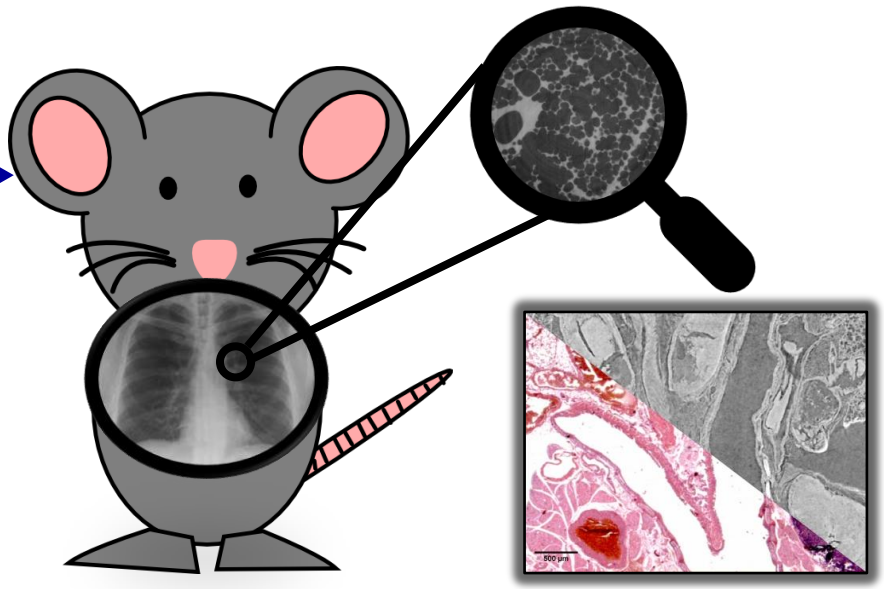

1-2 µm voxel size region of interest scan

Combined CT / histology analysis

Zoom CT - Visualization of lung

E = 22 keV,
pixel size = 9 μm
Slice of the entire lung

Lesion produced by cancer cells labeled by Ba np injected in blood stream

Pink beam,
pixel size = 2 μm
Phase retrieval,
δ/β = 1950

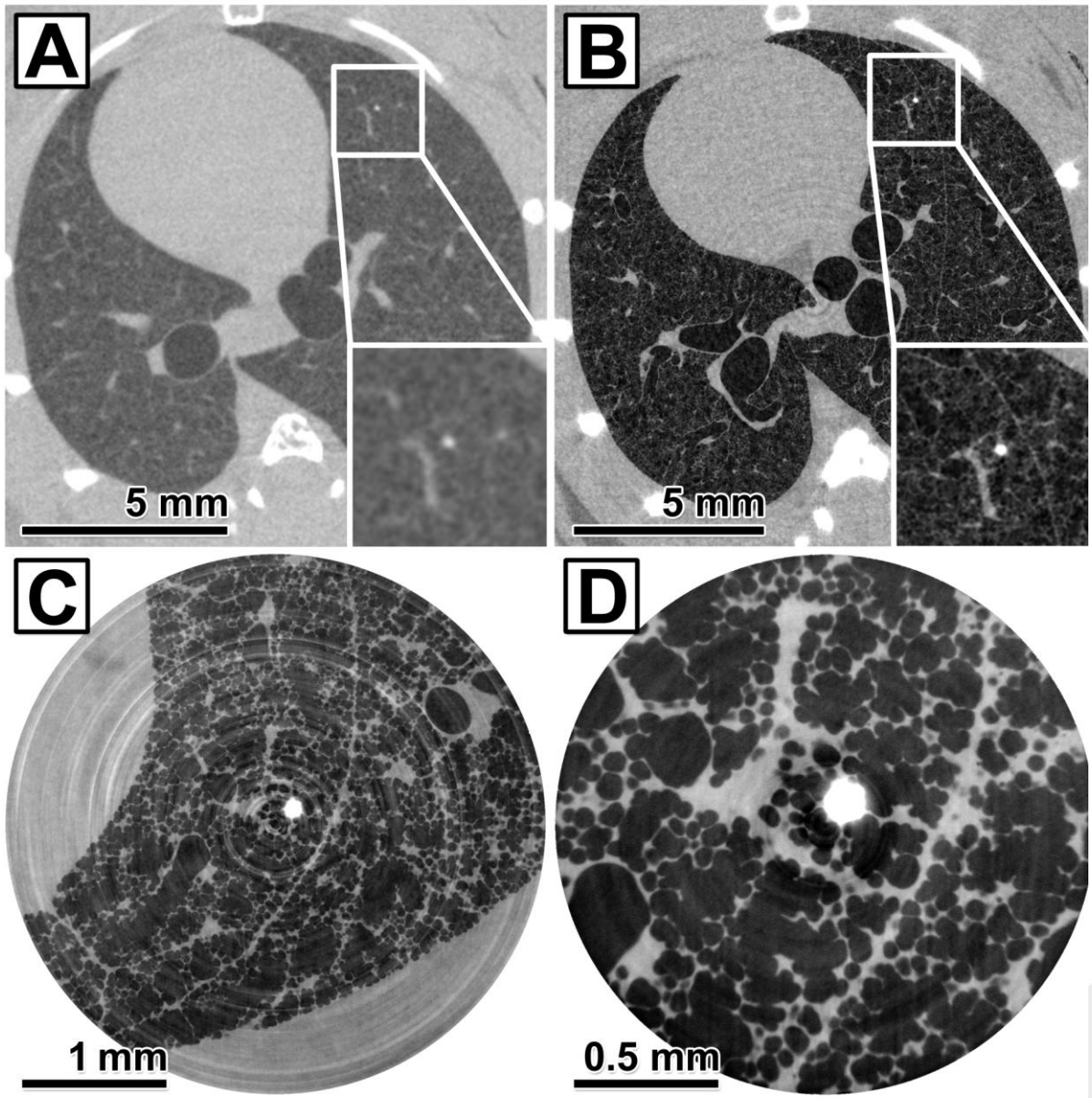

E = 22 keV,
pixel size = 9 μm
Phase retrieval,
δ/β = 1950

Pink beam,
pixel size = 1 μm
Phase retrieval,
δ/β = 1950

(Courtesy of J. Albers)

Brain studies

Technique:	Propagation based Imaging + contrast agent (gold nano particles)
Purpose:	tracking tumor development
Modality:	micro-CT *ex-vivo* imaging on mice
	(recent development: first *in-vivo* experiment)

Cell tracking studies for imaging brain tumors in rats

Glioblastoma multiforme (GBM) is the most common and aggressive primary brain tumor in humans.
An animal model based on Wistar rats have been developed.

Aim of the cell tracking technique:
monitor the dynamic of tumour growth
follow the migration of tumour cells
understand the dynamic of metastasis spread

Protocol: Glioma cells exposed to colloidal Gold Nano Particles (GNP) were implanted into the brain of adult male Wistar rats under general anesthesia. The animals were allowed to recover and were sacrificed two weeks later.

E.Schultke et al., Eur. J. Radiol.,Vol. 68, 2008

Elettra Sincrotrone Trieste

E = 24 keV
PHC dist. = 80 cm
Num. projections = 720
Ccd pixel size = 14μm

3D rendering of a 4 mm thick volume.

A1 and A2:
Tumor without colloidal gold

B1 and B2:
Tumor developed after implantation of 300,000 gold-loaded cells

In the skull segments (A2 and B2), the hole created for cell implantation is well visible (diameter 0.6 mm).

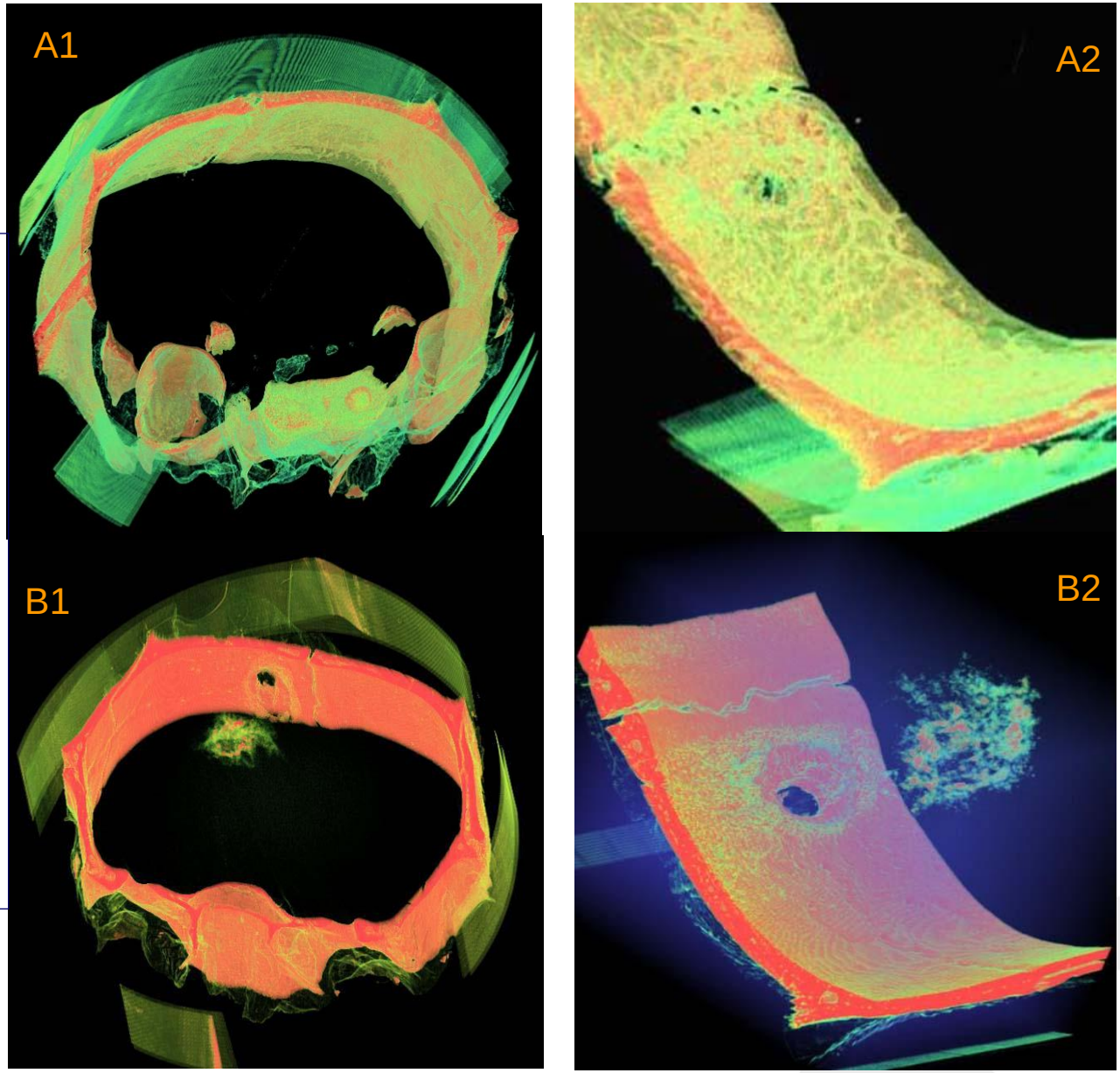

E.Schultke et al., Eur. J. Radiol.,Vol. 68, 2008

Metastasis spread in the spine

Loaded C6 cell are clearly visible in in the periphery of the chord. There is indication that the lesions penetrate into the vertebral bone.

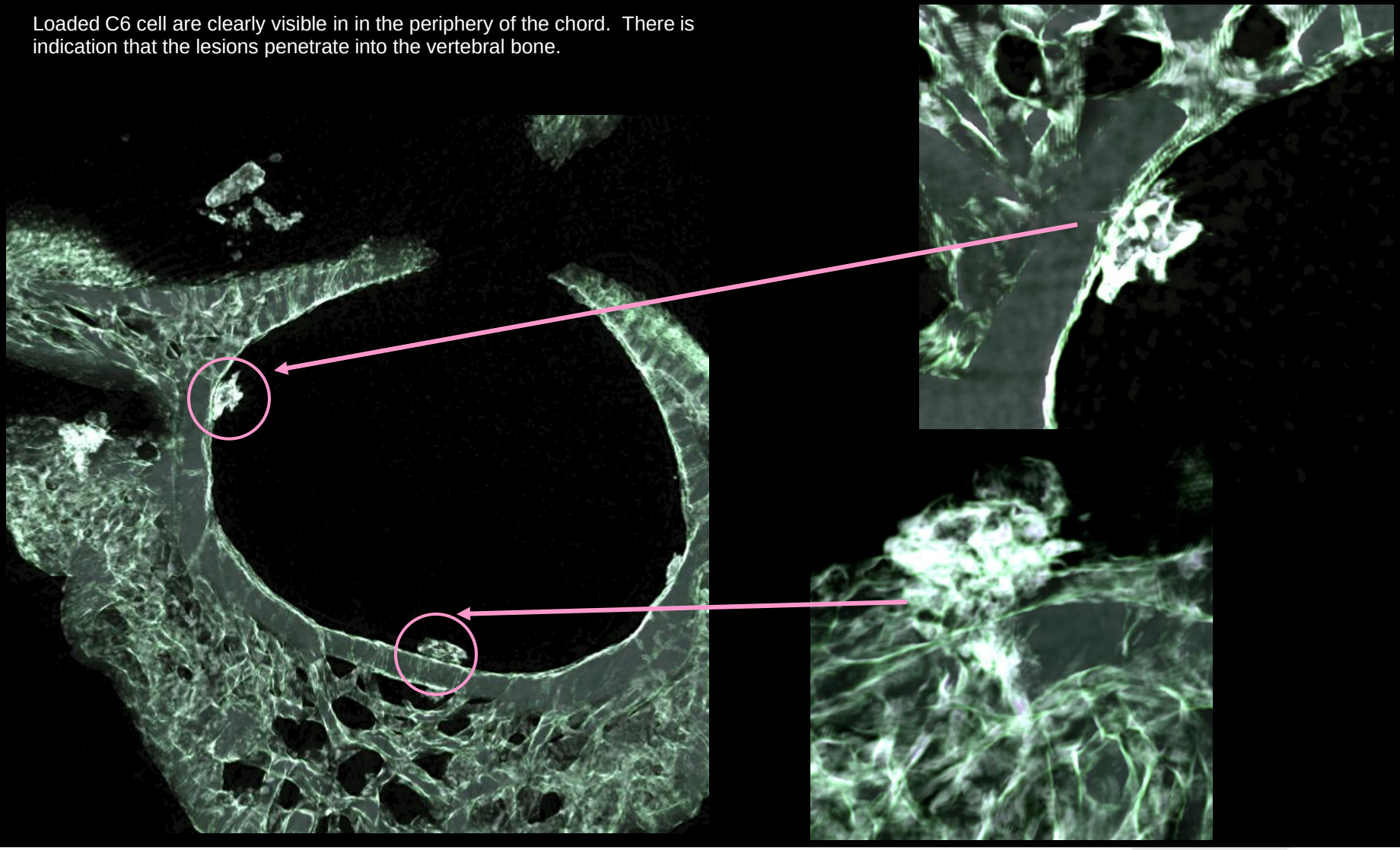

Thick slice obtained with SR

FIRST In-vivo low dose μ-CT of brain tumors

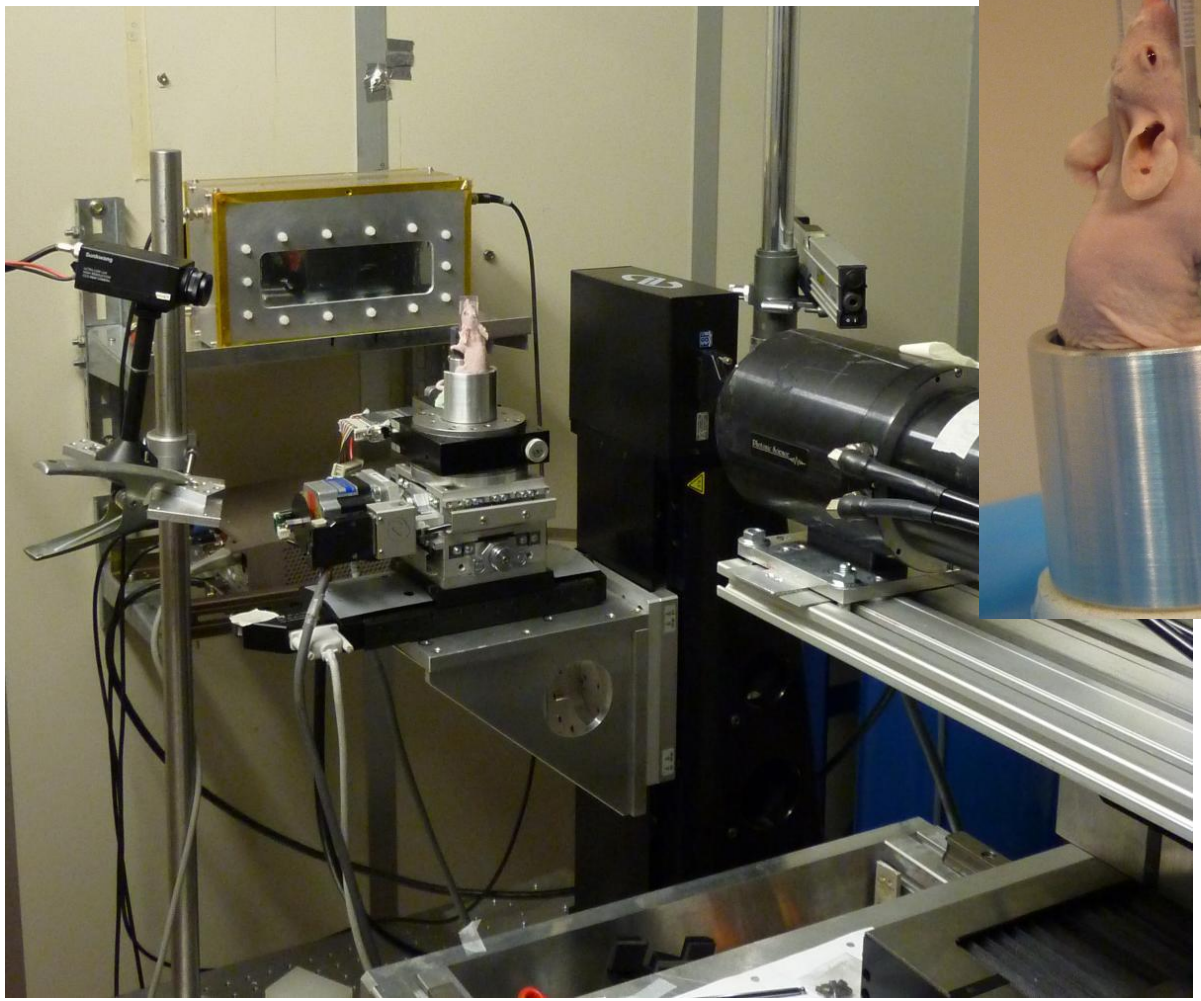

First experiment *in vivo*

A. Astolfo et al., Nanomedicine: Nanotech., Biology and Medicine, Vol. 9, Issue,2013

Low dose High dose

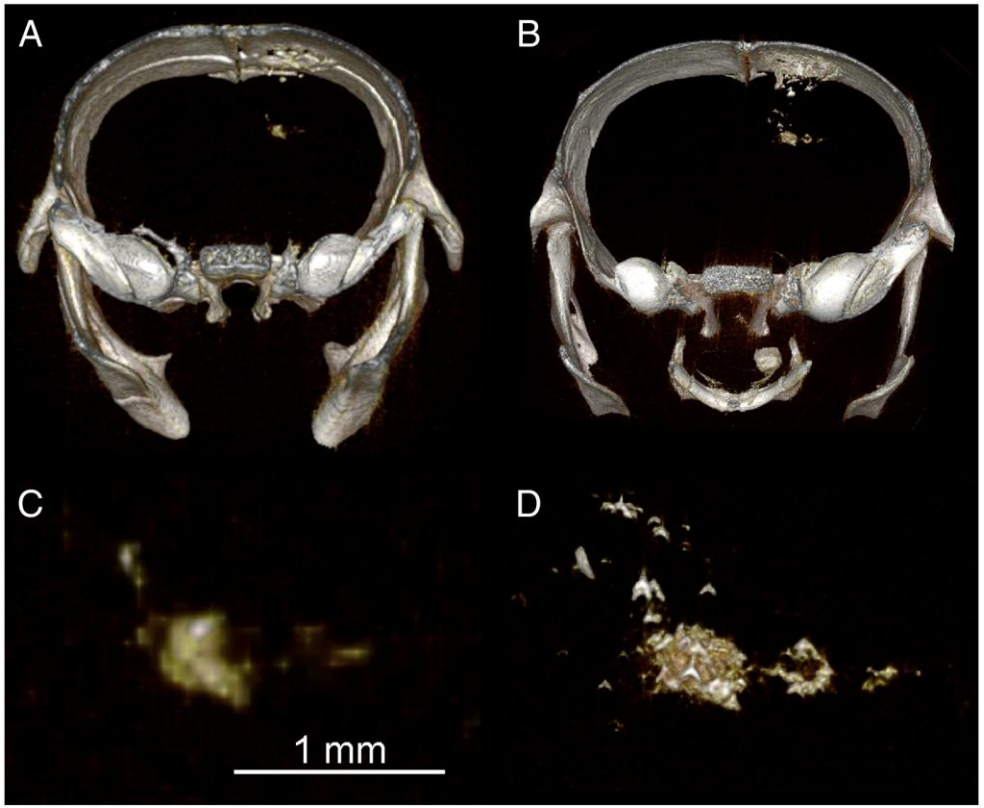

Comparison of two 3D renderings of a CT of a mouse injected with 100,000 GNP-loaded F98 cells depicts (A–C) the low x-ray dose in vivo data and (B–D) the high x-ray dose ex vivo data. The images in panels C and D are enlargements at full system resolution of the developed tumor depicted in panels A and B, respectively.

A. Astolfo et al., Nanomedicine: Nanotech., Biology and Medicine, Vol. 9, Issue,2013

Virtual Histology: high resolution imaging of Atherosclerotic plaques

Technique: Propagation- based + staining

Modality: micro-CT *in-vitro* imaging of mice aortas

Virtual histology: visualizing atherosclerosis plaques in mice

E = 27 keV,
FP dist = 30 cm
Pixel size = 9 µm

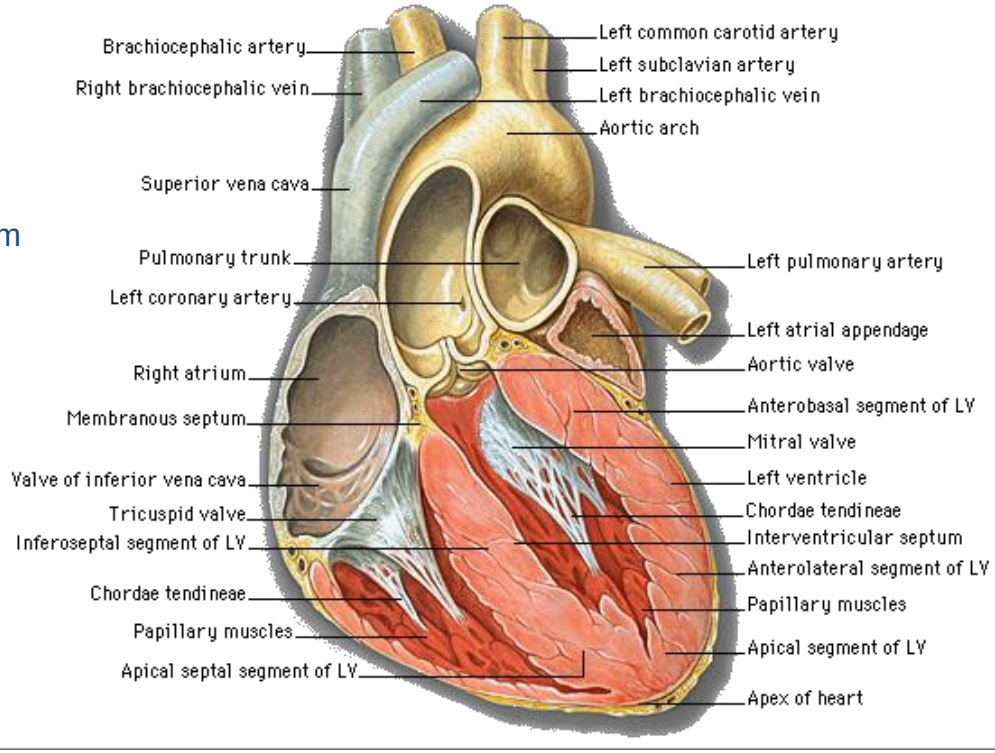

Animal model: atherosclerotic mouse

Apolipoprotein E-deficient (apoE−/−) mouse (deficient transgenic mice demonstrates a strong tendency to develop hyper-cholesterolemia

Aim: evaluate the capability of µCT to highlight the formation of atherosclerotic plaques in normal and Apo mice - All mice were fed with a high fat diet for 70 days.

Combination of soft tissue staining by phosphotungstic acid (PTA)* and sample embedding in paraffin or agarose gel allows direct overlay of **µ**CT data sets and microscopy after immunochemical staining

*B.Metscher, BMC Physiology 2009,

UNIVERSITÄTSMEDIZIN GÖTTINGEN UMG

Elettra Sincrotrone Trieste

Comparing CT slice with histology

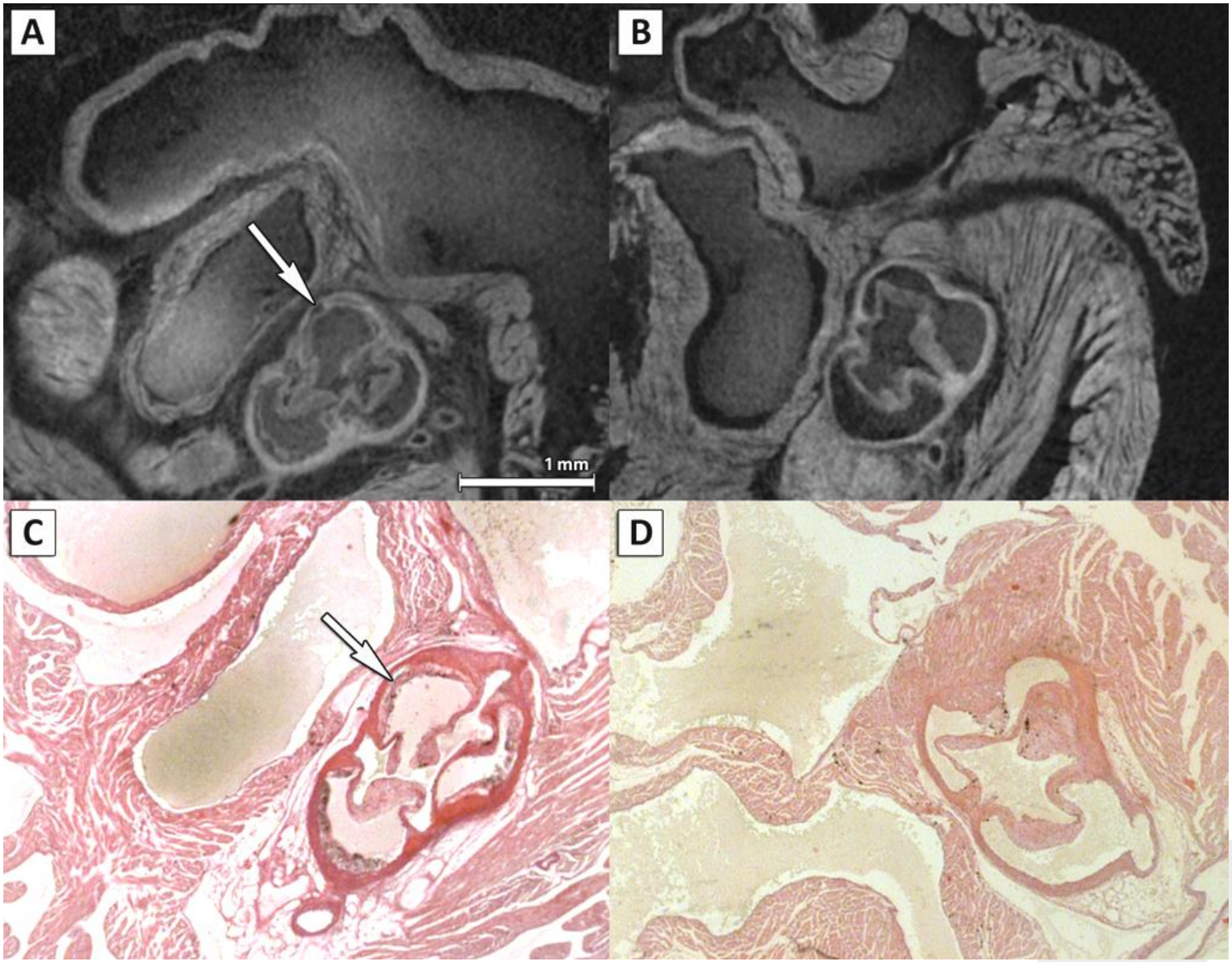

4DCT - Application to entomology

Visualizing fast micrometer scale internal movements of small animals is a key challenge for functional anatomy, physiology and biomechanics.

Phase contrast tomographic microscopy (down to 3.3 µm voxel size) was combined with retrospective, projection-based gating (in the order of hundreds of microseconds) to visualize the fast internal movements of the blowfly flight motor on sub-millisecond and micrometre scales.

Technique: Propagation- based

Modality: Dynamic micro-CT - *in-vivo* imaging

Elettra Sincrotrone Trieste

4DCT: *in vivo* X-ray microscopy with projection-guided gating

Visualizing fast micrometer scale internal movements of small animals

Application of phase contrast microCT (~ 3.3 μm voxel size) with retrospective, projection-based gating

20 CT scans selected through the 150 Hz oscillations of the blowfly flight

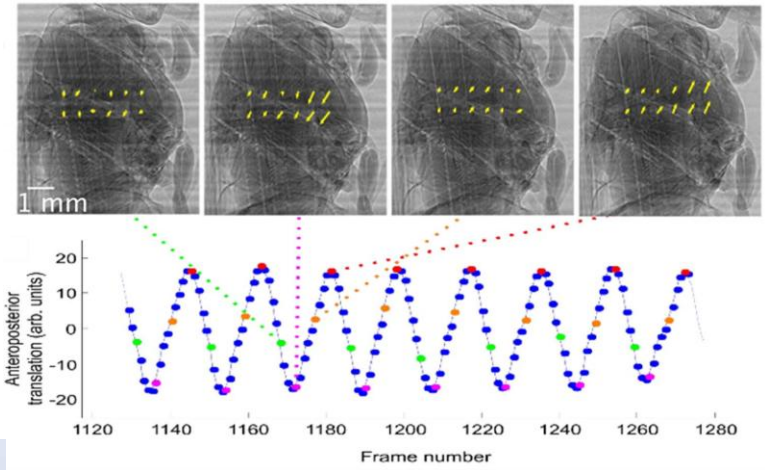

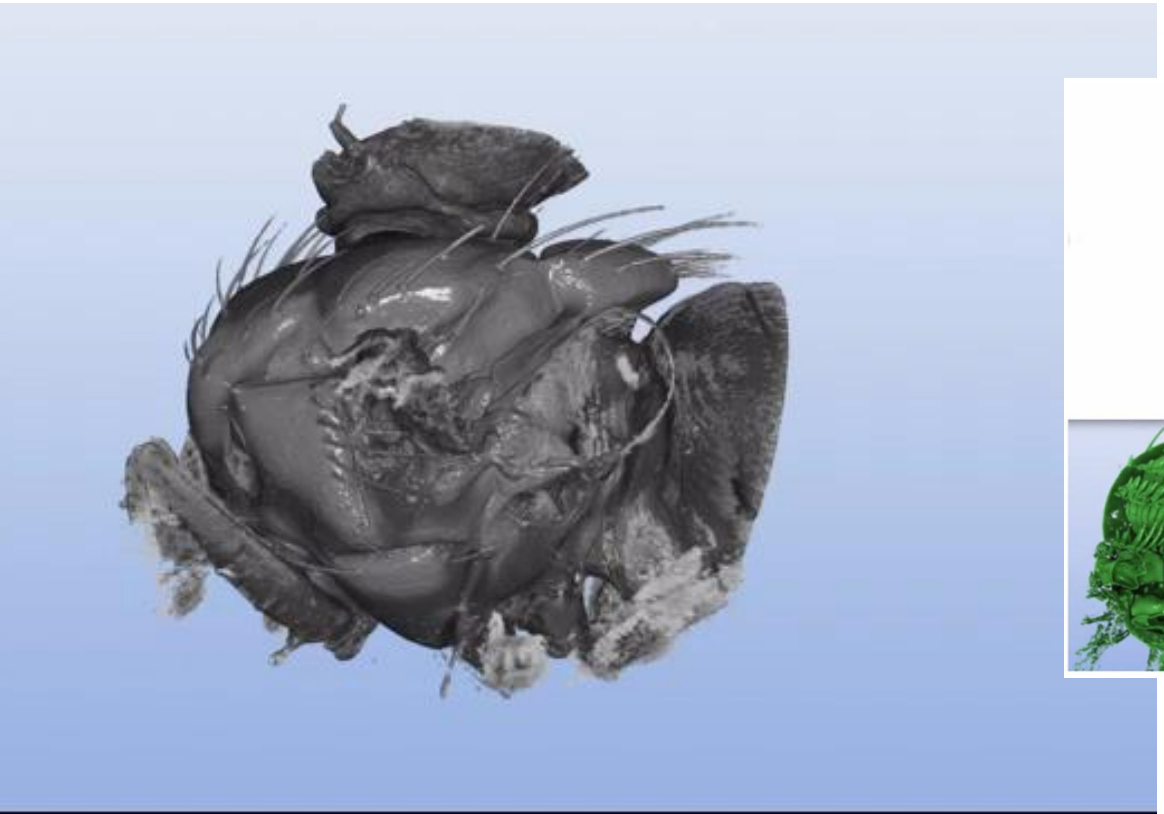

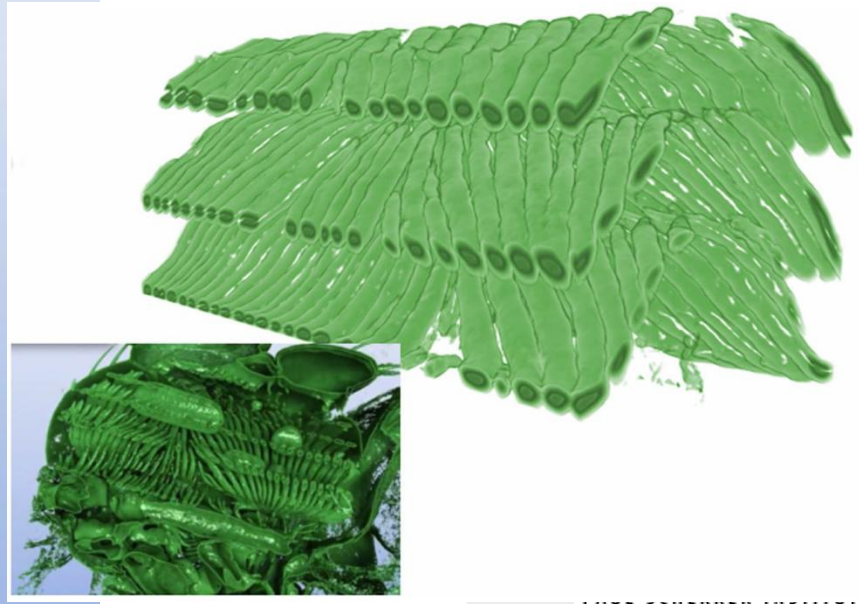

Rajmund Mokso et al.: Sci. Rep. | 5 : 8727 | (2015)

Elettra
Sincrotrone
Trieste

Research in Cultural Heritage and Anthropology

Historical musical instruments

Paleoanthropological finds (bones and theeth)

Investigation of ancient violins by µCT: feasibility study with a recent student violin

Aim: evaluate the conservation of the external protective layer ('varnish'), find defects in the wood, localize patches, identify its origin from the analysis of the annual rings

PICASSO detector (single photon counting by INFN Trieste) based on Si microstrip has been used with its wide sensitive area and its dynamic range

E = 23 keV
Sample-det. distance = 14 cm
Exposure time = 1 s
N. Proj = 3600 over 180
Pixel size = 50 µm

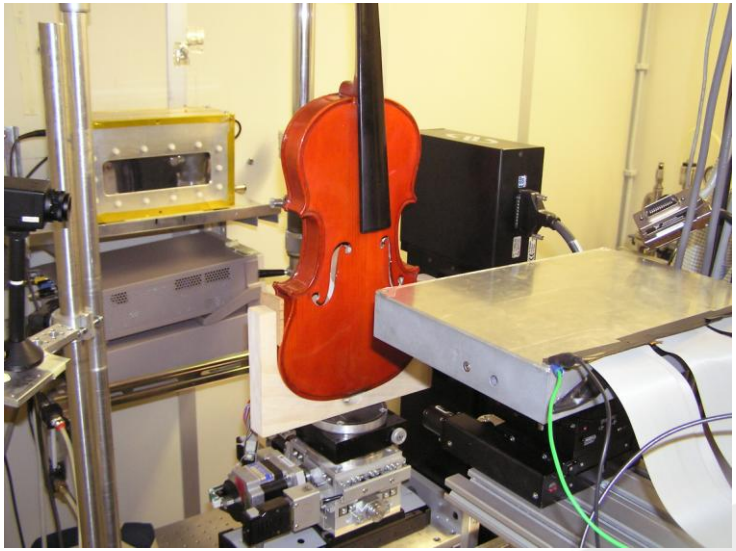

Reconstructed µCT slice of a student violin obtained with PICASSO detector developed by INFN - Trieste. The section has been taken at the middle bout, at the level of the f-holes.

L.Rigon et al, submitted to e-Preservation Science

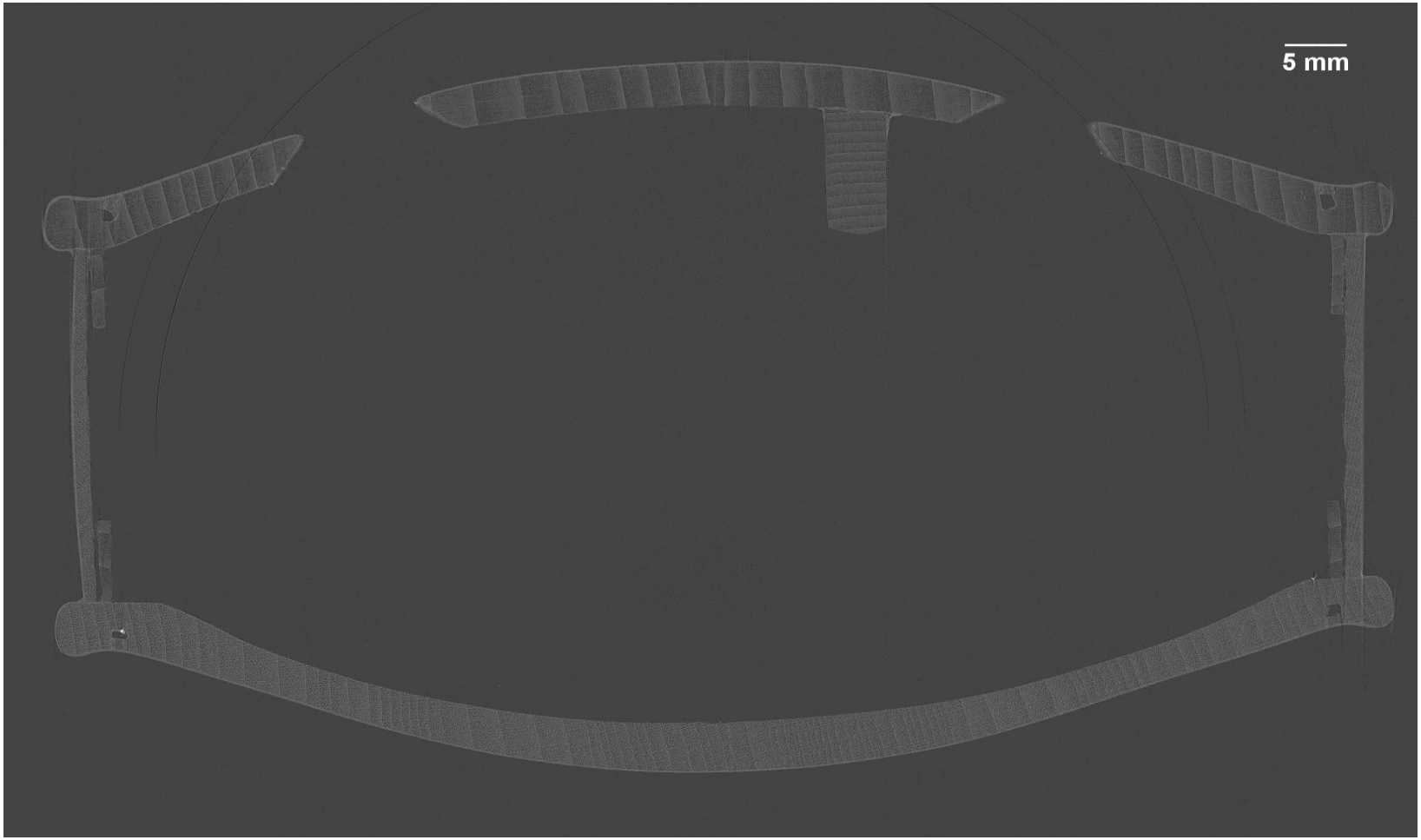

Reconstructed μCT slice of a student violin obtained with PICASSO detector developed by INFN - Trieste. The section has been taken at the middle bout, at the level of the f-holes.

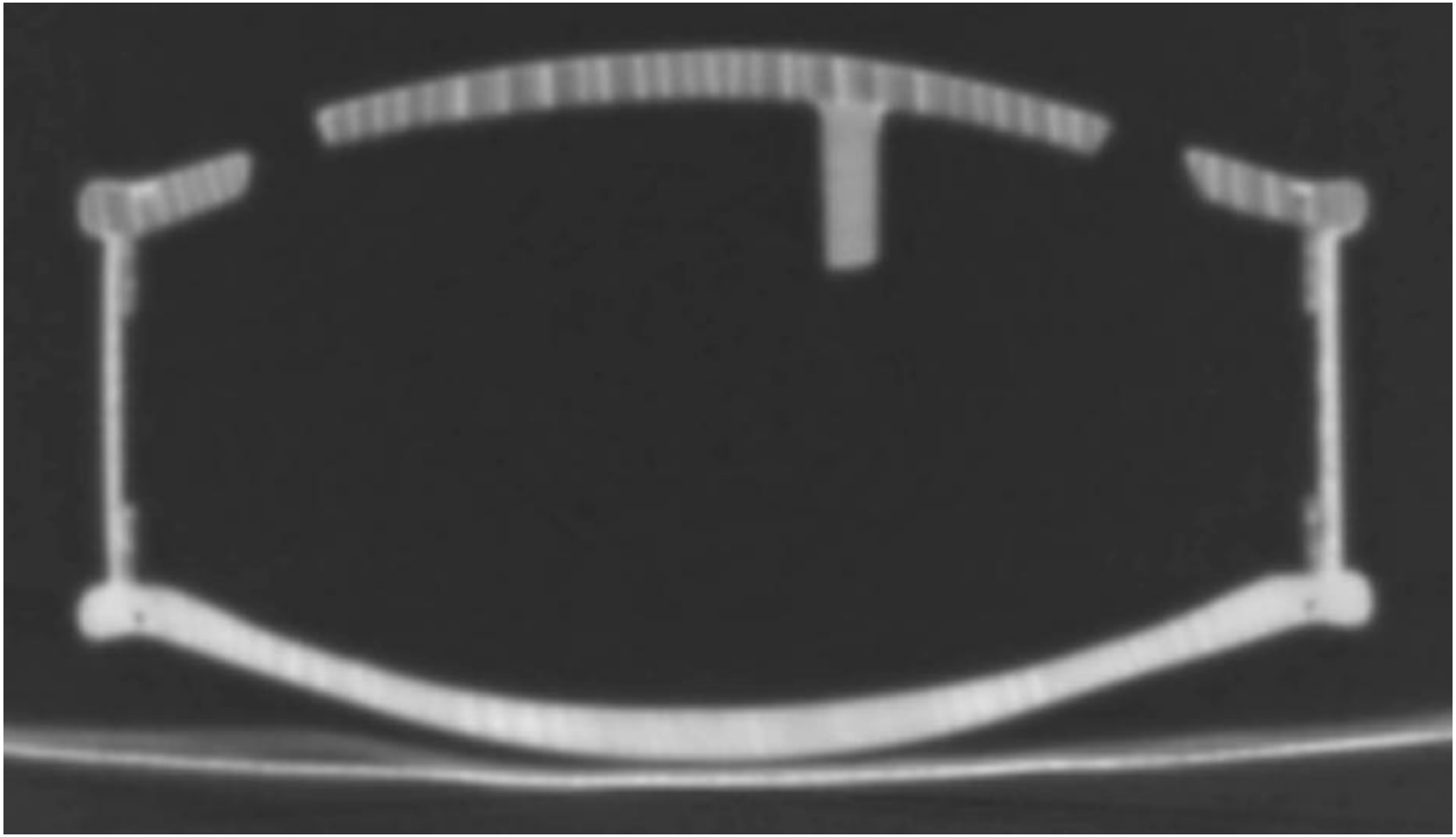

Transaxial CT taken with a state-of-the-art clinical instrument
(Toshiba Aquilion, helical scan 120 kVp, 512x512 matrix, 0.5 mm slice thickness,
0.5 s exposure time, 0.485/0.485 pixel spacing, Torax protocol)

Elettra Sincrotrone Trieste

Peter Herresthal and his Giovanni Battista Guadagnini (1753)

The experimental hutch

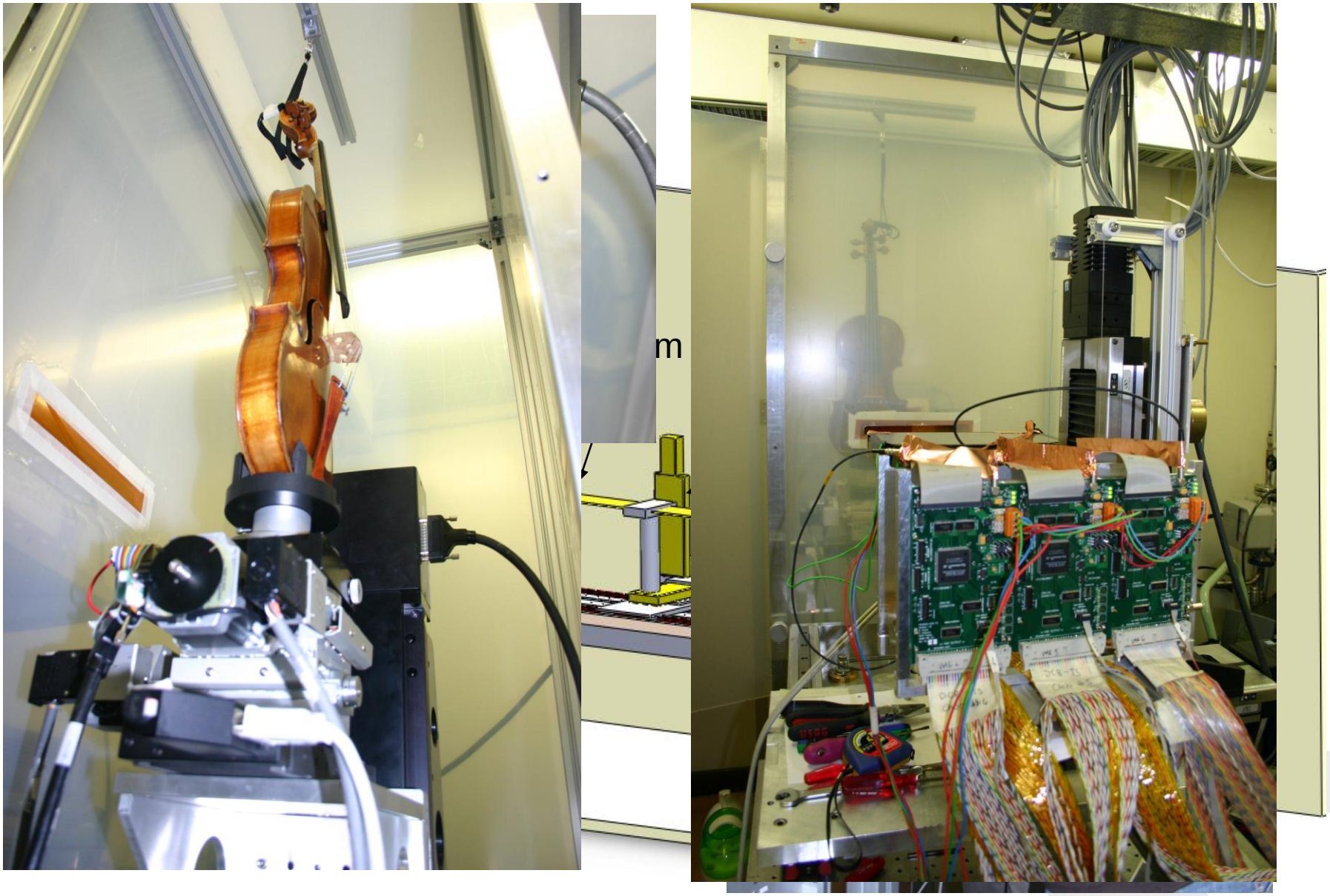

The planar image

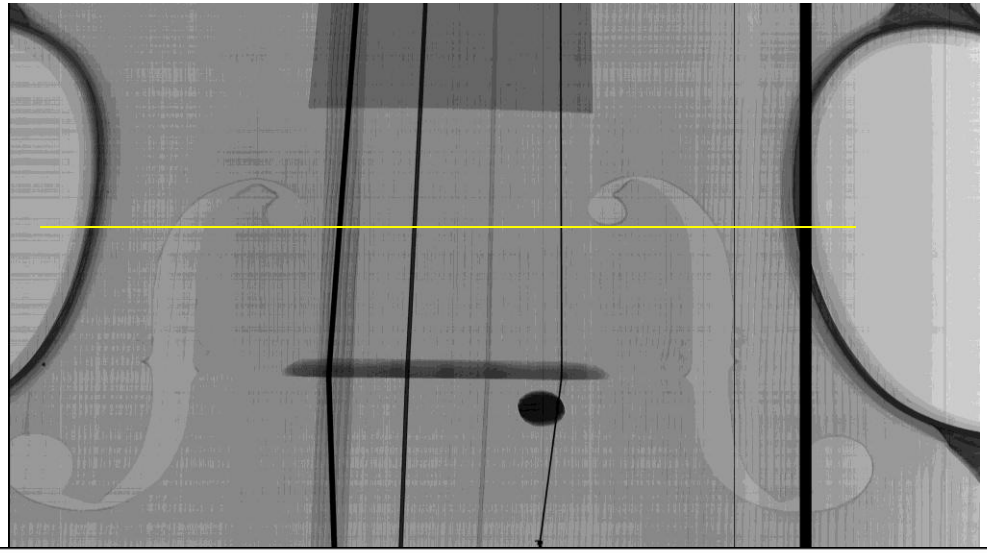

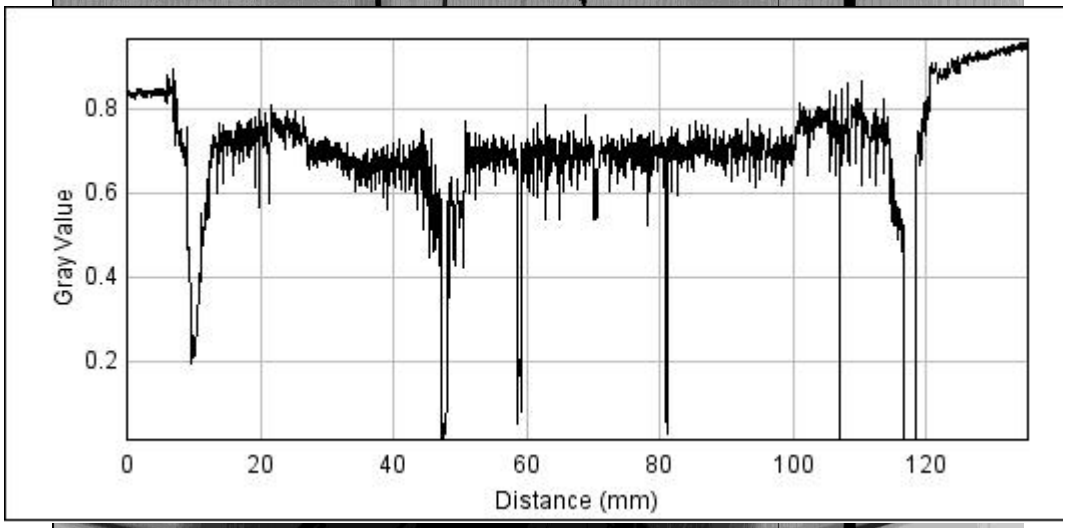

N.Sodini et al., Journal of Cultural Heritage, Vol. 13 - 3 (2012)

The planar image

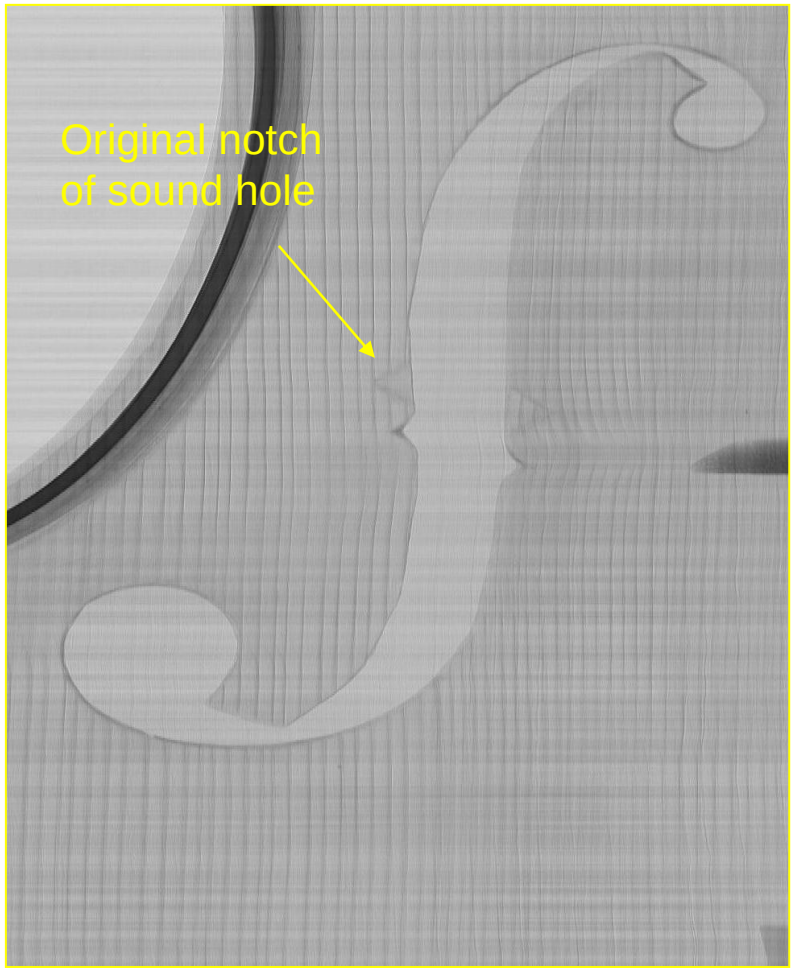

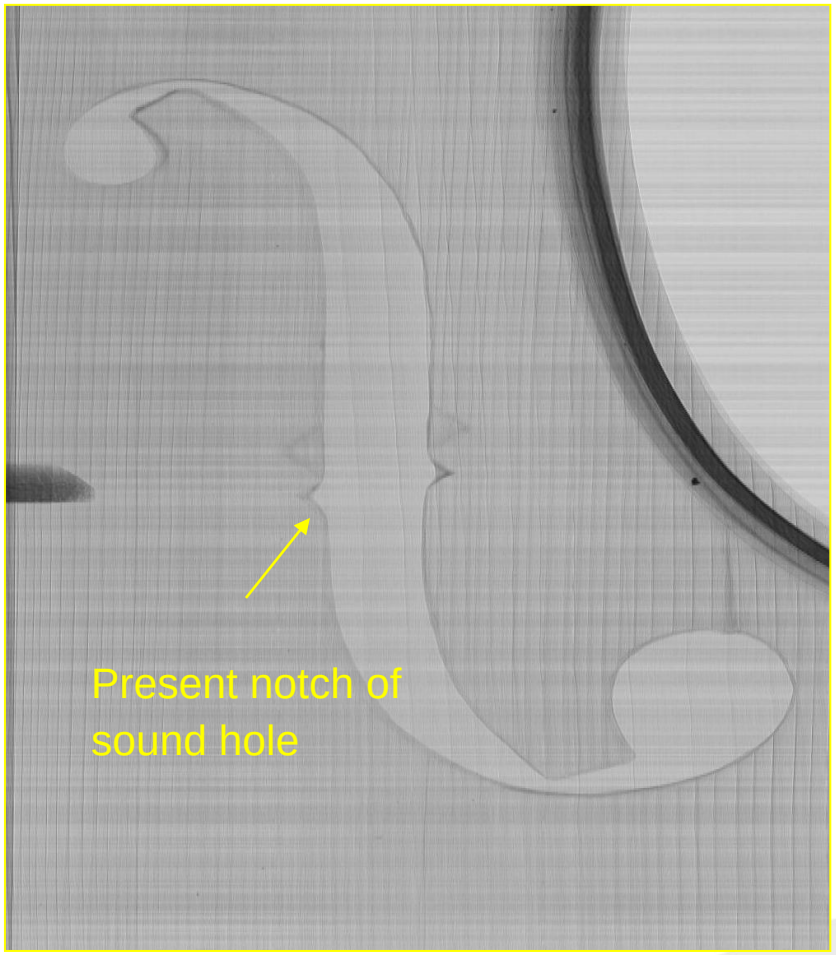

N.Sodini et al., Journal of Cultural Heritage, Vol. 13 - 3 (2012)

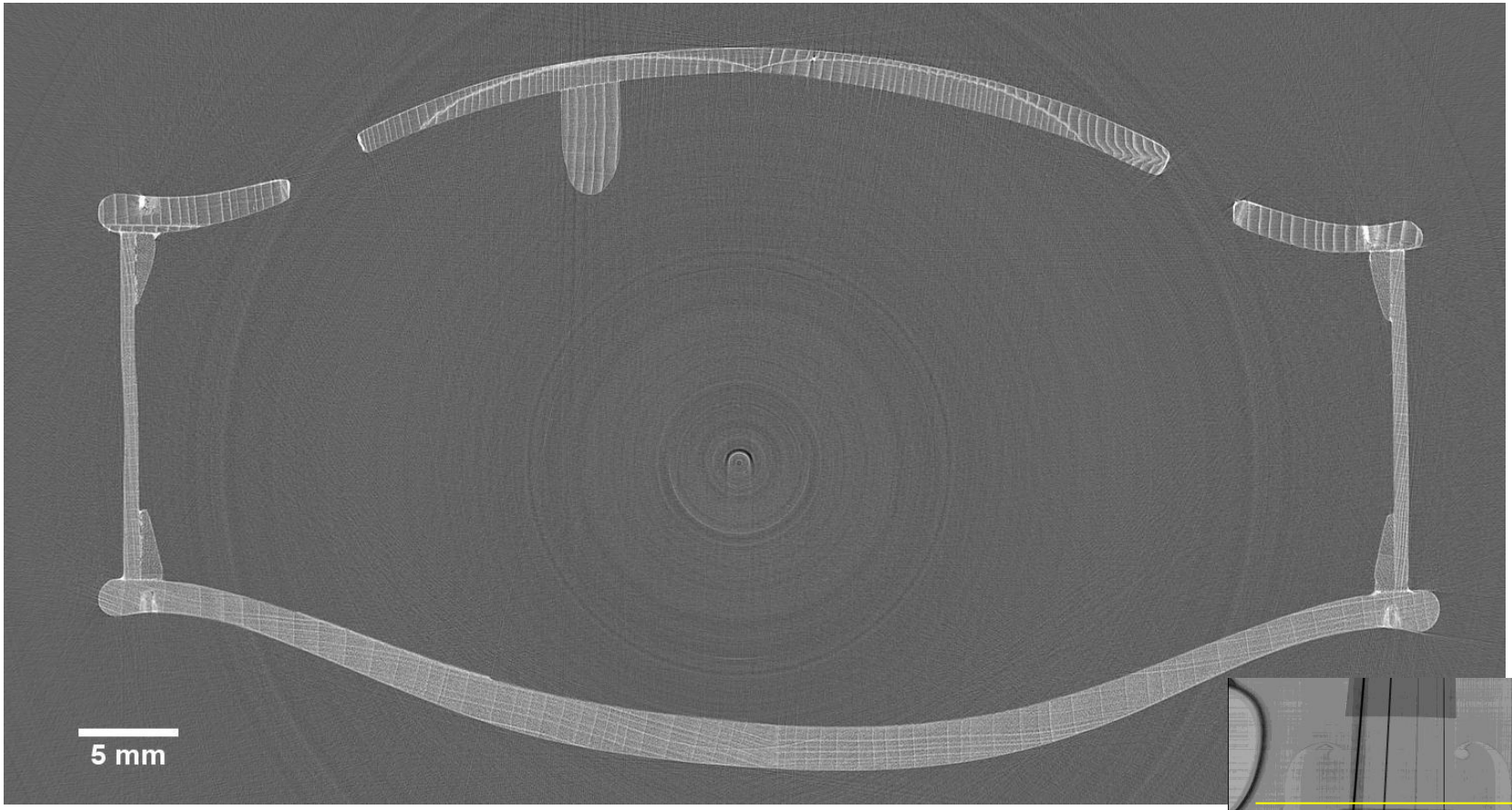

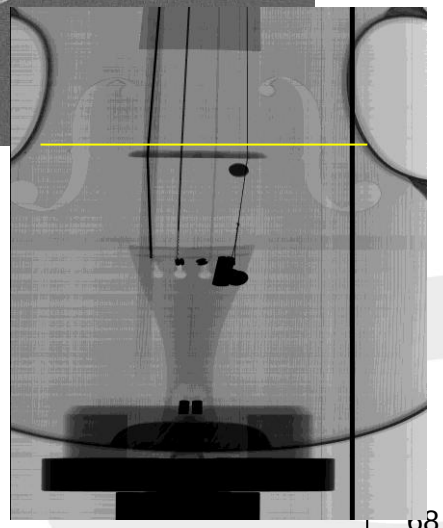

- Two patches are glued on the top plate
- The grain of the patches is good
- Thickness of the back is very thin

N.Sodini et al., Journal of Cultural Heritage, Vol. 13 - 3 (2012)

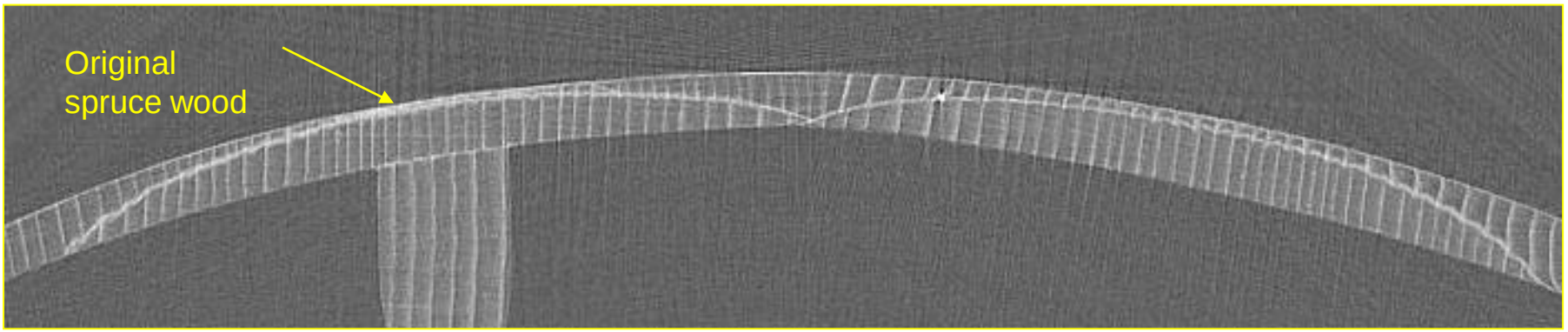

- Two patches are glued on the top plate
- The grain of the patches is good
- Thickness of the back is very thin

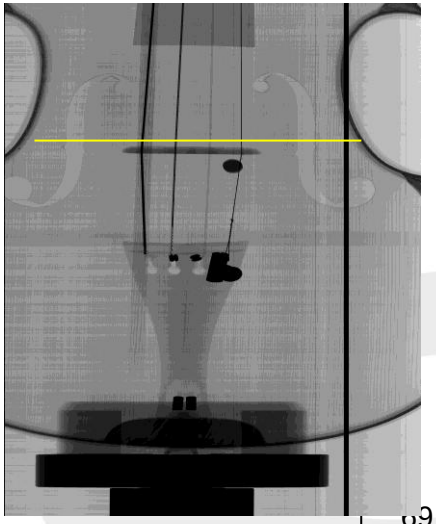

N.Sodini et al., Journal of Cultural Heritage, Vol. 13 - 3 (2012)

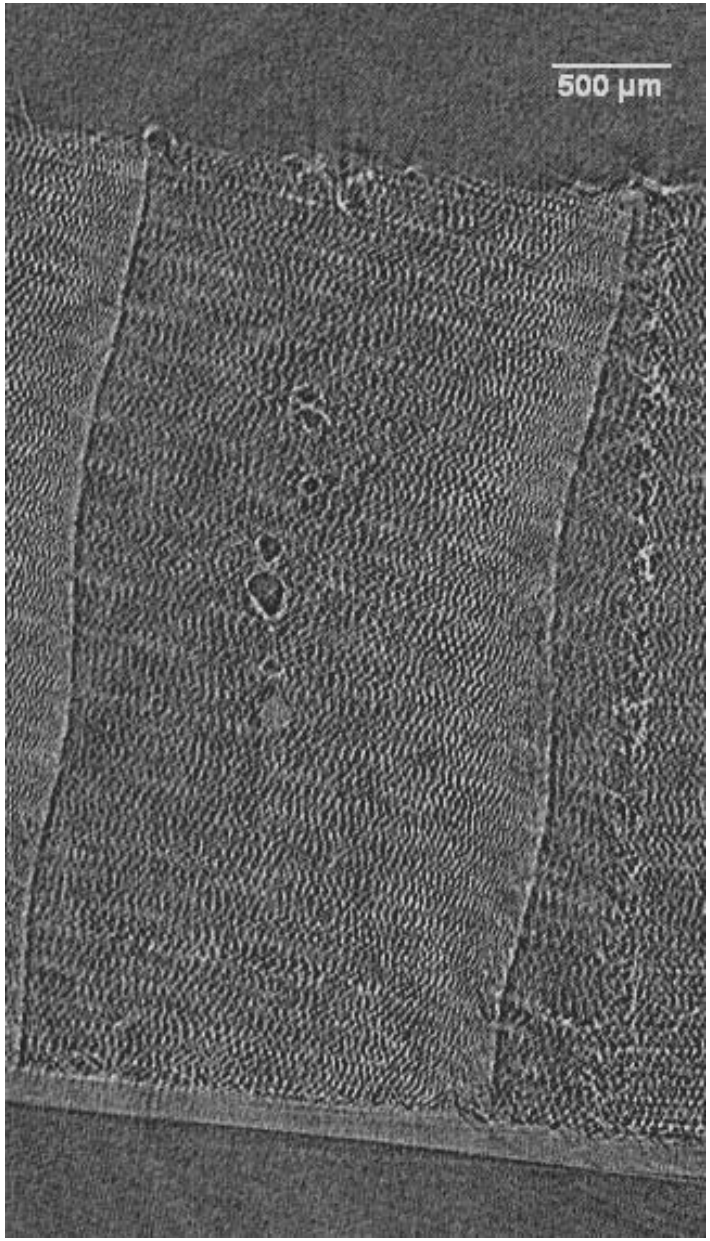

In principle, it is impossible to reconstruct, with the usual experimental and mathematical tools, an object with lateral dimensions larger than the FOV of the detector. This is the case of most musical instruments. We overcame this limit with *local area* tomography techniques.

This approach allowed us to analyze a violin at level of cellular structure, visualizing in detail the external varnish layer. *In an absolutely non-invasive way.*

Virtual section of the front plate obtained with local area tomography

Protodentistry

The Lonche jaw from a karsic cave of Slovenia

-First evidence of prehistoric dentistry (6500 BC)
-Multi modal analysis conducted on the upper part of a canine showed that beewax was used to fill a vertical crack affecting enamel and dentin tissue

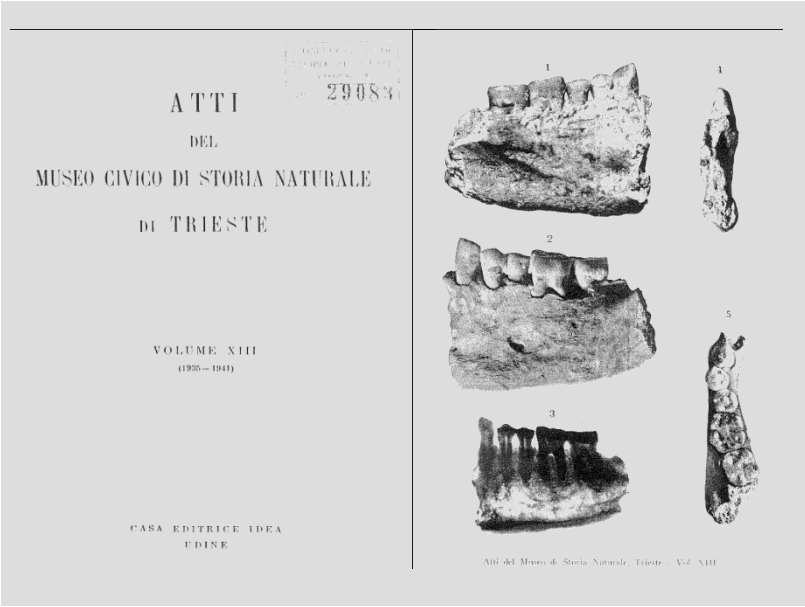

The Lonche jaw from a karsic cave of southern Slovenia Discovered in northern Istria in 1911

(Natural History Museum of Trieste)

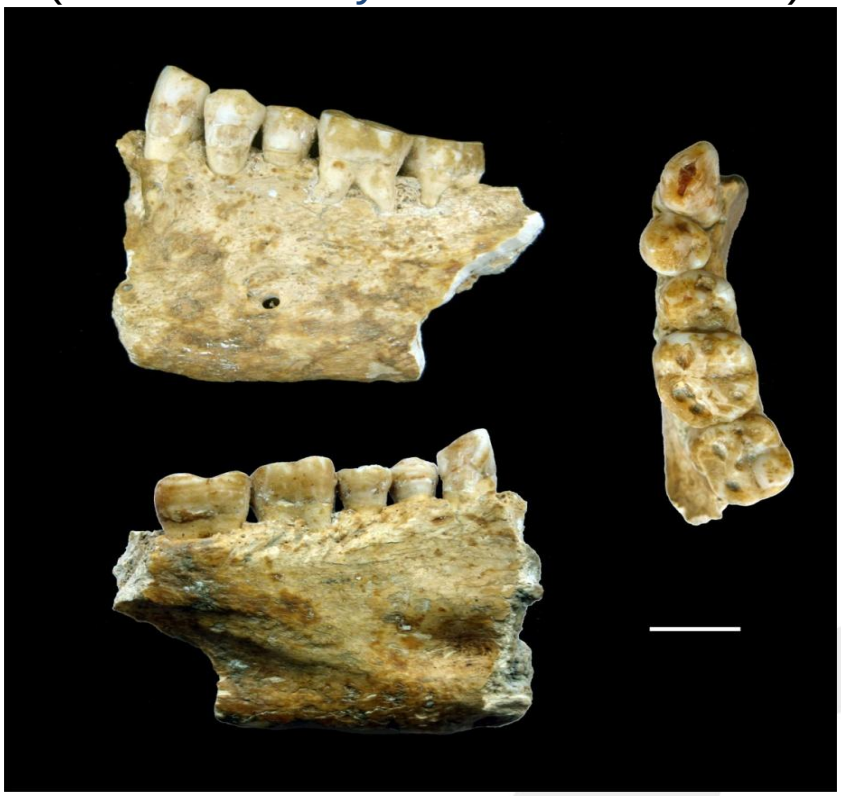

Bernardini et al., PLoS ONE 7 (2012) e44904

Elettra Sincrotrone Trieste

ICTP

Volume renderings of part of the Lonche jaw

by TomoLab @ Elettra (cubic voxel size = 18 mm)

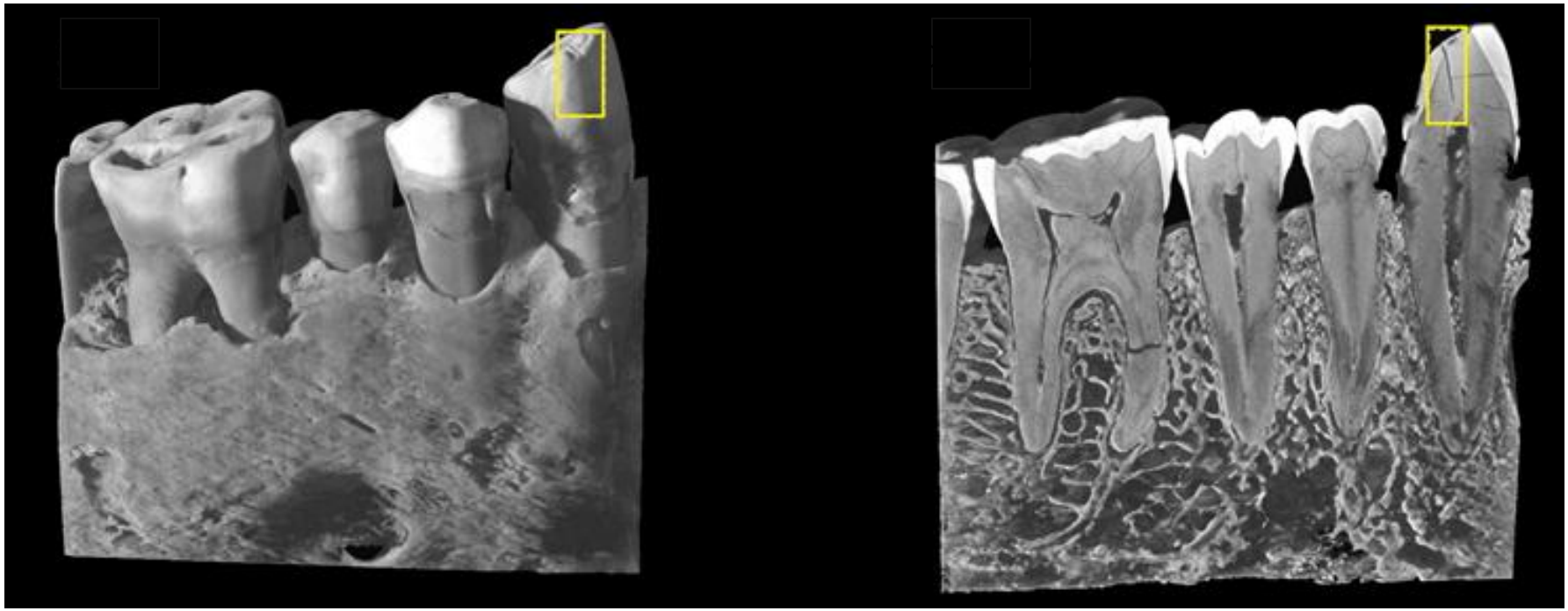

Dotted yellow rectangle: the position of the longitudinal crack partially filled with beeswax

Bernardini et al., PLoS ONE 7 (2012) e44904

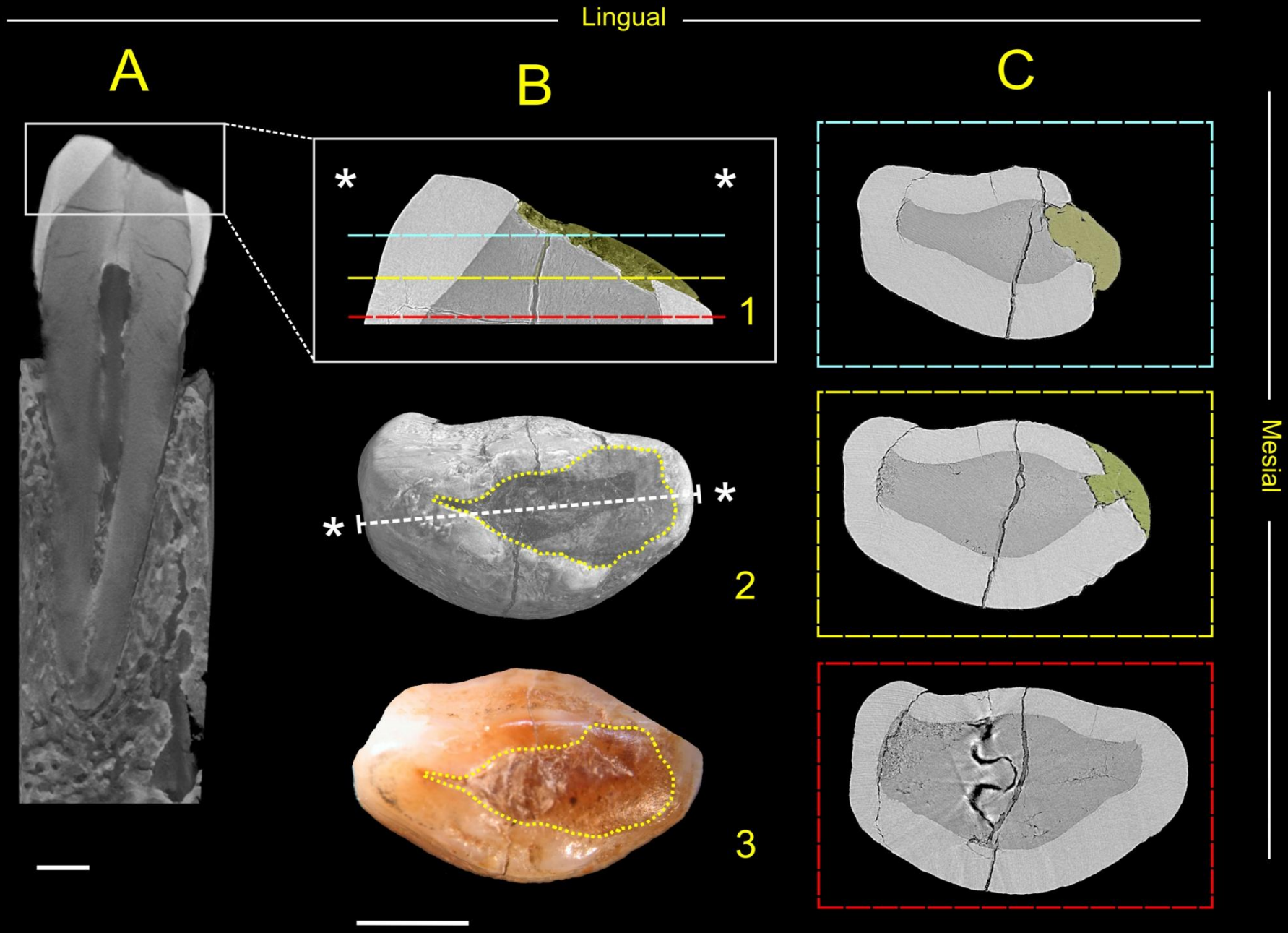
Lingual
A
B
C
Mesial
1
2
3

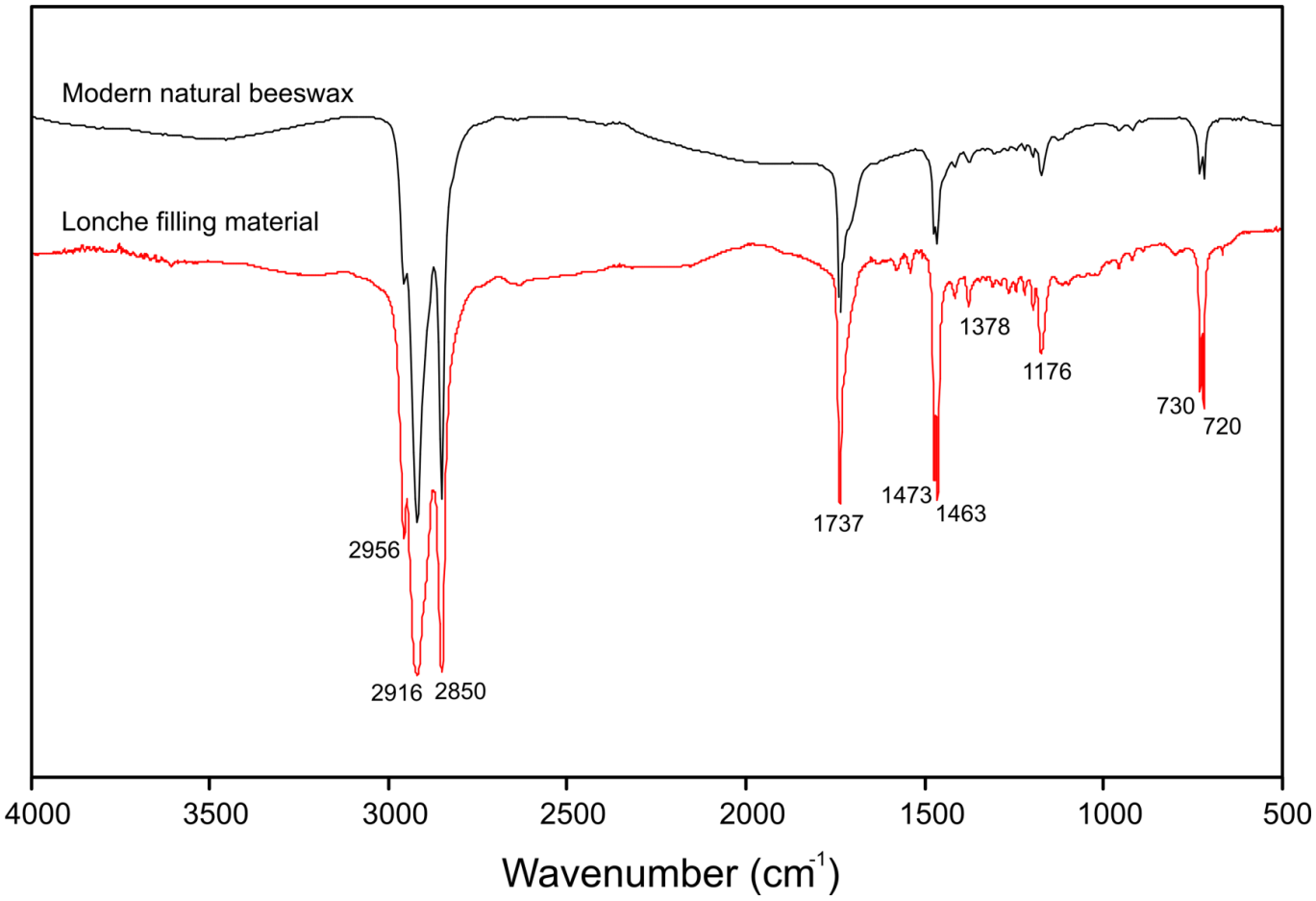

- Infrared spectroscopy characterized the extraneous filling material as beeswax.
- Accelerator Mass Spectroscopy radiocarbon used for dating showed that the filling was performed shortly before or after the person's death

Bernardini et al., PLoS ONE 7 (2012) e44904

3D quantitative analysis of volcanic rocks

• **The Formation of a volcanic rock** is a complex process with many steps involved, from magma ascent in the conduit to fragmentation and emplacement beyond the crater's rim.

•All these **processes** are somehow **recorded in the morphology** and in the **texture of the rock**.

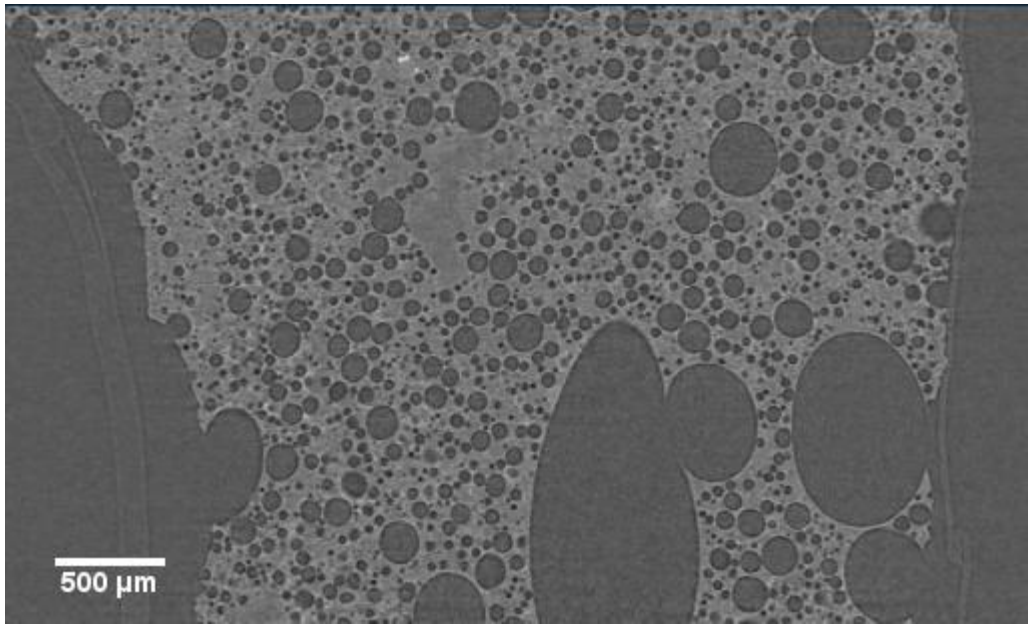

Reconstructed slices of a pumice sample from Ambryn volcano

D.R. Baker, et al.:, Lithos (2012)

Elettra Sincrotrone Trieste

Scoria from Ambryn, vesiculated, low crystallized

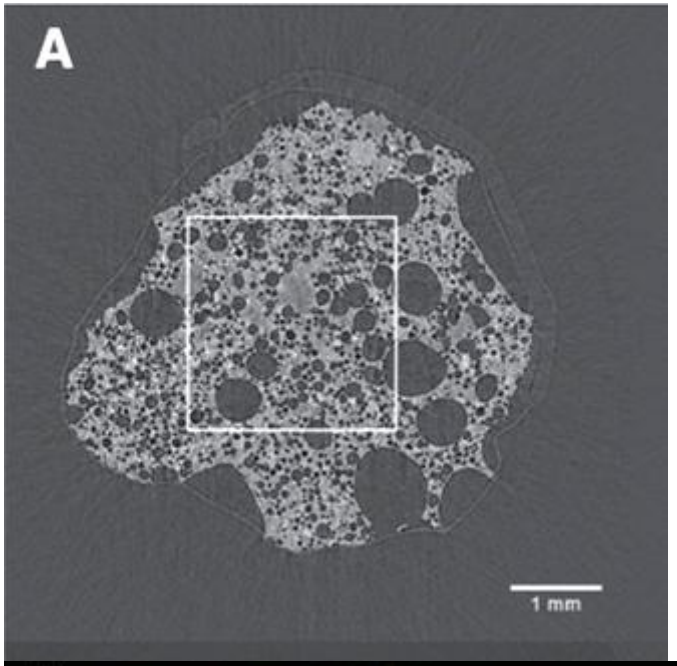

Vesicles colored after connected component analysis.

Red connected component

Yellow: the others

Vesicles isolated after watershed segmentation and border cleaning.

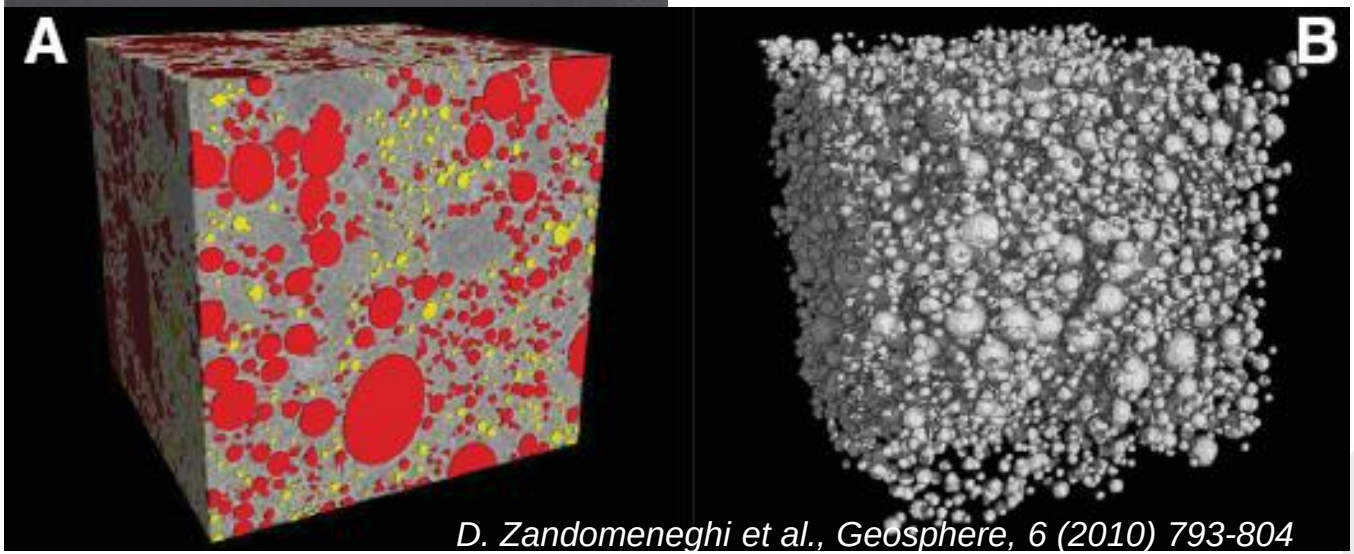

D. Zandomeneghi et al., Geosphere, 6 (2010) 793-804

Elettra Sincrotrone Trieste

Scoria from Stromboli, poorly to moderately vesiculated, highly crystallized

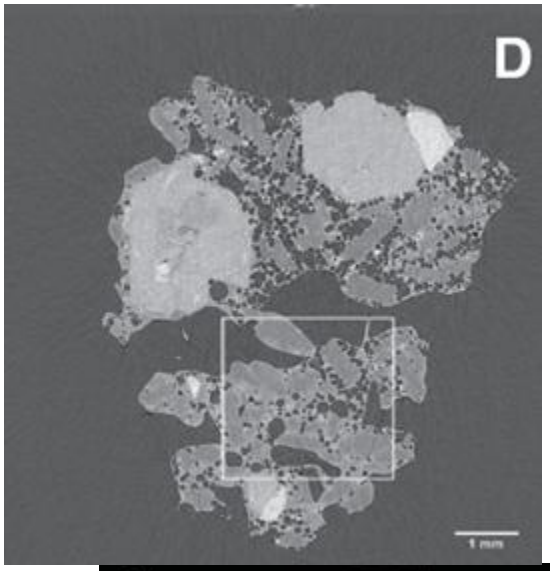

Blue pyroxene crystals
Yellow: feldspar crystals
vesicles -> 36 %
pyroxenes -> 28%
feldspars -> 12%,

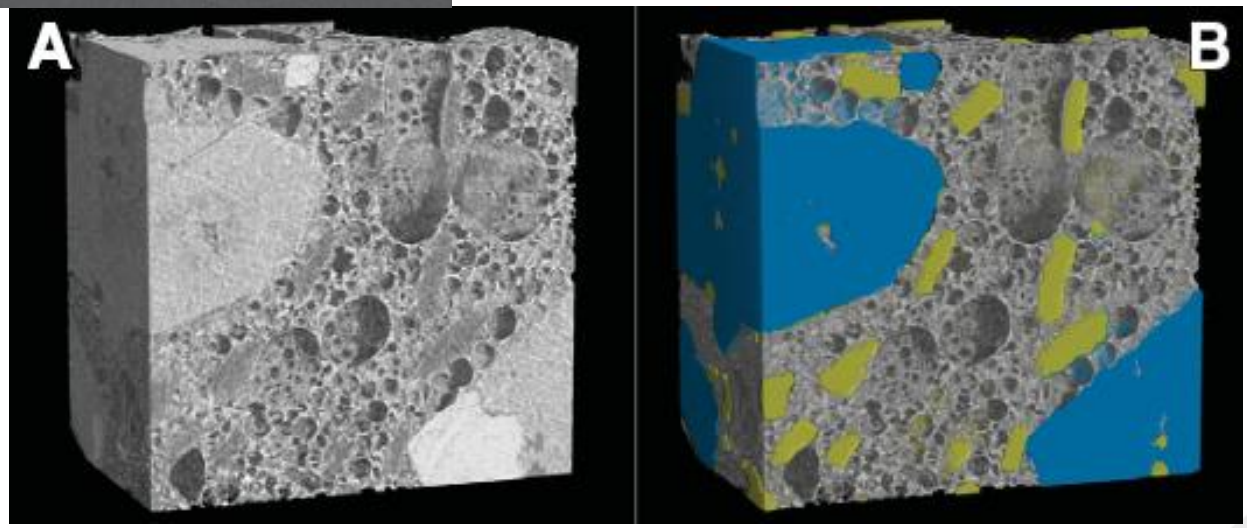

D. Zandomeneghi et al., Geosphere, 6 (2010) 793-804

Scoria from Etna

Complementary studies performed at PSI

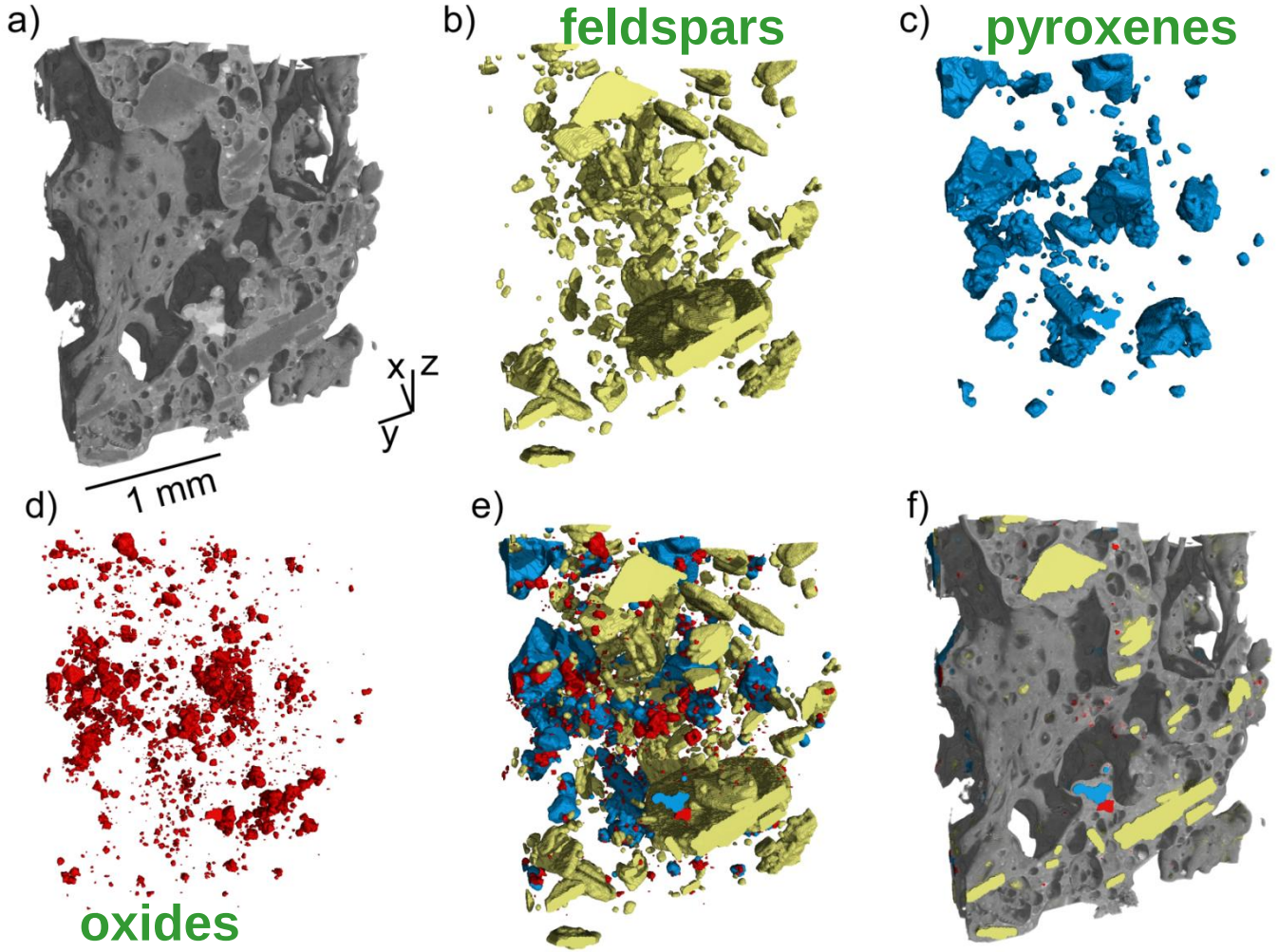

voxel size: 1.85 µm

vesicles -> 68.9%, plagioclases -> 4.3%, pyroxenes -> 3.2%, “oxides” -> 0.7%, glass -> 22.9%

Baker DR et al., Nat. Commun., Vol. 3, pp. 1135 (2012)

4D X-ray micro-CT study of bubble growth in basaltic foams – I experiment

The study of bubble formation in magma is fundamental for understanding the volcanic eruption mechanisms

Dynamic CT studies performed in-situ with basaltic samples brought at 600-1200 °C – white beam

Quantitative analysis allowed to measure bubble size, wall thickness distributions, connectivity, and calculate permeabilities and tensile strengths of basaltic foams imaged during bubble growth in hydrated basaltic melts.

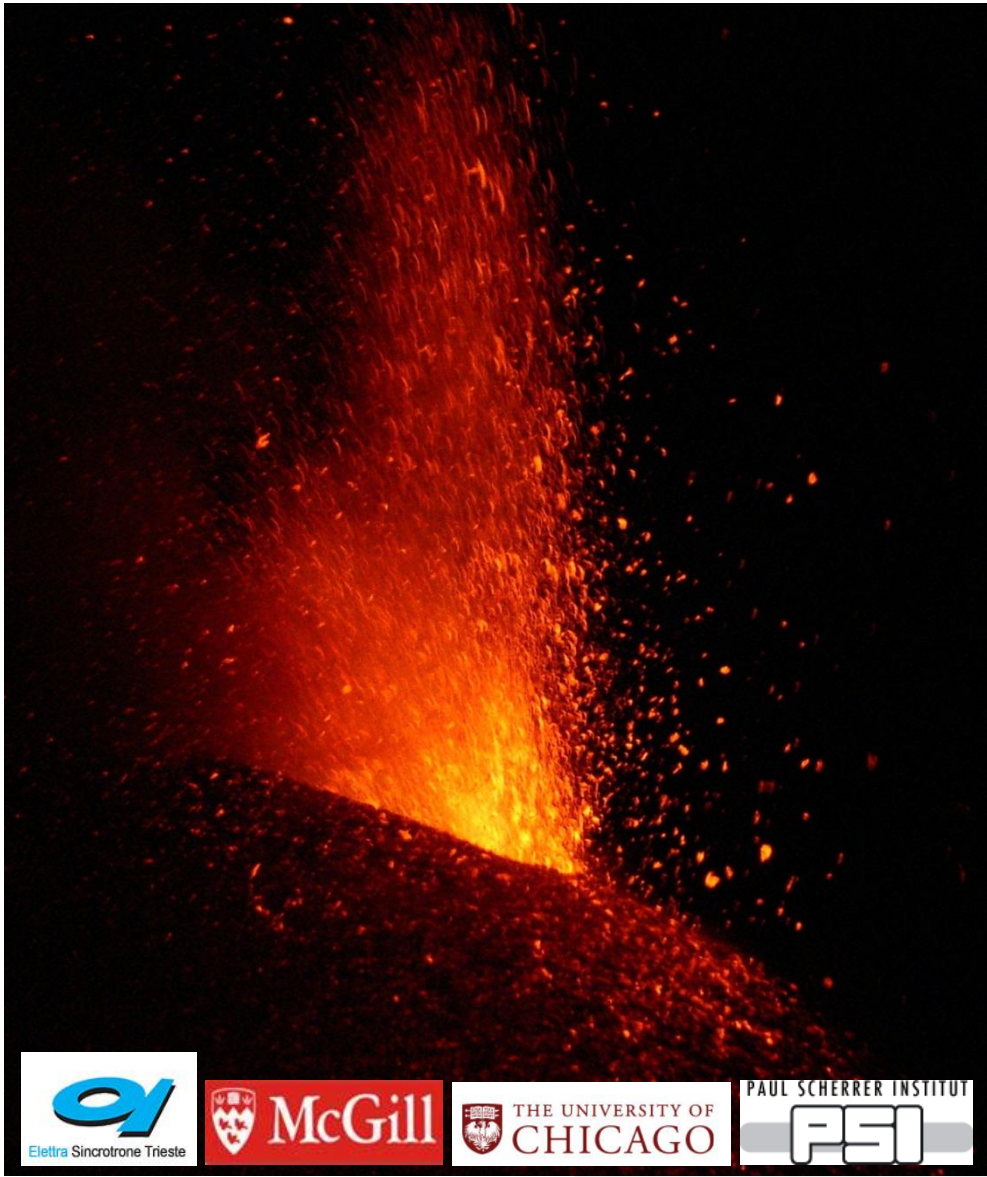

D.R. Baker, F. Brun, C. O'Shaughnessy, L. Mancini, J. Fife, M. Rivers, Nature Comm., 3 (2012) 1135

3D movie of the evolving sample

- Hydrated glasses (3 and 7 wt.% H_2O content) heated by a laser furnace
- As **T increased from 600 to ~1200° C**, full 3D data sets collected every second for 18 s.

Skeletonization used to measure bubble and pore throat sizes on reconstructed data

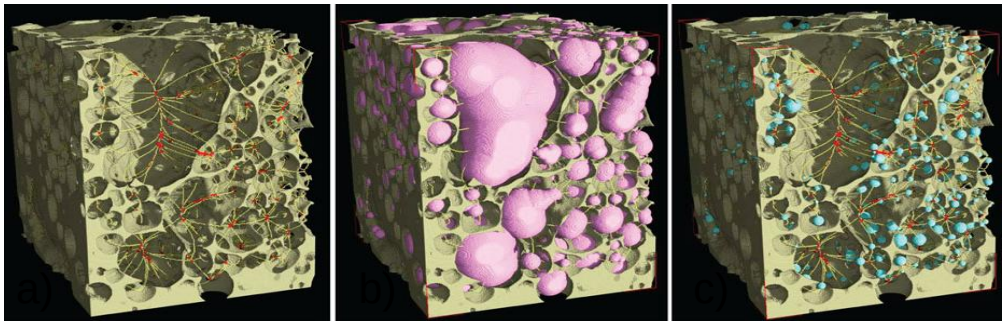

a) Topology preserving skeleton with nodes at the intersections of the branches
b) Maximal inscribed spheres to calculate bubble volumes
c) Maximal inscribed spheres to calculate pore throat diameters and wall thicknesses

D.R. Baker, F. Brun, C. O'Shaughnessy, L. Mancini, J. Fife, M. Rivers, Nature Comm., 3 (2012) 1135

Experiments vs. natural Bubble Size Distributions

4D experiments
Number of produced
Vescicles vs Vescicle Volume

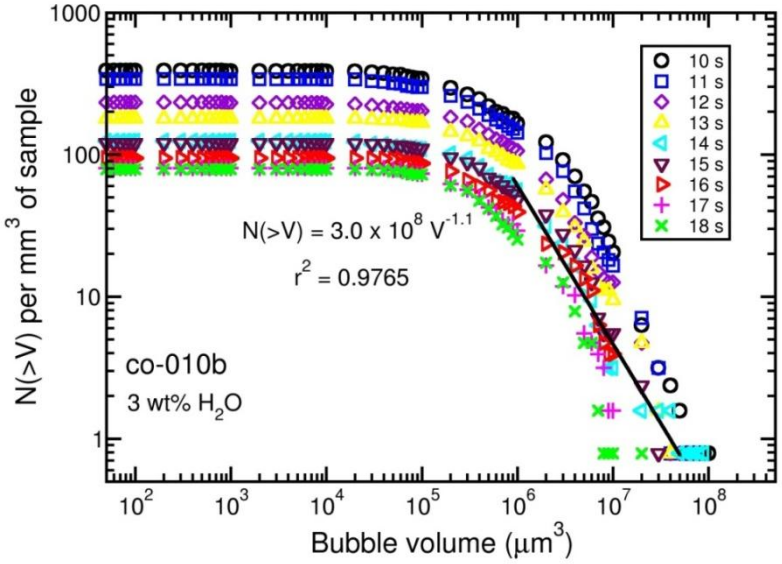

Normal Strombolian eruption

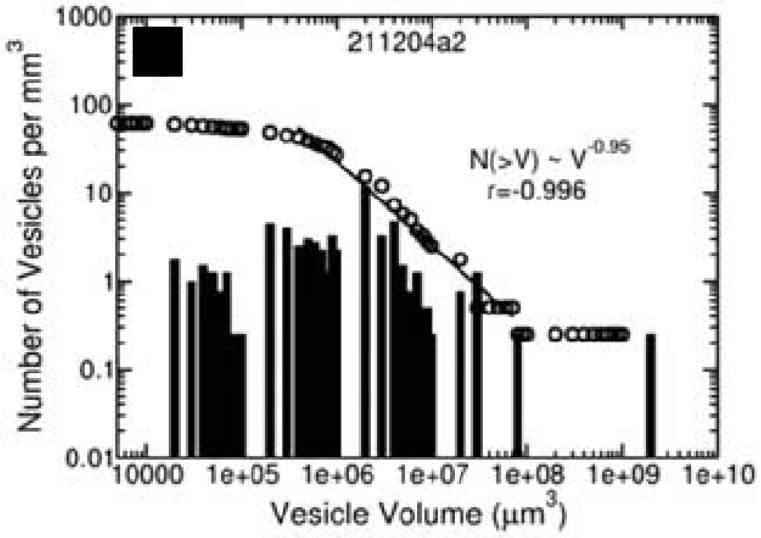

Paroxysmal eruption

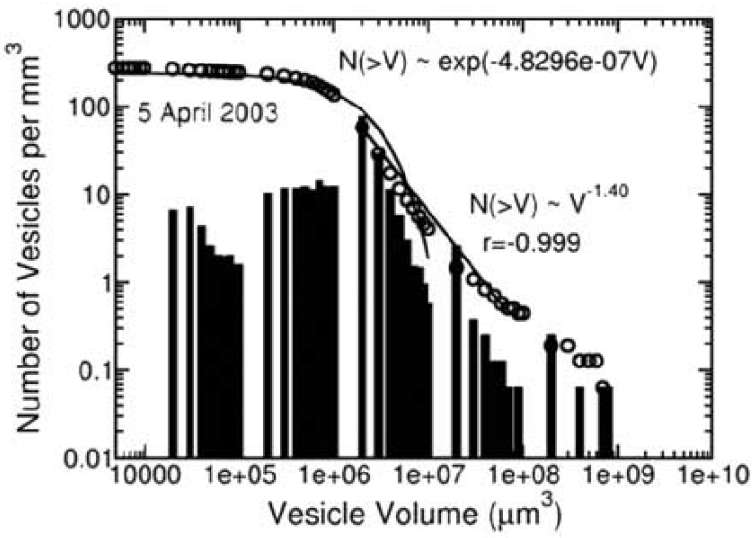

D.R. Baker, F. Brun, C. O'Shaughnessy, L. Mancini, J. Fife, M. Rivers, Nature Comm., 3 (2012) 1135

Elettra
Sincrotrone
Trieste

Contact:
giuliana.tromba@elettra.eu

Thank you for your attention